NASA-CR-205549

NASA GRANT NAG-1-244

NUMERICAL SOLUTIONS OF THE COMPLETE NAVIER-STOKES EQUATIONS

FINAL REPORT

Prepared by

David F. Robinson and H. A. Hassan

Department of Mechanical and Aerospace Engineering
Post Office Box 7910
North Carolina State University
Raleigh, North Carolina 27695-7910

Abstract

This report details the development of a new two-equation turbulence closure model based on the exact turbulent kinetic energy k and the variance of vorticity, ζ. The model, which is applicable to three dimensional flowfields, employs one set of model constants and does not use damping or wall functions, or geometric factors.

Table of Contents

List of Tables

List of Figures

List of Symbols

b	Wake half-width
b_{ij}	Anisotropy tensor, $\left[\frac{-\overline{u_i' u_j'}}{k} + \frac{2}{3}\delta_{ij}\right]$
c	Airfoil chord
B	Log-law constant
C_μ	Structural factor, 0.09
C_1, C_{ζ_1}	Compressibility closure coefficients
$C_{\mu 1}, C_{\mu 2}$	Wall damping function, f_μ closure coefficients
E	Non-dimensional Enstrophy for free shear flow analysis
e	Specific internal energy
f_μ	Wall damping function for the eddy viscosity
h	Specific enthalphy
k	Turbulent kinetic energy (per unit mass)
K	Non-dimensional turbulent kinetic energy for free shear flow analysis
l_{mfp}	Molecular length scale based on mean free path
M	Mach number
N	Non-dimensional eddy viscosity for free shear flow analysis
P, p	Mean and instantaneous Pressure
Pr_l	Laminar Prandtl number
Pr_t	Turbulent Prandtl number
q_j	Laminar Heat flux vector
q_{t_j}	Turbulent Heat flux vector
R	Reynolds number
R_k	Square root of turbulent Reynolds number
R_t	Turbulent reynolds number
S	Magnitude of strain rate tensor, $\sqrt{S_{ij}S_{ij}}$
S_{ij}, s_{ij}, s'_{ij}	Mean, instantaneous, and fluctuating strain rate tensors, respectively
t	Time
t_{ij}	Laminar stress tensor
T	Temperature
T_o	Stagnation (total) temperature
U_i, u_i, u'_i	Mean, instantaneous, and fluctuating velocity vector, respectively
U_τ	Frictional velocity, $\sqrt{\frac{\tau_w}{\rho}}$
v_{th}	Velocity scale based on thermal velocity
W	Defect velocity for planar wake flows
x_i	Spatial coordinates

α	Angle of attack
α_3	k-ζ closure coefficient
$\beta_4, \beta_5, \beta_6, \beta_7, \beta_8$	k-ζ closure coefficients
δ	k-ζ closure coefficient
δ_{ij}	Kronecker delta
$\delta\rho$	Compressibility correction for pressure gradient term
ϵ	Dissipation of turbulent kinetic energy
ϵ_{ijk}	Permutation tensor
η	Transformed similarity coordinate
κ	Karman constant, 0.40
μ	Molecular viscosity coefficient
ν	Kinematic molecular viscosity, $\frac{\mu}{\rho}$
$\mathcal{N}$	Navier-Stokes operator
ω	Specific dissipation rate
$\Omega_i, \omega_i, \omega_i'$	Mean, instantaneous, and fluctuating vorticity vectors, respectively
Ω	Magnitude of mean vorticity, $\sqrt{\Omega_i \Omega_i}$
$\Omega_{ij}, r_{ij}, r_{ij}'$	Mean, instantaneous, and fluctuating rotation tensor, respectively
Π_{ij}	Pressure dilatation term in Reynolds stress equation
ρ	Density
σ_k, σ_r, σ_ζ, σ_ρ, σ_p	k-ζ closure coefficients
τ	Turbulent time scale
τ_{ij}	Turbulent stress tensor
$\mathcal{T}$	Turbulent intensity
θ	Momentum thickness
ζ	Enstrophy

Subscripts:

$1, 2$	Denotes a quantity evaluated at the first or second point off the wall
char	Denotes a characteristic quantity
i, j, k	Denotes spatial coordinates or cell indices
l	Denotes a laminar quantity
o	Denotes a quantity evaluated at a centerline
t	Denotes a turbulent quantity
w	Denotes a quantity evaluated at the wall
∞	Denotes a freestream quantity

Superscripts:

n	Denotes a generic counter index
$'$	Denotes a time averaged fluctuating component
$''$	Denotes a Favre averaged fluctuating component
$+$	Denotes a log-law variable

Accents:

$\bar{}$	Denotes a time averaged quantity
$\tilde{}$	Denotes a Favre averaged quantity

Abbreviations:

CFD	Computational Fluid Dynamics
CFL	Courant-Friedrichs-Levy stability parameter
DNS	Direct Numerical Simulation
HSCT	High speed civil transport
LES	Large Eddy Simulation
NASP	National Aerospace Plane
NS	Navier-Stokes
ODE	Ordinary differential equation
PDE	Partial differential equation
RMS	Root Mean Square
TKE	Turbulent kinetic energy

1 Introduction

The use of Computational Fluid Dynamics, CFD as an engineering design tool has been accelerating in recent years primarily due to improvements in three major areas. The first is grid generation, where there are now a multitude of grid generation software packages available which can generate very complex three-dimensional grids. The other two areas are somewhat inter-related. Namely, computational speed and numerical algorithm efficiency. A combination of these two have reduced computational run times for two-dimensional flowfields from hours to minutes and have scaled three-dimensional calculations from days or weeks to hours. As the above three areas are continually refined the cost effectiveness of CFD as a design tool should continually increase. However, one of the major limitations of existing CFD solvers still remains. Namely, the inability to accurately solve complex turbulent flowfields. And, since the majority of flows of practical engineering interest are turbulent, this has become one of the most significant hindrances in the use of CFD as an engineering design tool.

CFD is being applied to a wide variety of applications: jet inlet design, weather prediction, High Speed Civil Transport (HSCT), National Aerospace Plane (NASP), missile aerodynamics, combustor design, and high angle of attack airfoils, just to name a few. One common feature of all of the above is that an accurate prediction of drag, heating, and mixing rates is paramount in the design/analysis process. In

turn, these parameters are highly dependent on an accurate solution of the turbulent flowfield. Inaccurate turbulent solutions can cause order of magnitude variations in these design parameters. Therefore, the goal of the current work is to develop a computational model which improves the accuracy of CFD solutions when analyzing extremely complex turbulent flowfields. Concentration will be focused on flows which contain a combination of free shear layers, shockwaves, large adverse pressure gradients, and large separated regions.

Before a discussion of the solution can begin a general description of turbulence is warranted. The most notable feature of a turbulent flowfield is seen by examining the velocity, or pressure, at a point in space, and noting that they are not constant in time. Rather, they exhibit very high frequency, irregular, three-dimensional fluctuations. Note that these fluctuations are three-dimensional, even for flows with a mean (time averaged) velocity field which is two-dimensional. The fluctuations cause three primary difficulties to arise when attempting to describe a turbulent flowfield. First, because it is a largely random process, we must rely on statistical methods to describe a turbulent flowfield. Second, we know that turbulent flows are highly rotational and three-dimensional. This inherent three-dimensionality is seen by examining the vorticity equation and noting that the vortex stretching term (absent for two-dimensional flows) is required to maintain the rotationality seen in a turbulent flow. This implies that there can be no adequate two-dimensional approximations to describe a turbulent flowfield. Finally, turbulence is not a fluid property (e.g. molec-

ular viscosity or thermal conductivity), rather, it is a property of the flow. Therefore, the initial/boundary conditions will play a major role and an *a priori* description of turbulence is not possible. Note that the preceding discussion was by no means an attempt to completely describe the physics behind a turbulent flow. Instead, it is an attempt to explain the difficulties associated with the CFD solution of a turbulent flowfield. For a more complete description of the physics of turbulence see Tennekes and Lumley[1].

To date, there are three basic approaches to solving a turbulent flowfield. The first, Direct Numerical Simulation (DNS), is a time dependent, three-dimensional solution of the Navier-Stokes (NS) equations. In order to accurately capture the turbulent features of the flowfield, all of the relevant scales (time and length) must be resolved. An estimate for the number of grid points required[1] to capture the spatial scales is typically given as $Re^{\frac{9}{4}}$, and therefore, for practical Reynolds numbers on the order of 10^6, this method is obviously not a feasible approach. It should be noted, however, that DNS is extremely useful for a limited range of low Reynolds number cases and, therefore, can be used as an invaluable tool in the testing/development of more practical turbulence models.

The next approach, Large Eddy Simulation (LES), involves splitting the flowfield such that the larger scales are computed directly and the smallest scale are modeled. As a result LES is also a relatively expensive calculation and turbulence modeling is still required for the smallest scales.

The final method does not attempt to resolve the turbulent scales. Rather, a model is derived which predicts the 'effect' of the turbulence on the mean (time averaged) flow. The 'effect' of the turbulence on the mean flow is determined by employing the Reynolds Averaging procedure, whereby, each quantity of interest (velocity, pressure) is decomposed into a mean and a fluctuating component. After substituting the decomposed variables into the instantaneous Navier-Stokes (NS) equations and applying a time average, two additional unknowns are produced due to the non-linearity of the NS equations. These unknowns, the turbulent stresses and the turbulent heat fluxes, represent the effect of the turbulence on the mean (time averaged) equations. The problem of turbulence modeling is, therefore, to devise a method of accurately calculating these two unknown quantities.

There are a variety of methods which can be used to calculate the effect of the turbulence on the mean flow (Algebraic, One-Equation, Two-Equation, Reynolds Stress). We chose a two-equation turbulence closure model so that, at a minimum, the following criterion are met. First, the model should be "complete", where complete refers to the fact that we only want to have to specify the initial and boundary conditions. This criterion requires that the closure coefficients must be constant (or a function of turbulent Reynolds number, R_t) for all of the flows considered. Next, the turbulence model must be able to solve both free shear (wakes, jets, and mixing-layers) and wall bounded flows. General design problems typically will include a combination of the above flow regimes for a given problem and it is not feasible to

have to use different turbulence models for each of the different regions of the flowfield. Finally, the turbulence model should be able to solve both two and three-dimensional flows and should be computationally efficient when used in either a boundary-layer or Navier-Stokes solver.

Given the above requirements, and noting that existing two-equation models are unable to meet these criterion, we chose to develop a new turbulence closure model. The decision to develop a new model, rather than modify an existing model, was influenced primarily by the following limitations of existing two-equation models. First, linear $k-\epsilon$ and $k-\omega$ models are incapable of describing wall bounded and free shear flows using the same set of model constants and boundary conditions[2]. Also, existing two-equation models are, in general, unable to predict separated flows[2, 3]. Finally, existing models were originally developed for high R_t flows, but are being employed in situations where R_t is low through the addition of asymptotic expansions or *ad hoc* terms. Based on the above, we chose not to modify an existing model, but rather, to develop a new model based on the exact turbulent kinetic energy ($k = \frac{1}{2}\overline{u_i' u_i'}$) and the variance of vorticity, or enstrophy ($\zeta = \overline{\omega_i' \omega_i'}$).

The development of the current model is shown beginning with a derivation of the exact k-ζ equations. Then the modeling is provided along with an explanation of how the closure coefficients were evaluated. Once the development has been presented the capabilities of the k-ζ model are examined, and modifications made, by considering a variety of flows. First, several free shear flows are considered and the k-ζ results

are compared with the k-ϵ model as well as with an abundance of experimental data. Next, a flat plate and its wake are considered. The flat plate results are compared with the near wall measurements of Schubauer[4] and Laufer[5] and the wake results were compared to the experimental data of Pot [6] and Weygandt and Mehta[7]. Additionally, a variety of two-dimensional airfoils are examined and the results are compared with the Johnson-King model[8], the k-ω model[2], and with experiment. Finally, the model is examined for a supersonic three-dimensional Cylinder-Flare and is compared with the experimental data of Wideman et al[9] as well as the k-ϵ model.

2 Turbulence Modeling

2.1 Reynolds Averaging

The instantaneous Navier-Stokes equations in a compressible medium are given as

$$\frac{\partial \rho}{\partial t} + \frac{\partial (\rho u_i)}{\partial x_i} = 0 \tag{2.1}$$

$$\frac{\partial (\rho u_i)}{\partial t} + \frac{\partial (\rho u_j u_i)}{\partial x_j} = -\frac{\partial p}{\partial x_i} + \frac{\partial (t_{ji})}{\partial x_j} \tag{2.2}$$

$$\frac{\partial}{\partial t}\left[\rho\left(e + \frac{1}{2}u_i u_i\right)\right] + \frac{\partial}{\partial x_j}\left[\rho u_j\left(h + \frac{1}{2}u_i u_i\right)\right] = \frac{\partial}{\partial x_j}(u_j t_{ij}) - \frac{\partial q_j}{\partial x_j} \tag{2.3}$$

with the following constitutive relations

$$t_{ij} = 2\mu s_{ij} - \frac{2}{3}\mu \frac{\partial u_m}{\partial x_m}\delta_{ij} \quad , \quad s_{ij} = \frac{1}{2}\left(\frac{\partial u_i}{\partial x_j} + \frac{\partial u_j}{\partial x_i}\right) \tag{2.4}$$

$$q_j = \frac{-\mu}{Pr_l}\frac{\partial h}{\partial x_j} \tag{2.5}$$

where t_{ji}, μ, s_{ij}, and Pr_l are the viscous stress tensor, molecular viscosity, strain rate tensor, and laminar Prandtl number, respectively. It should be noted that in order to simplify the current discussion, only incompressible flows (constant ρ) are considered. For an incompressible medium the Navier-Stokes equations (2.1-2.3) reduce to

$$\frac{\partial u_i}{\partial x_i} = 0 \tag{2.6}$$

$$\rho\frac{\partial u_i}{\partial t} + \rho u_j \frac{\partial u_i}{\partial x_j} = -\frac{\partial p}{\partial x_i} + \frac{\partial t_{ji}}{\partial x_j} \tag{2.7}$$

and the constitutive (Eq. 2.4-2.5) relations become

$$t_{ij} = 2\mu s_{ij} \quad , \quad s_{ij} = \frac{1}{2}\left(\frac{\partial u_i}{\partial x_j} + \frac{\partial u_j}{\partial x_i}\right) \tag{2.8}$$

It should be noted that the energy equation was omitted from the previous equation set. This is due to the fact that, for an incompressible flow, the energy equation is completely decoupled from the conservation of mass/momentum and, therefore, will be excluded from the current discussion. An in depth discussion of the energy equation and its relation to solving turbulent flows can be found in Refs.[10, 11].

The solution procedure for the current work does not attempt to resolve (spatially or temporally) all of the high frequency fluctuations which occur in a turbulent flowfield. Rather, the goal is to calculate the mean (time averaged) effect of these fluctuations on the mean flow. This statistical approach is achieved through the Reynolds averaging procedure which begins by decomposing the instantaneous quantities of interest (velocity and pressure) into a mean and fluctuating component.

$$q(\vec{x},t) = Q(\vec{x}) + q'(\vec{x},t) \tag{2.9}$$

where $Q(\vec{x})$ is the time averaged mean component, i.e.

$$Q(\vec{x}) = \lim_{T\to\infty} \frac{1}{T} \int_t^{t+T} q(\vec{x},t)dt \tag{2.10}$$

and $q'(\vec{x},t)$ is the turbulent fluctuation. Since it is not feasible to resolve the turbulent fluctuations, we are instead interested in determining the effect of these fluctuations on the mean flow.

After decomposing the Navier-Stokes equations (Eqs. 2.6-2.7) and applying the above time average we are left with the Reynolds Averaged Navier-Stokes equations

for an incompressible fluid.

$$\frac{\partial U_i}{\partial x_i} = 0 \tag{2.11}$$

$$\rho\frac{\partial U_i}{\partial t} + \rho U_j\frac{\partial U_i}{\partial x_j} = -\frac{\partial P}{\partial x_i} + \frac{\partial}{\partial x_j}\left(t_{ij} - \overline{\rho u_i' u_j'}\right) \tag{2.12}$$

where U_i, P, S_{ij} are the mean velocity, pressure, and strain rate, respectively, and u_i' represents the fluctuating velocity. By comparing eqs. (2.6-2.7) with eqs. (2.11-2.12) it is seen that aside from the replacement of the instantaneous variables by the mean values, the only difference between the instantaneous equations and the time-averaged equations is the appearance of a momentum flux which acts as an apparent stress. This additional parameter

$$\tau_{ij} = -\overline{\rho u_i' u_j'} \tag{2.13}$$

is referred to as the turbulent or Reynolds stress tensor. In order to solve the time averaged equations of motion for the mean flow properties, we must have a means of computing τ_{ij}. A similar procedure applied to the energy equation produces an unknown turbulent heat flux vector, $q_{t_j} = -\overline{\rho u_j' h'}$. Since the current work concentrated on incompressible flows the procedure for calculating the turbulent heat flux vector is deferred to Refs.[10, 11]).

The calculation of a turbulent flowfield has now become dependent on the accurate calculation of the Reynolds stress tensor. It should be noted that an equation for the Reynolds stress, $-\overline{\rho u_i' u_j'}$ can be derived (see Appendix A), by taking higher moments of the Navier-Stokes equations. However, when these moments are taken,

additional unknowns are generated (third order correlations). This inability to close the equation set (i.e. more unknowns than equations) is known as the 'turbulence closure' problem and is due to the non-linearity of the Navier-Stokes equations. The purpose of turbulence modeling is to devise approximations for the unknowns in terms of the known flow properties in such a way that the number of equations is equal to the number of unknowns.

2.2 Eddy Viscosity

By examining the molecular transport of momentum [2], the kinetic theory of gases provides an expression which relates the viscous stress tensor to the strain rate tensor through a coefficient of viscosity, μ.

$$t_{ij} = 2\mu S_{ij} \tag{2.14}$$

$$\mu = \frac{1}{2}\rho v_{th} l_{mfp} \tag{2.15}$$

where v_{th} is the thermal velocity and l_{mfp} is the mean free path. By making an analogy between the behavior of turbulent fluctuations and random molecular fluctuations, an expression for the turbulent viscous stress tensor (Reynolds stress) in terms of an apparent or eddy viscosity, μ_t is obtained.

$$\tau_{ij} = 2\mu_t S_{ij} \quad (i \neq j) \tag{2.16}$$

$$\mu_t = \frac{1}{2}\rho v_{char} l_{char} \tag{2.17}$$

where v_{char} and l_{char} are some characteristic velocity and length scales representative of the turbulence. The problem of turbulence modeling has now been reduced to one

of calculating Eq.(2.17). Keep in mind that although Eqs. (2.15) and (2.17) appear very similar, they do have one major difference. Namely, the thermal velocity and mean free path are properties of the fluid, whereas the characteristic velocity and length scales are flowfield properties. This difference is the reason why it is possible to give an *a priori* description of μ but not μ_t.

2.2.1 Levels of Modeling

There are several levels of turbulence modeling to consider ranging from the simplest algebraic model to very complex Reynolds stress formulations. A brief description of each method will be included for completeness, however, readers interested in a more in depth analysis should see Ref. [2].

The first, and simplest method considered, is an algebraic turbulence model. Typically, the characteristic velocity is given by a simple algebraic relation and the mixing length is based on some characteristic length of the flow. For wall bounded flows l_{char} is often based on normal distance from the wall, and for free shear flows it is typically proportional to the width of the shear layer. Herein lies the problem for algebraic models. This proportionality constant varies for each of the different types of free shear flows. This type of model, which requires *a priori* information about the flowfield (other than initial and boundary conditions) is referred to as an "incomplete" model.

The next level of modeling is termed a one-equation model. Instead of using an algebraic relation, an equation is solved (typically the turbulent kinetic energy) for the

characteristic velocity. This formulation still requires the specification of a turbulent length scale, and therefore, by analogy with the algebraic method, the one-equation model is also an incomplete model.

The next level of complexity for turbulence modeling involves solving two equations for the two characteristic scales. A two-equation formulation is desirable because it is the simplest form of a 'complete' model, where complete refers to the fact that only initial and boundary conditions for the two-equations must be specified. No *a priori* information about the flowfield is required. Higher order 'complete' turbulence models are available such as the Reynolds Stress model, however, solving this imposes a great deal of complexity since five new equations must be solved for the five independent components of the Reynolds stress tensor. Another reason for the choice of a two-equation model over a stress model is due to the fact that most of the problems with existing turbulence closure models have been traced to an inadequate dissipation rate equation[12]. When this is taken into consideration along with the fact that solving a Reynolds stress model requires a dissipation rate equation, the choice of a two-equation model becomes obvious. It should be noted, however, that once an improved dissipation equation is developed, an extension of the model to a Reynolds stress formulation becomes the obvious next step.

From Eq. (2.17) it is seen that you can solve one equation for a velocity scale and one equation for a length scale, or alternatively, you can solve for a velocity and a time scale. This is explained by noting that on dimensional grounds alone, a characteristic

velocity and length can be combined to give a characteristic time scale. For the current work we have chosen to solve one equation for the turbulent kinetic energy (characteristic velocity scale) and one equation for the dissipation rate of turbulent kinetic energy (characteristic time scale). Since the TKE equation is assumed to be a well defined/modeled equation, and since most of the debate over two-equation models focuses on the dissipation equation, the current formulation uses the standard k equation (see Appendix B) and a new dissipation equation based on the fluctuating vorticity. It should be pointed out that a variety of other dissipation rate equations could have been considered (i.e. ω, ϵ), however, the reason an equation based on the fluctuating vorticity was chosen can be seen by noting some predominant processes occurring in a turbulent flowfield.

Turbulent flows are dominated by three dimensional, highly rotational processes. Furthermore, vortex stretching is noted to be the most effective means of extracting energy from the mean flow and transferring it from the large eddies to the smallest eddies[1]. The smallest eddies, in turn, dissipate the energy into heat through molecular viscosity. This predominance of fluctuating vorticity in maintaining a turbulent flow suggests that a natural route in our search for a second equation (i.e. a characteristic time scale) would be through an examination of the vorticity equation. More specifically, it will be shown that the fluctuating vorticity can be used to calculate the dissipation rate as required to close our equation set (see Appendix B). A derivation of the Enstrophy equation is provided in Appendix D. It should be noted that the

Enstrophy equation has also been the subject of detailed investigations by Bernard and Berger [13] and Raul and Bernard [14]. It should also be noted that the current formulation for a dissipation equation can be easily incorporated into existing CFD codes by substituting the enstrophy equation for the 'ϵ' or 'ω' equations.

As previously mentioned, the current method is based on solving one equation for the turbulent kinetic energy (per unit mass)

$$k \equiv \frac{1}{2}\overline{u_i' u_i'} = \frac{1}{2}\left(\overline{u'^2 + v'^2 + w'^2}\right) \tag{2.18}$$

and one equation for the enstrophy (vorticity variance)

$$\zeta \equiv \overline{\omega_i' \omega_i'} \tag{2.19}$$

where u_i' is the fluctuating velocity and ω_i' is the fluctuating vorticity. We now define the eddy viscosity as

$$\mu_t = \frac{C_\mu \rho k^2}{\nu \zeta} \tag{2.20}$$

where C_μ is the structural factor (see Appendix G), ρ is the density, k is the turbulent kinetic energy, ν is the kinematic molecular viscosity, and ζ is the enstrophy. In order to determine the turbulent stresses we apply the Bousinesq approximation for an incompressible medium.

$$\tau_{ij} = 2\mu_t S_{ij} - \frac{2}{3}\rho k \delta_{ij} \tag{2.21}$$

where δ_{ij} is the Kronecker delta. Note that $(-\frac{2}{3}\rho k \delta_{ij})$ has been added to the stress relation (Eq. 2.16) to ensure that

$$\tau_{ii} \equiv -\overline{\rho u_i' u_i'} \tag{2.22}$$

$$= -2\rho k \tag{2.23}$$

as defined in Eq. 2.18.

From the above two-equation formulation it is seen that only the initial and boundary conditions for k and ζ must be specified, therefore, this type of turbulence model is a 'complete' model.

3 Modeling Unknown Correlations

The derivation of the exact incompressible k-ζ equations are given in Appendices B and D. The final forms have been reproduced here for convenience.

$$\frac{Dk}{Dt} = \frac{\tau_{ij}}{\rho}\frac{\partial U_i}{\partial x_j} - \nu\overline{\frac{\partial u_i'}{\partial x_k}\frac{\partial u_i'}{\partial x_k}} + \frac{\partial}{\partial x_j}\left[\nu\frac{\partial k}{\partial x_j} - \frac{1}{2}\overline{u_i'u_i'u_j'} - \overline{\frac{p'u_j'}{\rho}}\right] \tag{3.1}$$

$$\frac{D\zeta}{Dt} = -2\overline{u_j'\omega_i'}\frac{\partial \Omega_i}{\partial x_j} - \frac{\partial}{\partial x_j}\left(\overline{u_j'\omega_i'\omega_i'}\right) + 2\overline{\omega_i'\omega_j's_{ij}'} + 2\overline{\omega_i'\omega_j'}S_{ij} + 2\Omega_j\overline{\omega_i's_{ij}'}$$
$$+\nu\frac{\partial^2\zeta}{\partial x_m^2} - 2\nu\overline{\frac{\partial\omega_i'}{\partial x_j}\frac{\partial\omega_i'}{\partial x_j}} \tag{3.2}$$

Now that we have our equation set the next step is to model the unknown quantities in terms of known flow variables. The manner in which this is done represents the primary difference between the k-ζ model and other two-equation models. Traditionally, the high turbulent Reynolds number hypothesis is employed, whereby, the largest scales are unaffected by the fluid's viscosity and the smallest scales are isotropic, or independent of the larger scales. If the smallest scales are independent of the mean flow, this implies the following terms (which are dependent on the mean flow) from Eq. (3.2) can be neglected

$$2\overline{u_j'\omega_i'}\frac{\partial\Omega_i}{\partial x_j} \quad , \quad 2\overline{\omega_i'\omega_j'}S_{ij} \quad , \quad 2\Omega_j\overline{\omega_i's_{ij}'} \tag{3.3}$$

The above terms represent the fine scale correlations which describe the detailed mechanism of the dissipation process and thereby control the near wall behavior.

Thus, these terms must be retained if one hopes to accurately predict the skin friction and heat transfer. Therefore, the current model retains and models each of the above described terms.

In addition to retaining all of the fine scale terms in the exact equations a set of modeling guidelines were developed in order to impose a consistency to the modeling process and also in the hopes of more accurately capturing the underlying physics. It should be noted that these guidelines are necessary, but not sufficient conditions, for modeling the unknown correlations.

1) Dimensional consistency was enforced.

2) All modeling maintained coordinate system independence.

3) Gallilean Invariance was imposed.

4) All modeling was based on linear relationships ; this is consistent with Eq. 2.21

During the modeling we encountered a number of second order symmetric and skew-symmetric tensors which required modeling. In order to be mathematically consistent the unknown symmetric tensors are modeled using known symmetric tensors, namely, τ_{ij}, S_{ij}, and δ_{ij}. Similarly, the skew-symmetric tensors are modeled using Ω_{ij}, ϵ_{ijk}, and $\left(\frac{\partial k}{\partial x_i}\frac{\partial \zeta}{\partial x_j} - \frac{\partial k}{\partial x_j}\frac{\partial \zeta}{\partial x_i}\right)$. The modeling for each of the six unknown terms is shown in Appendix E, with the resulting equation set shown below.

$$\rho\frac{Dk}{Dt} = \tau_{im}\frac{\partial U_i}{\partial x_m} - \mu\zeta + \frac{\partial}{\partial x_m}\left[\left(\frac{\mu}{3} + \frac{\mu_t}{\sigma_k}\right)\frac{\partial k}{\partial x_m}\right] \tag{3.4}$$

$$\rho\frac{D\zeta}{Dt} = \frac{\epsilon_{mij}}{2}\left[\frac{\partial\left(\overline{u'_m u'_l}\right)}{\partial x_l} - \frac{\partial k}{\partial x_m}\right] + \frac{\partial}{\partial x_j}\left[\left(\mu + \frac{\mu_t}{\sigma_\zeta}\right)\frac{\partial \zeta}{\partial x_j}\right] - \frac{\rho\beta_5}{R_k}\zeta^{\frac{3}{2}}$$

$$+ \left(\alpha_3 \rho \zeta b_{ij} + \frac{2}{3}\delta_{ij}\rho\zeta\right) S_{ij} - \frac{\beta_4 \zeta \tau_{ij} \Omega_i \Omega_j}{k\Omega} + 2\beta_8 \epsilon_{ilm} \left(\frac{\tau_{ij}}{k}\right) \left(\frac{\partial k}{\partial x_l}\frac{\partial \zeta}{\partial x_m}\right) \frac{\Omega_j}{S^2}$$

$$- 2\frac{\beta_6 \tau_{ij} \nu_t}{k\nu} \Omega \Omega_i \Omega_j + \frac{\beta_7 \rho \zeta}{\Omega^2} \Omega_i \Omega_j S_{ij} + \frac{\sigma_p \left(\frac{\partial P}{\partial x_i}\right)^2 \left(\frac{\Omega}{P}\right) R_t^{\frac{3}{2}}}{1 + \left[\sigma_\rho \frac{a^2 M_T^{\frac{5}{2}}}{\nu S^2} \left(\frac{\partial U_i}{\partial x_i}\right)\right]^2} \tag{3.5}$$

where

$$\tau_{ij} = 2\mu_t S_{ij} - \frac{2}{3}\delta_{ij}\rho k \quad , \quad \nu_t = C_\mu \frac{k^2 f_\mu}{\nu\zeta}$$

$$S^2 = S_{ij}S_{ij} \quad , \quad \Omega^2 = \Omega_i \Omega_i$$

$$R_k = \frac{k}{\nu\sqrt{\zeta}} \quad , \quad R_t = R_k^2$$

Now that we have the modeled k-ζ equation set, all that is remaining is to determine the appropriate boundary conditions and calculate the unknown closure coefficients $(\alpha_3, \beta_4, \beta_5, \beta_6, \beta_7, \beta_8, \sigma_k, \sigma_\zeta, \sigma_p, \sigma_\rho)$.

4 Boundary Conditions

With the current formulation for solving turbulence we have introduced two additional unknowns to our equation set, namely, k, and ζ. A wall and free stream (subscripts w and ∞, respectively) boundary condition is required for each of the added variables.

At the wall it can be shown that k and its derivative are zero and ζ is finite (see Appendix I). Therefore, we have

$$k_w = 0 \tag{4.1}$$

$$\left.\frac{\partial k}{\partial \eta}\right|_w = 0 \tag{4.2}$$

ζ has no physical boundary condition at a solid surface.

For the current work we have examined two boundary conditions for ζ_w. The first was a simple first order extrapolation, i.e. we set

$$\left.\frac{\partial \zeta}{\partial \eta}\right|_w = 0 \tag{4.3}$$

where η is the normal coordinate from the surface. The second boundary condition for ζ_w was developed from Eq. (4.2) and the k equation. In the near wall region both the convection and production terms are negligible, and therefore, for an incompressible flow Eq. (3.1) reduces to

$$\frac{\partial}{\partial y}\left[\frac{1}{3}\frac{\partial k}{\partial y}\right] = \zeta_w \tag{4.4}$$

If we define a one-sided difference as

$$\frac{\partial q}{\partial y} = \frac{q_{j+1} - q_j}{y_{j+1} - y_j} \tag{4.5}$$

and we use a subscript convention of 1 and 2 to denote the the first and second points off of the wall, respectively, then we end up with

$$\zeta_w = \frac{1}{3\triangle y_1}\left[\left.\frac{\partial k}{\partial y}\right|_1 - \left.\frac{\partial k}{\partial y}\right|_w\right] \tag{4.6}$$

or, using Eq. (4.2)

$$\begin{aligned}\zeta_w &= \frac{1}{3\triangle y_1}\left.\frac{\partial k}{\partial y}\right|_1 \\ &= \frac{(k_2 - k_1)}{3\triangle y_1 \triangle y_2}\end{aligned} \tag{4.7}$$

where,

$$\triangle y_1 = y_2 - y_1 \tag{4.8}$$

The merits of both boundary conditions will be discussed in the results section where the simple extrapolation is labeled as bc_1 and the above formula (Eq. 4.7) is labeled as bc_2.

Now, all that is remaining is to specify the free stream values for each of the three variables. This is done by specifying a turbulent intensity, $\mathcal{T}$ and a ratio of turbulent to laminar stresses, $\left(\frac{\mu_t}{\mu}\right)_\infty$ and solving for the remaining variable, ζ_∞.

The turbulent intensity is defined as

$$\mathcal{T} = \frac{|u'|}{U_\infty} \tag{4.9}$$

and if you assume the flow is isotropic ($u' = v' = w'$) in the free stream k can be written as

$$k_\infty = \frac{3}{2} u'^2 \tag{4.10}$$

Eqs. 4.9-4.10 can be combined to give

$$k_\infty = \frac{3}{2} (\mathcal{T} U_\infty)^2 \tag{4.11}$$

The turbulent intensity is often provided by experiment and is typically $\mathcal{O}(1\%)$.

It should be noted that as you leave the boundary layer and approach the free stream all variables, k, ζ, and μ_t, decay to small values. Transients during the solution procedure can cause large spikes in the $\frac{\mu_t}{\mu}$ ratio since μ_t is defined as a ratio of $\frac{k^2}{\zeta}$. In order to prevent numerical difficulties resulting from dividing by a very small number, a bound is placed on the allowable values of $\frac{\mu_t}{\mu}$. This limit is derived by examining the isotropic decay of homogeneous turbulence (see Appendix K) and is given as

$$\left(\frac{\mu_t}{\mu}\right)_\infty < C_\mu \left(\frac{2\delta}{(\beta_5 - 2)}\right)^2$$

where C_μ, β_5, and δ are constants (see Table 9.3)

5 Evaluation of Closure Coefficients

The final step in the development of the k-ζ model is the determination of the unknown closure coefficients. This procedure was accomplished in four stages: a log-law analysis, an examination of similarity solutions for free shear flows, a boundary layer solution of a flat plate and its wake, and a number of Navier-Stokes solutions for more complex flowfields. A brief description of each method will be provided along with an explanation of why the method was chosen.

5.1 Log-Law Analysis

The log-law refers to a region of the boundary layer over which a logarithmic velocity profile is valid. If we examine the k-ζ equation set in this region, and ensure that the correct scaling is met, the following relation is obtained.

$$\sigma_\zeta = \frac{6\kappa^2}{\left[3\beta_5\sqrt{C_\mu} - 3\alpha_3\sqrt{C_\mu} - 4\beta_4 - 8\beta_6\right]} \tag{5.1}$$

This has allowed us to express one of our unknown closure coefficients in terms of the others, thereby, reducing the amount of unknowns by one. A more in-depth explanation of the log-law region, as well as a derivation of Equation (5.1) is provided in Appendix G.

5.2 Similarity Solutions

A number of model constants were chosen in order to optimize the solutions for a variety of free shear flows. The free shear flows considered for the current research include wakes, mixing-layers and a variety of jets (planar, round, and radial).

This method of determining model constants was chosen for several reasons, the first of which being, free shear flows, by definition, are not bounded by solid surfaces, and therefore, the complications imposed by solid boundaries can be avoided during the initial evaluation of the turbulence model. These complications include, amongst others, a vanishing turbulent Reynolds number and the lack of physical boundary conditions for the dissipation equation (ζ) at a solid surface.

Another reason free shear flows were chosen was due to the fact that, for each of the flows under consideration, a self-similar (or self-preserving) mean flow state is attained far downstream of the generating body. This self-similarity implies that, at a sufficient distance downstream, the profiles become invariant if plotted against a similarity variable, η. In other words, the equations are transformed from an x-y to an x-η coordinate system (where $\eta = yf(x)$). Then, for the types of flows under consideration, it is possible to eliminate the x-dependence, thereby reducing the partial differential equations to ordinary differential equations (ODE). These ODE's are not computationally intensive, and therefore, a large number of model constants can be evaluated with very little effort.

An additional reason for choosing free shear flows to calibrate the turbulence

model is because of the vast database of experimental data. This abundance of turbulent data for free shear flows allows one to easily evaluate a given model for a wide variety of flowfields. It should be noted, however, that there was a lack of consistency amongst the various experiments in measurements of the turbulent kinetic energy and the normal stresses. Therefore, the constants were optimized by emphasizing a comparison with measured growth rates and maximum shear stresses, which were in close agreement (within 10%) in the various experiments.

The final reason free shear flows were used as a starting point for determining closure coefficients stems from the consideration that if the new model is incapable of predicting growth rates and shear distributions of all free shear layers, then it can not have any advantage over existing k-ϵ and k-ω models and, as such, merits no further development.

It seems logical that if a model can not predict simple free shear flows, then it would have difficulty in accurately predicting a turbulent flowfield over a complex vehicle. Therefore, the obvious place to begin an optimization of a generalized turbulence model was through the examination of a variety of free shear flows.

5.3 Boundary Layer Solutions

The next step in determining the model constants is to test and refine the model for a wall bounded flow. A boundary layer solution[15] was chosen for this task due to its computational simplicity. This is a result of the fact that boundary layer code run times are much smaller than for a Navier-Stokes solver. A brief description of the

methodology used in the boundary layer code is provided in Appendix H. Because boundary layer codes cannot handle separated flows, further development required the use of a Navier-Stokes solver.

5.4 Navier-Stokes Solutions

Up to this point we have considered a variety of methods which make a number of simplifying assumptions about the flowfield in order to reduce the complexity of the Navier-Stokes equations. However, there are many flowfield features which cannot be examined using the simplified methods discussed up to this point. These include, but are not limited to, stagnation points, shockwaves, large adverse pressure gradients, and separated flows. In order to assess the models performance in and around these types of flow features, a Navier-Stokes solver must be employed. A description of the two Navier-Stokes solvers[10, 16] employed in the current research will be included in the results section.

Initially, the Navier-Stokes solver was used to examine a variety of two-dimensional airfoils, the purpose of which was twofold. First was the development and evaluation of a pressure gradient term, and second was an assessment of the k-ζ's numerical stability. Once the development and validation was completed for the two-dimensional cases, the performance of the model for a three-dimensional supersonic Cylinder-Flare was examined.

6 k-ζ Modifications

The previous section described how the closure coefficients were evaluated, however, it is important to recognize that this was an iterative procedure. As the research progressed from the simpler to the more complex flows it was often discovered that a particular choice of modeling was inappropriate. Terms were re-modeled and the procedure was repeated until we reached the current state of the model. The modifications of the original model warrant special attention, and therefore, a discussion of each has been included below. The final form of the modeled k-ζ equation set, including all of the modifications discussed below are shown in Appendix L

6.1 β_5 Term

The β_5 term is one of the dominant dissipation terms in the enstrophy equation. Originally it was modeled as

$$\frac{\beta_5 \zeta^{\frac{3}{2}}}{R_k} \tag{6.1}$$

for the free shear layers. However, when examining wall bounded flows R_k is zero at the wall. It should be noted that for the current work the finite volume approach was used so this term is never actually evaluated at the wall. However, as the wall is approached R_k can become extremely small, thus causing numerical problems. This numerical difficulty is a result of allowing the turbulence time scale to be less than Kologomorov's time scale. Calculation of R_k using Kolomogorov's microscales[1] yields

a value of about unity, $\mathcal{O}(1)$. To enforce the requirement that the turbulent time scale can not be less than Kolmogorov's time scale, the dissipation term can be written as

$$\frac{\beta_5 \zeta^{\frac{3}{2}}}{R_k + \delta} \tag{6.2}$$

where $\delta = \mathcal{O}(1)$. Determination of δ will be explained in the next section on wall damping functions.

6.2 Wall Damping Functions

For high turbulent Reynold's numbers the eddy viscosity is defined as

$$\mu_t = \frac{\rho C_\mu k^2}{\nu \zeta} \tag{6.3}$$

For wall bounded flows the eddy viscosity and the turbulent Reynolds number are both zero at the wall. Because of this the above expression is traditionally multiplied by a wall damping function, f_μ.

$$\mu_t = \frac{\rho C_\mu k^2 f_\mu}{\nu \zeta} \tag{6.4}$$

There is no unanimity on the form of f_μ in the near wall region[17]. Initially[18] the k-ζ model was implemented using the following form for the wall damping function

$$f_\mu = min\left(f_\mu^*, 1.0\right) \tag{6.5}$$

$$f_\mu^* = \left(1 + \frac{C_{\mu 1}}{\sqrt{R_t^{1.5}}}\right)\left[1 - exp\left(\frac{-\sqrt{k}y}{\nu C_{\mu 2}}\right)\right] \tag{6.6}$$

An examination of the above expression reveals that this term is unity except for a very small region near the surface ($y^+ < 100$). The problem with employing a wall

damping function is the introduction of geometrical dependence into the model. The 'y' is the normal distance to the nearest wall, however, for complex three-dimensional flows its calculation is somewhat cumbersome. Therefore, in order to make the k-ζ model more amenable to three-dimensional solutions, the wall damping function has been eliminated in recent implementations[19].

During the modeling process (see Appendix E) the following

$$-\overline{2u_j'\omega_i'}\frac{\partial \Omega_i}{\partial x_j} \tag{6.7}$$

was re-written using a symmetric and a skew-symmetric term with the symmetric portion being modeled as

$$\frac{\nu_t}{2\sigma_r}\left[\frac{\partial \Omega_i}{\partial x_j}+\frac{\partial \Omega_j}{\partial x_i}\right]\left(\frac{\partial \Omega}{\partial x_j}\right) \tag{6.8}$$

The above term does not contribute to the similarity solution of free shear flows, and as a result, σ_r was assigned a value based on log-layer considerations which was inappropriate. Later, it was shown that the value of σ_r was somewhat dependent on the model constants that appeared in the damping function, f_μ. A previous investigation[18] showed that it was possible to eliminate the σ_r term by simply modifying the f_μ constants. This result raised an interesting question: if one can develop an f_μ that eliminates Eq. (6.8), then can one eliminate f_μ and keep the above term. It turned out that this was indeed possible by choosing the model constants σ_r and δ as

$$\delta = 0.1 \ , \ \sigma_r = 0.07 \tag{6.9}$$

From our previous analysis it was shown that $\delta = \mathcal{O}(1)$. A major consideration that entered into the selection of δ is transition from laminar to turbulent flow. In the absence of a transition model, small values of δ are required to allow transition to take place.

6.3 Symmetric Portion of $-\overline{2u_j'\omega_i'}\frac{\partial \Omega_i}{\partial x_j}$

The symmetric portion of this term is written as (See Appendix E)

$$\frac{\epsilon_{mij}}{2}\left[\frac{\partial\left(\overline{u_m'u_l'}\right)}{\partial x_l} - \frac{\partial k}{\partial x_m}\right] \tag{6.10}$$

An evaluation of Eq. 6.10 has shown its impact to be negligible for all of the cases considered. Furthermore, an examination of this term in a three-dimensional coordinate system reveals that you are required to calculate the derivative of each of the Reynolds stresses in each direction. This can be quite costly computationally, and therefore, in order to simplify the k-ζ model this term has been neglected. No noticeable change in results was noticed from the omission of this term.

6.4 Pressure Gradient

In eddy viscosity models such as the k-ϵ and k-ω, the production of turbulent kinetic energy is related to the mean strain rate. This is large in regions of significant curvature, and therefore, eddy viscosity models typically generate excessive production of k in these regions. This in turn increases the value of μ_t which delays or inhibits separation.

The successful models that were developed to address separated flows were aimed at mimicking conditions that exist in separated regions by reducing eddy viscosity or turbulent energy production. Thus, the Johnson and King[8] model was designed to reduce the eddy viscosity in the wake region of boundary layer flows characterized by adverse pressure gradients. Reduction of the eddy viscosity is also the motivation behind the shear stress transport model of Mentor[20, 21]. For the current model a reduction of eddy viscosity in adverse pressure gradient regions can be imposed in one of two ways. First, one can model the term

$$\frac{\partial}{\partial x_j}\left[\overline{p'u_j}\right] \tag{6.11}$$

that appears in the k equation (Eq. 3.1) in terms of a mean pressure gradient. This was attempted by Rao and Hassan[3] but proved to be unsatisfactory. Alternatively, one can develop a term in the enstrophy equation based on the mean pressure gradient. Although the pressure does not appear explicitly in the exact (incompressible) ζ equation, the effect of the pressure is noted by examining the term $\frac{\partial \Omega_i}{\partial x_j}$. This term can be expressed as a second derivative of mean velocity which is related to the mean pressure gradient through the momentum equation. Thus, the ζ equation can have an explicit dependence on the mean pressure gradient. Based on this, the following term was originally added to the k-ζ model

$$\sigma_p \left(\frac{\partial P}{\partial x_i}\right)^2 \left(\frac{\Omega}{P}\right) R_t^{\frac{3}{2}} \tag{6.12}$$

This term produces ζ, and therefore, reduces the eddy viscosity in an adverse pressure gradient flow as desired. However, the problem with a term of the above

form is that its always positive, and therefore, always dissipative of μ_t, regardless of whether favorable or adverse pressure gradients are considered. The result was that the above term was excessively dissipative around the leading edge of airfoils. In order to correct this problem we were looking to develop a term which took into account the sign of the pressure gradient (i.e. favorable or adverse). This was done by re-modeling the above term as

$$\frac{\partial\left(\rho U_i P\right)}{\partial x_i}\frac{k\Omega}{\nu P \sigma_P}\frac{1}{(1+\delta\rho)} \tag{6.13}$$

where

$$\delta\rho = \frac{\sigma_\rho}{\rho}\sqrt{\frac{kR_t}{\zeta}\left(\frac{\partial\rho}{\partial x_i}\right)^2} \tag{6.14}$$

This term (Eq. 6.13) represents the derivative of pressure along a streamline, and therefore, is negative (produces μ_t), and positive (dissipates μ_t) for favorable and adverse pressure gradients, respectively. The $(1+\delta\rho)$ is a compressibility correction and has been added to prevent the pressure gradient term from becoming excessive around strong shocks. Note that, in the absence of mean pressure gradients, the modeling reverts to that appropriate for constant pressure solutions. Thus, no adjustments in the previously calibrated model constants are necessary. It should also be noted that there are a number of possible methods for modeling the pressure gradient term. Therefore, Eq. 6.13 should be considered a tentative term until the efficacy of other forms can be examined.

6.5 Compressibility and Transition Modifications

Modifications to the k-ζ model which take into account compressibility effects are currently being developed by Alexopoulos[11, 22]. He has developed a number of compressibility terms (see C_1, C_{ζ_1} terms in Appendix L), all of which have been included in the current results. These additional terms have had very little effect, as expected, since the cases currently being considered were all either subsonic or transonic, or assumed adiabatic walls (Cylinder-Flare). Also, a transition model has been developed by Warren[23, 24, 25] based on the k-ζ model. This transition model was not used for the current results. For an in depth discussion of both compressibility and transition and how they relate to the k-ζ model the reader is referred to Refs.[11] and [25].

6.6 Numerical Stability Modifications

The current model, like all turbulence closure models, requires some modification to improve its numerical stability. The first stability improvement is made by setting a minimum ζ in the Navier-Stokes codes. The reason for this minimum can be seen by examining the typical behavior of k and ζ. The enstrophy is finite at the wall, attains a maximum in the boundary layer, and decays to some small value outside of the boundary layer. Similarly, k is zero at the wall, reaches a maximum in the boundary layer, and then decays to some small value outside the boundary layer. An examination of μ_t

$$\mu_t = \frac{C_\mu \rho k^2}{\nu \zeta} \tag{6.15}$$

shows that since both k and ζ are rapidly approaching very small values at the edge of the boundary layer, numerical instabilities can arise. In order to improve the stability and prevent oscillations in μ_t a floor is typically set for the dissipation, ζ. For the current work a minimum ζ is set as

$$\zeta = max\left(\zeta, \frac{\zeta_\infty}{10^6}\right) \tag{6.16}$$

Minimums as large as $\frac{\zeta_\infty}{10^2}$ were evaluated and shown to have no effect on the final converged solution.

Two additional modifications were made in order to improve the numerical stability of the model. Namely, both the pressure gradient and β_8 terms are maxed with zero (See Appendix L. This forces both terms to be shut off in regions where they dissipate ζ (produce μ_t). For the pressure gradient term this was done because this term produced excessive μ_t around the leading edge of the airfoils. It should be noted that this is only a transient phenomena which occurs during the convergence of the solution. Once the solution converges the max can be removed without adversely effecting the final solution. A similar procedure applies for the β_8 term.

6.7 Summary of Modifications

It should be noted that as modifications to the model are made one underlying assumption must hold. Namely, that the modification does not affect the previously considered cases. In other words, the addition of the δ to the β_5 term to improve the results for the wall bounded flows can not affect the free shear results. Similarly, the

addition/removal of a wall damping function can not affect either the boundary layer solution of the flat plate or the free shear results. This assumption holds for each of the additional modifications made in this section. Also, as additional modification are made which take into account more complex flowfield features (e.g. compressibility, combustion, etc), this assumption must remain valid in order to develop a generalized turbulence closure model capable of solving complex three-dimensional flows.

The final form of the k-ζ model with all of the aforementioned modifications, including the compressibility terms developed by Alexopoulos[11, 22], can be seen in Appendix L.

7 Results

7.1 Free Shear Layer

For the free shear layers we have compared the current model to both experimental data and the results from the k-ϵ turbulence model. The results from the k-ω model were not included due to the fact that the free stream boundary condition for ω must be adjusted for each of the different types of shear flows.

We begin with the results for the self-similar incompressible planar wake. A schematic of this flowfield is shown in Figure (10.1). Figure (10.2) shows the defect velocity, W (non-dimensionalized by centerline defect velocity W_o) versus y (non-dimensionalized by wake width). For this case we have compared with a variety of profiles at various $\frac{x}{\theta}$ locations from the experiments of Patel[26] as well as with the k-ϵ turbulence model. Note that the experimental data shows that a self-similar velocity profile is obtained at an $\frac{x}{\theta}$ of approximately 79. The k-ζ model shows excellent agreement with experiment and also shows a noted improvement over the k-ϵ model. Figure (10.3) shows a similar comparison for the shearing stress, τ along with the experimental data of Pot[6]. Note, that two sets of data were included at an $\frac{x}{\theta}$ of 960 in order to show the level of asymmetry in the experimental data. Also included was a comparison with the asymptotic solution obtained by assuming a constant eddy viscosity, μ_t. Once again the k-ζ model shows excellent agreement with experiment as well as with the asymptotic solution. Figure (10.4) shows the turbulent kinetic

energy profile, and while there was no available experimental data for this case, it has been included for completeness. The effect of the improvements in the velocity and stress profiles can also be seen in Table 9.1 which shows a percent error in the growth rate of 14% and 30% for the k-ζ and k-ϵ models, respectively.

The next set of Figures (10.6-10.8) show the comparisons for velocity, shear stress, and turbulent kinetic energy for the two-dimensional planar jet (see schematic in Figure 10.5) compared with experiment[27, 28, 29] and the k-ϵ model. The results between the k-ζ and k-ϵ models are essentially identical except for the formers slight over prediction of shear stress. Both models agree extremely well with experimental profiles and, therefore, both do a very good job of predicting the growth rate (Table 9.1). Bradbury[28] indicates that his measured spreading rate is not exactly proportional to x. The departure from true self-preservation, however, is so small than no adjustment is necessary in Fig. (10.6).

Figures (10.9-10.11) show the comparison of mean velocity, shear stress, and turbulent kinetic energy for the round (axisymmetric) jet along with the results of the k-ϵ model and experiment[30, 31]. The k-ζ model does an excellent job of predicting the velocity and shear stress profiles. Note, however, that the centerline TKE is under predicted. This is explained by noting that during the optimization process we were primarily concerned with accurately reproducing growth rates, velocity profiles, and peak shearing stresses. The primary reason for considering the TKE prediction to be of secondary importance can be seen by noting that there was a large degree

of variation in the measured TKE for the various experiments, and therefore, these measurements were deemed to be less reliable. Therefore, we primarily concentrated on matching velocity and shear profiles as well as growth rates. Note that the k-ζ models prediction of growth rate lies within the experimental range while the k-ϵ shows a 26% error if compared with the upper bound (Table 9.1).

Figures (10.12-10.14) shows a similar comparison for the radial jet. Although no experimental data was available, other than growth rates, the plots were included for completeness and to show the similarity between the k-ζ and k-ϵ models. Available data[32, 33, 34] suggests that profiles for the radial jet approach those for the plane jet. Since both models were in good agreement with experiment for the plane jet, the indicated agreement in Figures (10.12-10.14) is expected. Note that both models did an excellent job of predicting the growth rate for this case.

The final set of figures (10.16-10.18) show the comparisons for the mixing layer (see schematic in figure 10.15). In these figures η is defined as

$$\eta = -\frac{\left(\frac{y}{x}\right) - \left(\frac{y}{x}\right)_{0.5}}{\left(\frac{y}{x}\right)_{0.9} - \left(\frac{y}{x}\right)_{0.1}} \tag{7.1}$$

where $\left(\frac{y}{x}\right)_{0.1}$, etc., denotes the locations where the ratio of the mean velocity to the free stream velocity is 0.1, etc. For this case the mean velocity is accurately predicted, however, the shear stress and TKE both failed to reproduce the experimental data. The growth rates were within 5% for the k-ζ model compared to 15% for the $k-\epsilon$ model. It should be noted that the theory shows good agreement with the predicted shear stress in the streaming side of the measurements but not with the zero velocity

side. Patel[35] points out that measurements with a normal hot-wire probe became unreliable in the zero velocity side. However, no estimate of inaccuracies were given. Thus, a more accurate measurement in the zero velocity side is needed before a definitive statement can be made regarding predictions of the theory in this region.

A summary of the calculated spreading rates is shown in Table 9.1. The spreading rates are defined in a manner consistent with that given in Ref. [2]. Moreover, the ϵ comparison values were obtained from Table 4.2, Ref. [2]. In general, computed growth rates represent a noted improvement over those obtained from the $k-\epsilon$ or $k-\omega$ models.

After optimizing the free shear flows and obtaining a tentative set of closure coefficients the next step was to examine the turbulence model for a wall bounded flow. This was done by examining the boundary layer solution of a flat plate and its wake.

7.2 Flat Plate

The next step is to calibrate the k-ζ turbulence model for a wall bounded flow. As was previously discussed, the original form of the model contained a wall damping function with two unknown closure coefficients (C_{μ_1}, C_{μ_2}). In order to evaluate these constants an incompressible flow $(M = 0.01)$ over a flat plate was considered.

Figures (10.19-10.21) show plots of k^+, ζ^+, and τ_{12}^+ vs. y^+ for the near wall region. The current model is compared with the experimental measurements of Schubauer[4] and Laufer[5] as well as the "average" of the available data[17]. As is seen from the figures,

the results compare well with the results summarized in Ref.[17]. From Figure (10.19), it is seen that the peak value of k^+ has been slightly under predicted, however, the current results occur within the range typical of two-equation models ($k^+ \approx 2.8-4.0$). Figure (10.20) shows that both ζ^+ and ϵ^+ have a "peak" near the wall. It should be mentioned that the ϵ^+ is not from a solution of the k-ϵ model, rather it is determined by comparing the k equation for the ζ model to that of the standard ϵ model and noting that

$$\epsilon = \nu\zeta + \frac{2\nu}{3}\frac{\partial^2 k}{\partial y \partial y} \tag{7.2}$$

Therefore, the ϵ^+ shown, is that calculated by using the above expression in conjunction with the solution of the k-ζ model. The current model accurately reproduces the experimental data of Laufer, however, there has been some recent controversy over the validity of this data in the very near wall region. The DNS data for this case[2] shows no such "peak" in the near wall region.

The constant, 'B' from the log-law relation

$$u^+ = \frac{1}{\kappa} ln\left(y^+\right) + B$$

is typically taken to be 5.0. A plot of $u^+ - \frac{1}{\kappa} lny^+$ shows that 'B' is not exactly constant, but rather, varies slightly from approximately 4.4 to 5.2 over a y^+ range from 50 to 1000.

The sublayer behavior of the TKE is shown in figure 10.23. Since n ($k = k_o y^n$) could not be evaluated at $y = 0$, a polynomial curve fit was used to obtain a value of

2.08 at $y = 0$. This is in very close agreement with the theoretical value of 2.0 (see Appendix I).

Figure (10.24) shows the skin friction coefficient (based on edge values) vs. the vanDriest[36] correlation. Excellent agreement with the current model is shown.

Figure (10.25) shows the wall damping function. Note that this parameter is non-unity only in a small region very close to the wall ($y^+ < 80$).

Once acceptable results were obtained for the flat plate, the boundary layer solution was used to examine the near wake properties and as a means of validating the self-similar wake results. This was done by marching off the end of a flat plate and continuing the solution procedure downstream until similarity profiles were attained.

Figs. (10.26-10.30) demonstrate the k-ζ's prediction of a variety of near wake parameters including growth rate, centerline defect velocity, and peak shearing stress. The results of the current model are compared with the experimental data of Pot [6] and Weygandt and Mehta [7]. Excellent agreement is indicated. Also shown are the stress and velocity profiles in the far downstream region. These figures show that a self-preserving state was attained and that the marching procedure has reproduced the similarity results within a few percent.

It should be mentioned that all of the figures considered up to this point used the wall damping function, f_μ. It should also be noted, however, that elimination of the wall damping function made no noticeable changes in the flat plate results. This was the criterion used for the elimination of the damping function. In other words,

the model had to give the same results with or without the f_μ. All of the results for the flat plate without the damping function were within a couple of percent, and therefore, they have not been reproduced here. Also, note that the elimination of the f_μ has no effect on the free shear flows since f_μ was unity for all of those cases. All of the remaining results were obtained after the elimination of the wall damping function.

7.3 Homogeneous Shear Flows

This section examines the predicted decay rates of turbulence in a homogeneous shear flow. It should be noted that even though the current model constants were not chosen by considering the decay of homogeneous turbulence, close agreement with the $k-\epsilon$ model, whose constants were chosen to give the correct decay rate for homogeneous turbulence, is shown in figures 10.32-10.33. This test case was examined per the suggestion of Reference [37] in order to determine if the current model would predict an acceptable value of the homogeneous shear parameter $\frac{SK}{\epsilon}$ and also to ensure that the k-ζ model would predict equilibrium (or constant steady state) values for the shear parameter and for the Reynolds stress anisotropy, b_{12}. Measurements and DNS[38] suggest that the shear parameter reaches an equilibrium value between 5 and 6. Figures (10.31-10.32) show that the current model does in fact reach a constant steady state value and also does predict an acceptible homogeneous shear parameter.

Figures (10.33-10.34) show the comparison of the k-ζ and the k-ϵ models in the prediction of k^+ and ϵ^+. These figures represent the time decay of the turbulent

quantities and show very similar results between the two models. One final note should be made regarding homogeneous shear flows. Namely, that for this case the k-ζ model gives $b_{11} = b_{22} = b_{33} = 0$, which has been shown to be incorrect [39]. This is not a limitation of the current two-equation model, rather, it is a limitation in the current Bousinesq approximation. In order to be able to accurately predict the Reynolds stress anisotropies, the Bousinesq approximation must be modified to include higher order terms.

7.4 Airfoils

For the airfoil cases a comparison is made with the k-ω model of Wilcox[2], the Johnson-King[8] model, as well as with experimental data where available. The k-ω model was chosen because it is widely known to have good agreement with experiment for attached wall bounded flows. The J-K model was included because it is widely known to accurately predict two-dimensional separated airfoils. The J-K results were obtained from the calculations of Rumsey and Anderson[40]. Mentor[20] made an issue of the sensitivity of the k-ω model to free stream conditions. In all of the calculations presented here, k_∞ and $\left(\frac{\mu_t}{\mu}\right)_\infty$ were selected and corresponding values of ζ_∞ and ω_∞ were computed. We believe this is the correct way to compare the two models.

The evaluation of the k-ζ model for two-dimensional airfoils begins by first examining the effect of the two boundary conditions. Recall that bc_1 is a simple of extrapolation of ζ to the wall, whereas, bc_2 imposes a $k = k_o y^2$ behavior to determine a wall value of ζ. The first case considered is a symmetric NACA 0012 airfoil at a

relatively low Mach number. This provides a simple flow free of both shockwaves and separated regions. Note from figures 10.35-10.36 that both boundary conditions give nearly identical results except for the skin friction, C_{fe} in a small region around the trailing edge. This is explained by noting that the first boundary condition (simple ζ extrapolation) gives a near wall k variation very close to the theoretical value (see Appendix I) of $n = 2$. Thus, imposing a y^2 variation of the near wall k has little to no effect, as expected. However, this is not the case for the more complex flowfields. Figures (10.37-10.38) show the same comparisons for the NACA 0012 run with a transonic Mach number. For this case small variations in C_p can be seen around the shock, however, large variations in C_{fe} are noted. When using simple extrapolation, bc_1 for more complex flows, large oscillations in the skin friction coefficient can occur, therefore, for the more complex flows bc_1 has proven to be inadequate around shocks (a similar behavior was noted near separated regions). It should also be noted that bc_1 proved to be much less numerically stable around shocks, separated regions, and stagnation points. Therefore, for the remainder of the results section, only bc_2 will be considered.

The next step in evaluating the k-ζ model was to ensure that grid independent solutions were being obtained. A grid study was performed for an RAE 2822 transonic airfoil with a small separated region. Figures (10.39-10.40) show the pressure distribution and skin friction for all grids considered. Both the pressure and skin friction distributions have proven to be grid independent. The results are nearly identical,

except for a slight variation in skin friction on the $143x51$ grid. From this grid analysis it has been determined that the k-ζ model requires a minimum of approximately 5 points within the sublayer ($y^+ < 10$). The $321x91$ grid had an initial y_1^+ of approximately 0.2, the $231x51$ used $y_1^+ \approx 1.8$, and the $143x51$ used $y_1^+ \approx 3.0$. Note, however, that the deviation in skin friction results were caused not by the initial y^+ spacing, but rather, is was primarily caused by the amount of resolution of the sublayer. In other words, as long as you have at least 5 points in the sublayer, you may begin with initial y_1^+ values of 2 or 3 and still obtain accurate solutions. This is important, and is being discussed in detail, because of the obvious influence on rate of convergence. Increasing the distance of the first y^+ point off of the surface can drastically increase the rate of convergence of the solution. Note, that for all of the remaining airfoil cases, an initial y^+ between 1 and 2 and approximately 8-10 points in the sublayer were employed.

Now that the boundary conditions and basic grid requirements have been determined the next step is to examine the results for a variety of two-dimensional airfoils beginning with a NACA 4412. The airfoil geometry is shown in figure 10.41. This case is a low subsonic ($M = 0.2$) stalled airfoil ($\alpha = 13.87°$) and was used to examine the k-ζ's performance on an airfoil with a large separated region but in the absence of shockwaves. Comparisons are made with the available experimental data[41] as well as with the standard k-ω model. Figure (10.42) shows that the pressure distribution is well predicted by both the current and k-ω models. Although no skin friction data

was available, the experiments of Coles and Wadcock[41] showed separation beginning between $\frac{x}{c}$ of $.75-.80$. Figure (10.43) shows that the k-ζ model predicts separation at $\frac{x}{c} = 0.81$, in excellent agreement with experiment, while the k-ω model predicts delayed separation and a somewhat smaller separated region. Figure (10.44) compares the mean velocity profiles for a variety of $\frac{x}{c}$ stations throughout the separated region. Again, prediction of the current theory is more consistent with the experiment.

The next set of comparisons (figures 10.45-10.47) involve a NACA 0012 (geometry shown in figure 10.45) at an angle of attack, α of 8.34° and a free stream Mach number, $M_\infty = 0.55$ compared with the experimental data of Harris[42]. All models predict the pressure distribution well . An absence of skin friction data prevents a meaningful discussion of which model is more accurate, however, it should be noted that both the current and k-ω models predict only one separated region while the J-K predicts two. Figures (10.48-10.49) show the same airfoil at an angle of attack of 2.26° and a transonic Mach number of 0.799. Both the current and J-K models give an accurate prediction of the pressure distribution and show similar results for the skin friction. The k-ω model predicts delayed separation which is not consistent with experiment.

Figures (10.50-10.54) show the results for the RAE 2822 (geometry shown in figure 10.50). For cases 9 and 10, we have compared with the experimental data of Cook et. al.[43] ; no definitive angle of attack or Mach number corrections to account for wall interference were given. As a result, the flow conditions assumed for these cases were those used by Rumsey and Vatsa[44]. For case 9 ($M_\infty = 0.73, \alpha = 2.80°, R_e =$

$6.5x10^6$), the flow is attached and the k-ω model does a better job of predicting the shock position and the pressure distribution. Figure (10.52) shows that all models do a fair job of predicting the skin friction for this case. The next case (10) involves shock induced separation. Both the k-ζ and J-K do a good job of predicting both the shock position and the skin friction. Note that the k-ω model predicts both a delayed shock and a milder separated region.

7.5 Cylinder-Flare

The Cylinder-Flare case was considered in order to examine the k-ζ models ability to accurately predict a complex three-dimensional supersonic flowfield. The geometry for this case is shown in Fig.(10.55) along with the test conditions. A schematic of the flare, along with the appropriate dimensions, are shown in Fig.(10.56). Also, in order for the reader to get a general idea of the flowfield being considered, a sketch of the postulated flowfield was provided in Fig.(10.57). This figure was taken from Ref.[9]. From this figure it it seen that at the $\theta = 0°$ plane, there is a small separated region between the intersection of the cylinder and the offset flare. This separation bubble turns the flow prior to reaching the juncture, and therefore, causes the oblique shockwave to move upstream of the flare. Also, as you consider planes with increasing θ, the extent of the separation region grows, and therefore, the amount of upstream influence is increased. This is due to the fact that as you progress from $\theta = 0°$ to $\theta = 90°$ the flow becomes increasingly three-dimensional in nature due to the crossflow caused by the offset flare.

A few notes about the solution procedure are warranted. First, in order to minimize the computational time required for this case the problem was split into two sections: an axisymmetric cylinder and a three-dimensional flare. A semi-infinite cylinder was computed assuming axisymmetric flow. At a given distance along the cylinder the $\frac{P}{P_t}$, C_f, and δ parameters were found to match the experimental results. The profiles for velocity, temperature, pressure, k, and ζ from this point on the cylinder were then used as initial profiles for the three-dimensional flare. Note, that for the full three-dimensional case, a small cylinder (10 cm length) was run upstream of the flare so that the initial profiles would not be affected by the upstream influence generated by the flare. In other words, instead of running the full cylinder (90 cm) in the three-dimensional code, only a smaller portion (10 cm) was considered. The remaining 80cm was run using an axisymmetric assumption to reduce computational time. The above procedure provided for a significant reduction in the number of grid points required.

The solution procedure used was a four stage Runge-Kutta, explicit, central difference (standard Jameson Damping) code developed by Baurle[16]. The grid contained $87 \times 99 \times 99$ points in the x,y,z directions, respectively and was run with an initial y_1^+ of 0.3 and approximately twelve points in the sublayer ($y^+ < 10$). Comparisons of the current model are made with the k-ϵ model as well as the data of Wideman et al [9]. The k-ϵ results were obtained from Ref.[45].

Figures (10.58-10.60) show the pressure ratio for the $\theta = 0°, 90°, 180°$ planes,

respectively. The pressure ratio is equal to the surface pressure over the freestream stagnation pressure. For the $\theta = 0$ plane both models accurately predict the initial pressure rise upstream of the juncture. This indicates that, for this plane, both models are accurately predicting the extent of the separation bubble. Downstream of the juncture the k-ζ models shows a pressure rise which is in closer agreement with the experimental data. Both models predict the asymptotic pressure region accurately. For the $\theta = 90°$ plane both models again do a good job of predicting the initial pressure rise. Aft of the juncture both models overpredict the pressure ratio, but they both return to acceptable levels in the downstream region. The $\theta = 180°$ plane once again shows that the k-ζ model does a slightly better job of predicting the pressure ratio upstream of the juncture. Aft of the juncture the k-ζ models shows a slightly larger peak, however, it returns to an acceptable level in the downstream region. From the three previous figures it should be noted that the upstream influence is a minimum at the $\theta = 0°$ plane where very little crossflow velocity exists. It continually increases until the $\theta = 90°$ plane is reached at which point the upstream influence is a maximum (noted by the distance between the juncture and the initial pressure rise). This value then remains relatively constant until the bottom symmetry plane is reached at $\theta = 180°$.

Figures (10.61-10.63) show the skin friction coefficient (non-dimensionalization uses free stream quantities) for the $\theta = 0°, 90°, 180°$ planes, respectively. For the $\theta = 0°$ plane the k-ζ model does a better job then the k-ϵ in predicting C_f downstream

of the juncture. The k-ϵ model overpredicts the asymptotic value for skin friction.

The C_f for the $\theta = 90°$ plane shows that both models mimic each other very closely, however, they also significantly overpredict the skin friction data in the downstream region. The validity of the experimental data for this plane has been called into question by one of the co-authors of the original paper[46], and therefore, a meaningful discussion of the results is not possible. It should be noted that even though the skin friction data for this plane is being questioned, the pressure data remains valid[46].

The final figures shows the skin friction comparison for the $\theta = 180°$ plane. The k-ζ model slightly overpredicts the separated region, however, the model does an excellent job downstream of the juncture.

In summary, the k-ζ model without damping functions has performed as well as the k-ϵ model which employs damping functions. Overall, good agreement is indicated with the current model.

8 Concluding Remarks

The current k-ζ model has proven to be a noteworthy step towards the development of a generalized three-dimensional turbulence closure model which can be used in the calculation of practical engineering problems. This model overcomes a number of limitations of existing two-equation models. First, the current model can accurately predict the growth rates, velocity, and shear stress profiles for a variety of free shear flows using only one set of closure coefficients and boundary conditions. Furthermore, the k-ζ model allows for the solutions of a wall bounded flow and its wake without a modification of the model constants or boundary conditions. Moreover, the current model compares favorably to both the Johnson-King and k-ω models for the prediction of two-dimensional airfoils. For these airfoils, the current model does a good job predicting skin friction and shock location, as well as the extent and location of the separated regions. Also, the current form of the k-ζ model is free of damping functions and geometrical factors. With this development, one of the major obstacles in applying the model to three-dimensional flows has been removed.

Because of the nature of the development process the current k-ζ model still has one primary limitation. This is the models tendency to overpredict the eddy viscosity around a strong shock wave. The reason for this limitation is due to the fact that the pressure gradient term was calibrated for low speed flows (subsonic and transonic airfoils) with relatively weak shocks. When the model was used for flows

with strong shocks (Mach > 2.5) excessive values of μ_t were generated, and therefore, an overprediction of skin friction and heat transfer occur in the vicinity surrounding the shock. It is to be noted that, near the shock, over 50% of the turbulent energy production is a result of the work of the normal stresses. Since such stresses are not well predicted by two-equation turbulence models it is possible that the observed behavior of μ_t near a shock is a result of inaccuracies in the normal stresses. This conjecture can not be ascertained without a solution based on a stress model.

References

[1] Tennekes, H., and Lumley, J.L. *"A First Course in Turbulence"*. The MIT Press., Cambridge, MA, 1989.

[2] Wilcox, D. C. *"Turbulence Modeling for CFD"*. DCW Industries, Inc., La Canada, CA, 1993.

[3] Rao, M.S., and Hassan, H.A. "Modeling of Turbulence in the Presence of Adverse Pressure Gradients". AIAA Paper 96-2429, AIAA 14th Applied Aerodynamic Conference, June 1996.

[4] Schubauer, G.B. "Turbulent Processes as Observed in Boundary Layers and Pipes". *Journal of the Applied Physics*, Vol. 25:188–196, 1954.

[5] Laufer, J. "The Structure of Turbulence in Fully Developed Pipe Flow". NACA Rept 1174, 1954.

[6] Pot, P.J. "Measurement in a Two-Dimensional Wake and in a Two-Dimensional Wake Merging into a Boundary Layer". Data Report NLR TR-79063 U, the Netherlands, 1979.

[7] Weygandt, J.H., and Mehta, R.D. "Asymptotic Behavior of a Flat Plate Wake". NASA CR-185917, 1989.

[8] Johnson, D.A., and King, L.S. "A Mathematically Simple Closure Model for Attached and Separated Turbulent Boundary Layers". *AIAA Journal*, Vol. 23, No. 11, November, 1985, pp. 1684-1692.

[9] Wideman, J.K., Brown, J.L., Miles, J.B., and Oktayan, O. "Surface Documentation of a 3-D Supersonic, Shock-Wave/Boundary-Layer Interaction". NASA Technical Memorandum 108824, NASA Ames Research Center, June 1994.

[10] Gaffney, R.L., Salas, M.D., and Hassan, H.A. "An Abbreviated Reynolds Stress Turbulence Model for Airfoil Flows". AIAA Paper 90-1468, June 1990.

[11] Alexopoulos, G. A. "Prediction of Compressible Flows with the k-ζ Turbulence Model". PhD Dissertation, North Carolina State University, Raleigh, North Carolina, August 1997.

[12] Morse, A.P. "Axisymmetric Free Shear Flows With and Without Swirl". PhD Dissertation, Imperial College of Science and Technology, University of London, May 1980.

[13] Bernard, P.S., and Berger, B.S. "A Method for Computing Three-Dimensional Turbulent Flows". *SIAM Journal of Applied Mathematics*, Vol. 43, No. 3, June 1982, pp. 453-470.

[14] Raul, R., and Bernard, P.S. "A Numerical Investigation of the Turbulent Flow Field Generated by a Stationary Cube". *Journal of Fluids Engineering*, Vol. 113, June 1991, pp. 216-222.

[15] Harris, J.E., and Blanchard, D.K. "Computer Program for Solving Laminar, Transitional, or Turbulent Compressible Boundary-Layer Equations for Two-Dimensional and Axisymmetric Flow". NASA TM 83207, NASA Langley, Feb 1982.

[16] Baurle, R. "Modeling of Turbulent Reacting Flows with Probability Density Functions for Scramjet Applications". PhD Dissertation, North Carolina State University, Raleigh, North Carolina, December 1995.

[17] Patel, V.C., Rodi, W., and Scheuerer, G. "Turbulence Models for Near-Wall and Low Reynolds Number Flows: A Review". *AIAA Journal*, Vol. 23, No. 9:1308–1319, July 1982.

[18] Robinson, D.F., and Hassan, H.A. "A Two-Equation Turbulence Closure Model for Wall Bounded and Free Shear Layers". AIAA Paper 96-2057, June 1996.

[19] Robinson, D.F., and Hassan, H.A. "Modeling of Separated Turbulent Flows". AIAA Paper 97-0207, January 1997.

[20] Mentor, F.R. "Two-Equation Eddy-Viscosity Turbulence Models for Engineering Applications". *AIAA Journal*, Vol. 32, No. 8:1598–1605, 1994.

[21] Mentor, F.R. "Performance of Popular Turbulence Models for Attached and Separated Adverse Pressure Gradient Flows". *AIAA Journal*, Vol. 30, No. 8:2066–2072, 1992.

[22] Alexopoulos, G.A., and Hassan, H.A. "A k-ζ (Enstrophy) Compressible Turbulence Model for Mixing Layers and Wall Bounded Flows". AIAA Paper 96-2039, June 1996.

[23] Warren, E. S., Harris, J. E., and Hassan, H. A. A transition model for high-speed flow. *AIAA Journal*, 33(8):1391–1397, August 1995.

[24] Warren, E.S., and Hassan, H.A. . An alternative to the e^n method for determining onset of transition. AIAA Paper 97–0825, January 1997.

[25] Warren, E. S. "A Closure Model for Predicting Transition Onset". PhD Dissertation, North Carolina State University, Raleigh, North Carolina, July 1997.

[26] Ramaprian, B.R., Patel, V.C., and Sastry, M.S. "The Symmetric Turbulent Wake of a Flat Plate". *AIAA Journal*, Vol. 20, No. 9:1228–1235, Sept 1982.

[27] Gutmark, E. and Wygananski, I. "The Planar Turbulent Jet". *Journal of Fluid Mechanics*, Vol. 73:465–495, 1976.

[28] Bradbury, L.J. "The Structure of the Self-Preserving Jet". *Journal of Fluid Mechanics*, Vol. 23:31–64, 1965.

[29] Heskestad, G. "Hot-Wire Measurements in a Plane Turbulent Jet". *Journal of Fluid Mechanics*, Vol. 32:721–734, 1965.

[30] Wygnanski, I. and Fiedler, H.E. "The Two-Dimensional Mixing Region". *Journal of Fluids Mechanics*, Vol. 41:327–361, 1970.

[31] Rodi, W. "A New Method of Analyzing Hot-Wire Signals in Highly Turbulent Flows and its Evaluation in Round Jets". Disa Information No. 17, 1975.

[32] Heskestad, G. "Hot-Wire Measurements in a Radial Turbulent Jet". *Journal of Fluid Mechanics*, Vol. 33:417–424, June 1966.

[33] Tanaka, T. and Tanaka, E. "Experimental Study of a Radial Turbulent Jet". Bulletin of the JSME Vol. 19, No. 133, July 1976.

[34] Witze, P.O., and Dwyer, H.A. "The Turbulent Radial Jet". *Journal of Fluid Mechanics*, Vol. 75, Part 3, 1976, pp. 401-417.

[35] Patel, R.P. "An Experimental Study of a Plane Mixing-Layer". *AIAA Journal*, Vol. 29:67–71, 1973.

[36] vanDriest, E.R. "On Turbulent Flow Near a Wall". *Journal of the Aeronautical Sciences*, Vol. 23:1007–1010, 1956.

[37] Speziale, C. G. Private communication.

[38] Bernard, P.S., and Speziale, C.G. "Bounded Energy States in Homogeneous Turbulent Shear Flows - An Alternative View". ICASE Rept. No. 90-66, Oct 1990.

[39] Speziale, C. G., and Gatski, T. B. "An Alternative Assessment of Second-Order Closure Models in Turbulent Shear Flows". NASA Contractor Report 194881, ICASE, March 1994.

[40] Rumsey, C.L., and Anderson, W. Kyle. "Parametric Study of Grid Size, Time Step, and Turbulence Modeling on Navier-Stokes Computations Over Airfoils". *AGARD Cp-437*, Vol. 1, May 1988, pp. 5.1-5.19.

[41] Coles, D., and Wadcock, A.J. "Flying Hot Wire Study of Flow Past an NACA 4412 Airfoil at Maximum Lift". *AIAA Journal*, Vol. 17, No. 4, 1979, pp. 321-328.

[42] Harris, C. "Two-Dimensional Aerodynamic Characteristics of the NACA 0012 Airfoil in the Langley 8-Foot Transonic Pressure Tunnel". NASA TM 81927, NASA Langley, 1981.

[43] Cook, P., McDonald, M., and Firmin, M. "Airfoil RAE 2822 - Pressure Distribution and Boundary Layer Measurements". AGARD AR-138, May 1979.

[44] Rumsey, C.L., and Vatsa, V.N. "A Comparison of the Predictive Capabilities of Several Turbulence Models Using Upwind and Central-Difference Computer Codes". AIAA Paper 93-0192, January 1993.

[45] Gaitonde, D., Shang, J.S., and Edwards, J.R. "The Computed Structure of a 3-D Turbulent Interaction Caused by a Cylinder/Offset flare Juncture". AIAA Paper 95-0230, January 1995.

[46] Brown, J. Private Communication, NASA Ames Research Center.

[47] Reynolds, W.C. "Fundamentals of Turbulence for Turbulence Modeling and Simulation". AGARD R-755, 1987.

[48] Paullay, A.J., Melnik, R.E., Rubel, A., Rudman, S., and Siclari, M.J. "Similarity Solutions for Plane and Radial Jets Using $k - \epsilon$ Turbulence Model". *Journal of Fluids Engineering*, Vol. 107:79–85, March 1985.

[49] Schetz, J. A. *"Foundations of Boundary Layer Theory for Momentum, Heat, and Mass Transfer"*. Prentice-Hall, Nov. 1984.

Appendices

A Reynolds Stress Derivation

In order to determine governing equations for the Reynolds stresses, moments are taken of the Navier-Stokes equations. This is accomplished by multiplying through by the fluctuating property and taking the time average of the product.

The Navier-Stokes equations are re-written as

$$\mathcal{N}(u_i) = \rho\frac{\partial u_i}{\partial t} + \rho u_j\frac{\partial u_i}{\partial x_j} + \frac{\partial p}{\partial x_i} - \mu\frac{\partial}{\partial x_j}\left(\frac{\partial u_i}{\partial x_j} + \frac{\partial u_j}{\partial x_i}\right) \tag{A.1}$$

$$= \rho\frac{\partial u_i}{\partial t} + \rho u_j\frac{\partial u_i}{\partial x_j} + \frac{\partial p}{\partial x_i} - \mu\frac{\partial^2 u_i}{\partial x_j \partial x_j} \tag{A.2}$$

$$= 0 \tag{A.3}$$

where $\mathcal{N}$ is the Navier-Stokes operator. Take the following time average in order to derive an equation for the Reynolds stress tensor,

$$\overline{u_i'\mathcal{N}(u_j) + u_j'\mathcal{N}(u_i)} = 0 \tag{A.4}$$

Consider each term separately, starting with the unsteady term

$$\overline{u_i'\rho\frac{\partial u_j}{\partial t} + u_j'\rho\frac{\partial u_i}{\partial t}} = \overline{u_i'\rho\frac{\partial}{\partial t}\left(U_j + u_j'\right) + u_j'\rho\frac{\partial}{\partial t}\left(U_i + u_i'\right)} \tag{A.5}$$

$$= \overline{\rho u_i'\frac{\partial U_j}{\partial t} + \rho u_i'\frac{\partial u_j'}{\partial t} + \rho u_j'\frac{\partial U_i}{\partial t} + \rho u_j'\frac{\partial u_i'}{\partial t}} \tag{A.6}$$

$$= \overline{\rho u_i'\frac{\partial u_j'}{\partial t} + \rho u_j'\frac{\partial u_i'}{\partial t}} \tag{A.7}$$

$$= \rho\overline{\frac{\partial(u_i'u_j')}{\partial t}} \tag{A.8}$$

$$= -\frac{\partial}{\partial t}(\tau_{ij}) \tag{A.9}$$

Next consider the convective term

$$\overline{u_i'\rho u_m\frac{\partial u_j}{\partial x_m} + u_j'\rho u_m\frac{\partial u_i}{\partial x_m}} = \overline{\rho U_m\frac{\partial(u_i'u_j')}{\partial x_m} + \rho u_m'\frac{\partial(u_i'u_j')}{\partial x_m} + \rho u_i'u_m'\frac{\partial U_j}{\partial x_m}}$$

$$+\overline{\rho u_j'u_m'\frac{\partial U_i}{\partial x_m}} \tag{A.10}$$

$$= \frac{\partial(\overline{\rho u_i'u_j'u_m'})}{\partial x_m} - U_m\frac{\partial \tau_{ij}}{\partial x_m} - \tau_{im}\frac{\partial U_j}{\partial x_m} - \tau_{jm}\frac{\partial U_i}{\partial x_m} \tag{A.11}$$

and for the pressure gradient term

$$\overline{u_i'\frac{\partial p}{\partial x_j} + u_j'\frac{\partial p}{\partial x_i}} = \overline{u_i'\frac{\partial p'}{\partial x_j} + u_j'\frac{\partial p'}{\partial x_i}} \tag{A.12}$$

Repeat for the viscous term

$$\overline{u_i'\mu\frac{\partial^2 u_j}{\partial x_m^2} + u_j'\mu\frac{\partial^2 u_i}{\partial x_m^2}} = \overline{u_i'\mu\frac{\partial^2 u_j'}{\partial x_m\partial x_m} + u_i'\mu\frac{\partial^2 u_i'}{\partial x_m\partial x_m}} \tag{A.13}$$

$$= \overline{\mu\frac{\partial}{\partial x_m}\left(u_i'\frac{\partial u_j'}{\partial x_m}\right) + \mu\frac{\partial}{\partial x_m}\left(u_j'\frac{\partial u_i'}{\partial x_m}\right)}$$

$$-\overline{\mu\frac{\partial u_j'}{\partial x_m}\frac{\partial u_i'}{\partial x_m} - \mu\frac{\partial u_i'}{\partial x_m}\frac{\partial u_j'}{\partial x_m}} \tag{A.14}$$

$$= \overline{\mu\frac{\partial}{\partial x_m}\left(u_i'\frac{\partial u_j'}{\partial x_m} + u_j'\frac{\partial u_i'}{\partial x_m}\right) - 2\mu\frac{\partial u_i'}{\partial x_m}\frac{\partial u_j'}{\partial x_m}} \tag{A.15}$$

$$= \overline{\mu\frac{\partial^2(u_i'u_j')}{\partial x_m\partial x_m} - 2\mu\frac{\partial u_i'}{\partial x_m}\frac{\partial u_j'}{\partial x_m}} \tag{A.16}$$

$$= \overline{\mu\frac{\partial}{\partial x_m}\left[u_i'\frac{\partial u_j'}{\partial x_m} + u_j'\frac{\partial u_i'}{\partial x_m}\right] - 2\mu\frac{\partial u_i'}{\partial x_m}\frac{\partial u_j'}{\partial x_m}} \tag{A.17}$$

$$= \overline{\mu\left[u_i'\frac{\partial^2 u_j'}{\partial x_m\partial x_m} + u_j'\frac{\partial^2 u_i'}{\partial x_m\partial x_m}\right]} \tag{A.18}$$

$$= \overline{\mu \left[u_i' \frac{\partial}{\partial x_m} \left(2s_{mj}' - \frac{\partial u_m'}{\partial x_j} \right) + u_j' \frac{\partial}{\partial x_m} \left(2s_{mi}' - \frac{\partial u_m'}{\partial x_i} \right) \right]} \quad \text{(A.19)}$$

$$= \overline{2\mu \left[u_i' \frac{\partial s_{mj}'}{\partial x_m} + u_j' \frac{\partial s_{mi}'}{\partial x_m} \right]} \quad \text{(A.20)}$$

$$= \overline{2\mu \left[\frac{\partial}{\partial x_m} \left(u_i' s_{mj}' + u_j' s_{mi}' \right) - s_{mj}' \frac{\partial u_i'}{\partial x_m} - s_{mi}' \frac{\partial u_j'}{\partial x_m} \right]} \quad \text{(A.21)}$$

Combine Equations A.9 - A.21 to obtain the Reynolds Stress equation

$$\frac{\partial}{\partial t}(\tau_{ij}) + U_m \frac{\partial \tau_{ij}}{\partial x_m} = \frac{\partial(\overline{\rho u_i' u_j' u_m'})}{\partial x_m} - \tau_{im} - \tau_{jm} \frac{\partial U_i}{\partial x_m} + + \overline{u_i' \frac{\partial p'}{\partial x_j} + U_j' \frac{\partial p'}{\partial x_i}}$$

$$+ \overline{2\mu \left[\frac{\partial}{\partial x_m} \left(u_i' s_{mj}' + u_j' s_{mi}' \right) - s_{mj}' \frac{\partial u_i'}{\partial x_m} - s_{mi}' \frac{\partial u_j'}{\partial x_m} \right]} \quad \text{(A.22)}$$

Rearrange the above equation into a more recognizable form.

$$\frac{\partial \tau_{ij}}{\partial t} + U_m \frac{\partial \tau_{ij}}{\partial x_m} = -\tau_{im} \frac{\partial U_j}{\partial x_m} - \tau_{jm} \frac{\partial U_i}{\partial x_m} + \epsilon_{ij} - \Pi_{ij} + \frac{\partial C_{ijm}}{\partial x_m}$$

$$\Pi_{ij} = \overline{p' \left(\frac{\partial u_i'}{\partial x_j} + \frac{\partial u_j'}{\partial x_i} \right)}$$

$$\epsilon_{ij} = \overline{2\nu \left(s_{mj}' \frac{\partial u_i'}{\partial x_m} + s_{mi}' \frac{\partial u_j'}{\partial x_m} \right)}$$

$$C_{ijm} = \overline{\rho u_i' u_j' u_m'} + \overline{p' u_i'} \delta_{jm} + \overline{p' u_j'} \delta_{im} - \overline{2\mu \left(u_i' s_{mj}' + u_j' s_{mi}' \right)} \quad \text{(A.23)}$$

The above expression provides six new equations (one for each independent component of the Reynolds Stress tensor) which must be solved in order to completely determine the Reynolds stress tensor.

B Turbulent Kinetic Energy Derivation

The equation describing the turbulent kinetic energy (per unit mass) is obtained by contracting the Reynolds Stress Eq.(A.23).

$$\frac{\partial \tau_{ii}}{\partial t} + U_m \frac{\partial \tau_{ii}}{\partial x_m} = -2\tau_{im}\frac{\partial U_i}{\partial x_m} + \rho\epsilon_{ii} - \Pi_{ii} + \frac{\partial C_{iim}}{\partial x_m} \tag{B.1}$$

$$\rho\frac{\partial k}{\partial t} + \rho U_m \frac{\partial k}{\partial x_m} = \tau_{im}\frac{\partial U_i}{\partial x_m} - \rho\frac{\epsilon_{ii}}{2} - \frac{\partial}{\partial x_m}\left[\frac{\overline{\rho u_i' u_i' u_m'}}{2} + \overline{p' u_m'} - 2\mu\overline{u_i' s_{mi}'}\right] \tag{B.2}$$

$$\rho\frac{Dk}{Dt} = \tau_{im}\frac{\partial U_i}{\partial x_m} - \frac{\rho\epsilon_{ii}}{2} - \frac{\partial}{\partial x_m}\left[\frac{\overline{\rho u_i' u_i' u_m'}}{2} + \overline{p' u_m'} - \mu\frac{\partial k}{\partial x_m}\right] \tag{B.3}$$

By contracting the Reynolds stress equation we have reduced the tensor equation to a scalar one for τ_{ii}. Since we are no longer dealing with a tensor equation, the scalar ϵ_{ii} will be replaced with ϵ. For an incompressible flow the pressure dilatation term, Π_{ij}, is zero and, therefore, if the Boussinesq approximation is used

$$\tau_{ij} = 2\mu_t S_{ij} - \frac{2}{3}\rho k\delta_{ij} \tag{B.4}$$

the k equation can be written in its standard form for an incompressible fluid.

$$\rho\frac{\partial k}{\partial t} + \rho U_m \frac{\partial k}{\partial x_m} = \tau_{im}\frac{\partial U_i}{\partial x_m} - \rho\epsilon + \frac{\partial}{\partial x_m}\left[\mu\frac{\partial k}{\partial x_m} - \frac{1}{2}\overline{\rho u_i' u_i' u_m'} - \overline{p' u_m'}\right] \tag{B.5}$$

The above equation can be re-written in terms of the enstrophy as

$$\frac{Dk}{Dt} = \frac{\tau_{ij}}{\rho}\frac{\partial U_i}{\partial x_j} + \frac{\partial}{\partial x_j}\left[\frac{\nu_t}{\sigma_k}\frac{\partial k}{\partial x_j}\right] - \nu\epsilon_{ijm}\frac{\partial}{x_j}\left(\overline{u_i'\omega_m'}\right) - \nu\zeta \tag{B.6}$$

From the enstrophy modeling we have

$$\overline{u_i'\omega_m'} = \frac{\nu_t}{2\sigma_r}\left[\frac{\partial\Omega_m}{\partial x_i} + \frac{\partial\Omega_i}{\partial x_m}\right] + \frac{\epsilon_{pmi}}{2}\left[\frac{\partial\left(\overline{u_p'u_l'}\right)}{\partial x_l} - \frac{\partial k}{\partial x_p}\right] \tag{B.7}$$

$$\overline{u_p'u_l'} = -2\nu_t S_{pl} + \frac{2}{3}k\delta_{pl} \tag{B.8}$$

Therefore, after neglecting the higher order derivatives we obtain

$$\frac{\partial}{\partial x_j}\left(\overline{u_i'\omega_m'}\right) = -\frac{\epsilon_{pmi}}{6}\frac{\partial}{\partial x_j}\left[\frac{\partial k}{\partial x_p}\right] \tag{B.9}$$

Substitute the above to obtain the modeled k equation (in an incompressible medium)

$$\rho\frac{\partial k}{\partial t} + \rho U_m\frac{\partial k}{\partial x_m} = \tau_{im}\frac{\partial U_i}{\partial x_m} - \mu\zeta + \frac{\partial}{\partial x_m}\left[\left(\frac{\mu}{3} + \frac{\mu_t}{\sigma_k}\right)\frac{\partial k}{\partial x_m}\right] \tag{B.10}$$

In order to relate the above equation to other two-equation models we can relate the dissipation ϵ to the enstrophy, ζ.

$$\epsilon \equiv 2\nu\overline{s_{ij}'s_{ij}'} \tag{B.11}$$

$$= 2\nu\frac{\overline{\omega_i'\omega_i'}}{2} + \frac{\partial^2\left(\overline{u_i'u_j'}\right)}{\partial x_i\partial x_j} \tag{B.12}$$

$$= \nu\zeta + \frac{\partial^2\left(\overline{u_i'u_j'}\right)}{\partial x_i\partial x_j} \tag{B.13}$$

or for a large Reynolds number the above can be re-written as [1]

$$\epsilon = \nu\zeta \tag{B.14}$$

C Vorticity Derivation

Begin with the incompressible Navier-Stokes

$$\rho\frac{\partial u_i}{\partial t} + u_j\frac{\partial u_i}{\partial x_j} = -\frac{\partial p}{\partial x_i} + \frac{\partial t_{ij}}{\partial x_j} \tag{C.1}$$

where

$$t_{ij} = 2\mu s_{ij} \tag{C.2}$$

Re-write the above as

$$\rho\frac{\partial u_i}{\partial t} + u_j\left(\frac{\partial u_i}{\partial x_j} - \frac{\partial u_j}{\partial x_i}\right) + u_j\frac{\partial u_j}{\partial x_i} = -\frac{\partial p}{\partial x_i} + \mu\frac{\partial}{\partial x_j}\left[\left(\frac{\partial u_i}{\partial x_j} - \frac{\partial u_j}{\partial x_i}\right) + \frac{\partial u_j}{\partial x_i}\right] \tag{C.3}$$

or

$$\rho\frac{\partial u_i}{\partial t} + 2r_{ij}u_j + u_j\frac{\partial u_j}{\partial x_i} = -\frac{\partial p}{\partial x_i} + \mu\frac{\partial}{\partial x_j}(2r_{ij}) \tag{C.4}$$

Where r_{ij} is the rotation tensor and can be re-written as [1]

$$r_{ij} = -\frac{1}{2}\epsilon_{ijk}\omega_k \tag{C.5}$$

Now, substitute Equation C.5 into Equation C.4 to obtain

$$\rho\frac{\partial u_i}{\partial t} - u_j\epsilon_{ijk}\omega_k + u_j\frac{\partial u_j}{\partial x_i} = -\frac{\partial p}{\partial x_i} + \mu\frac{\partial}{\partial x_j}(-\epsilon_{ijk}\omega_k) \tag{C.6}$$

which can be re-written as

$$\frac{\partial u_i}{\partial t} = -\frac{\partial}{\partial x_i}\left[\frac{p}{\rho} + \frac{u_j u_j}{2}\right] + \epsilon_{ijk}u_j\omega_k - \nu\epsilon_{ijk}\frac{\partial \omega_k}{\partial x_j} \tag{C.7}$$

From the definition of vorticity

$$\omega_i = \epsilon_{ijk}\frac{\partial u_k}{\partial x_j} \tag{C.8}$$

we see that in order to derive an equation for the vorticity you simply apply the curl operator to the above form of the Navier-Stokes (Eq. C.7).

$$\epsilon_{ilm}\frac{\partial}{\partial x_m}\left(\frac{\partial u_i}{\partial t}\right) = -\epsilon_{ilm}\frac{\partial}{\partial x_m}\left[\frac{\partial}{\partial x_i}\left(\frac{p}{\rho}+\frac{u_j u_j}{2}\right)\right] + \epsilon_{ilm}\frac{\partial}{\partial x_m}\left(\epsilon_{ijk}u_j\omega_k\right) - \nu\epsilon_{lmi}\frac{\partial}{\partial x_m}\left(\epsilon_{ijk}\frac{\partial \omega_k}{\partial x_j}\right) \tag{C.9}$$

Note that the first term on the right hand side is zero from the multiplication of a symmetric tensor ($\frac{\partial^2\left(\frac{p}{\rho}+\frac{u_j u_j}{2}\right)}{\partial x_m \partial x_i}$) and a skew-symmetric tensor (ϵ_{lmi}). Therefore, the above reduces to

$$\frac{\partial \omega_l}{\partial t} = \epsilon_{lmi}\epsilon_{ijk}\frac{\partial(u_j\omega_k)}{\partial x_m} - \nu\epsilon_{lmi}\epsilon_{ijk}\frac{\partial}{\partial x_m}\left(\frac{\partial \omega_k}{\partial x_j}\right) \tag{C.10}$$

Apply the following identity

$$\epsilon_{lmi}\epsilon_{ijk} = \delta_{lj}\delta_{mk} - \delta_{lk}\delta_{mj} \tag{C.11}$$

to obtain

$$\frac{\partial \omega_l}{\partial t} = \frac{\partial(u_l\omega_m)}{\partial x_m} - \frac{\partial(u_m\omega_l)}{\partial x_m} - \nu\frac{\partial}{\partial x_m}\left(\frac{\partial \omega_m}{\partial x_l}\right) + \nu\frac{\partial}{\partial x_m}\left(\frac{\partial \omega_l}{\partial x_m}\right) \tag{C.12}$$

The above equation can be simplified by noting that the divergence of the curl ($\nabla \times V$) is zero

$$\frac{\partial \omega_m}{\partial x_m} = 0 \tag{C.13}$$

and by switching the dummy indices to obtain the instantaneous incompressible vorticity equation.

$$\frac{\partial \omega_i}{\partial t} + u_j \frac{\partial \omega_i}{\partial x_j} = \omega_j \frac{\partial u_i}{\partial x_j} + \nu \frac{\partial^2 \omega_i}{\partial x_j \partial x_j} \tag{C.14}$$

or

$$\frac{D\omega_i}{Dt} = \omega_j \frac{\partial u_i}{\partial x_j} + \nu \frac{\partial^2 \omega_i}{\partial x_j \partial x_j} \tag{C.15}$$

D Enstrophy Derivation

Start with the instantaneous vorticity equation for an incompressible flow (see Appendix C).

$$\frac{D\omega_i}{Dt} = \omega_j \frac{\partial u_i}{\partial x_j} + \nu \frac{\partial^2 \omega_i}{\partial x_j \partial x_j} \tag{D.1}$$

The first step is to derive the fluctuating vorticity equation. This is done by decomposing the instantaneous variables into a mean and a fluctuating component and then applying a time average. This will provide an equation for the mean vorticity. If you then subtract the mean equation from the instantaneous, you will obtain the fluctuating vorticity equation.

$$\omega_i(x_i, t) = \Omega_i(x_i) + \omega_i'(x_i, t) \tag{D.2}$$

$$u_i(x_i, t) = U_i(x_i) + u_i'(x_i, t) \tag{D.3}$$

Substitute Equations D.2- D.3 into Equation D.1 and apply a time average.

$$\frac{\partial \Omega_i}{\partial t} + U_j \frac{\partial \Omega_i}{\partial x_j} + \overline{u_j' \frac{\partial \omega_i'}{\partial x_j}} = \Omega_j \frac{\partial U_i}{\partial x_j} + \overline{\omega_j' \frac{\partial u_i'}{\partial x_j}} + \nu \frac{\partial^2 \Omega_i}{\partial x_j \partial x_j} \tag{D.4}$$

$$\frac{D\Omega_i}{Dt} = \Omega_j \frac{\partial U_i}{\partial x_j} + \nu \frac{\partial^2 \Omega_i}{\partial x_j^2} + \overline{\omega_j' \frac{\partial u_i'}{\partial x_j}} - \overline{u_j' \frac{\partial \omega_i'}{\partial x_j}} \tag{D.5}$$

$$= \Omega_j \frac{\partial U_i}{\partial x_j} + \nu \frac{\partial^2 \Omega_i}{\partial x_j^2} + \frac{\partial}{\partial x_j} \left[\overline{u_i' \omega_j'} \right] \tag{D.6}$$

When the above equation is combined with the identity

$$\Omega_j \frac{\partial U_i}{\partial x_j} = \Omega_j S_{ij} \tag{D.7}$$

the Mean Vorticity equation for an incompressible medium is obtained.

$$\frac{D\Omega_i}{Dt} = -\frac{\partial}{\partial x_j}\left[\overline{u_j'\omega_i'} - \overline{u_i'\omega_j'}\right] + \Omega_j S_{ij} + \nu\frac{\partial^2\Omega_i}{\partial x_j^2} \tag{D.8}$$

Multiply Eq. D.8 by Ω_i to obtain an equation for $\Omega_i\Omega_i$ (mean equation)

$$\frac{D}{Dt}\left(\Omega_i\Omega_i\right) = -2\Omega_i\frac{\partial}{\partial x_j}\left[\overline{u_j'\omega_i'} - \overline{u_i'\omega_j'}\right] + 2\Omega_i\Omega_j S_{ij} + 2\nu\Omega_i\frac{\partial^2\Omega_i}{\partial x_j^2} \tag{D.9}$$

Multiply Eq. D.1 by ω_i to obtain an equation for $\omega_i\omega_i$ (instantaneous equation).

$$\frac{D}{Dt}\left(\omega_i\omega_i\right) = 2\omega_i\omega_j\frac{\partial u_i}{\partial x_j} + 2\nu\omega_i\frac{\partial^2\omega_i}{\partial x_j^2} \tag{D.10}$$

Now decompose the above equation using Equation D.2- D.3 and apply a time average to obtain

$$\begin{aligned}\frac{\partial}{\partial t}\left(\Omega_i\Omega_i\right) + \frac{\partial}{\partial t}\left(\overline{\omega_i'\omega_i'}\right) = {} & 2\Omega_i\Omega_j\frac{\partial U_i}{\partial x_j} + 2\Omega_j\overline{\omega_i'\frac{\partial u_i'}{\partial x_j}} + 2\Omega_i\overline{\omega_j'\frac{\partial u_i'}{\partial x_j}} + 2\overline{\omega_i'\omega_j'}\frac{\partial U_i}{\partial x_j} + 2\overline{\omega_i'\omega_j'\frac{\partial u_i'}{\partial x_j}} \\ & + 2\nu\Omega_i\frac{\partial^2\Omega_i}{\partial x_j^2} + 2\nu\overline{\omega_i'\frac{\partial^2\omega_i'}{\partial x_j^2}} - U_j\left(\frac{\partial}{\partial x_j}\left[\Omega_i\Omega_i + 2\Omega_i\omega_i' + \omega_i'\omega_i'\right]\right) \\ & - \overline{u_j'\frac{\partial}{\partial x_j}\left[\Omega_i\Omega_i + 2\Omega_i\omega_i' + \omega_i'\omega_i'\right]}\end{aligned} \tag{D.11}$$

Now subtract the mean and instantaneous equations to obtain a relation for $\overline{\omega_i'\omega_i'}$

$$\begin{aligned}\frac{D}{Dt}\overline{(\omega_i'\omega_i')} = {} & -2\overline{u_j'\omega_i'}\frac{\partial\Omega_i}{\partial x_j} - \frac{\partial}{\partial x_j}\left(\overline{u_j'\omega_i'\omega_i'}\right) + 2\overline{\omega_i'\omega_j's_{ij}'} + 2\overline{\omega_i'\omega_j'}S_{ij} + 2\Omega_j\overline{\omega_i's_{ij}'} \\ & + \nu\frac{\partial^2}{\partial x_m^2}\overline{(\omega_i'\omega_i')} - 2\nu\overline{\frac{\partial\omega_i'}{\partial x_j}\frac{\partial\omega_i'}{\partial x_j}}\end{aligned} \tag{D.12}$$

The above is the incompressible enstrophy equation where the enstrophy

$$\zeta = \overline{\omega_i'\omega_i'} \tag{D.13}$$

is the sum of the squares of the fluctuating vorticity components.

E Modeling of the ζ Equation

We begin with the incompressible Enstrophy equation (see Appendix D)

$$\frac{\partial \zeta}{\partial t} + U_j \frac{\partial \zeta}{\partial x_j} = -2\overline{u_j' \omega_i'} \frac{\partial \Omega_i}{\partial x_j} - \frac{\partial \left(\overline{u_j' \omega_i' \omega_i'} \right)}{\partial x_j} + 2\overline{\omega_i' \omega_j' s_{ij}'} + 2\overline{\omega_i' \omega_j'} S_{ij} + 2\overline{\omega_i' s_{ij}'} \Omega_j$$

$$+\nu \frac{\partial^2 \zeta}{\partial x_j \partial x_j} - 2\nu \overline{\frac{\partial \omega_i'}{\partial x_j} \frac{\partial \omega_i'}{\partial x_j}} \tag{E.1}$$

From Eq. E.1 we have six terms which require modeling.

E.1 Modeling of $\overline{\omega_i' u_j'}$

The first term is a second order tensor and is therefore re-written as the sum of a symmetric and skew-symmetric tensor.

$$\overline{\omega_i' u_j'} = \frac{1}{2} \left(\overline{\omega_i' u_j' + \omega_j' u_i'} \right) + \frac{1}{2} \left(\overline{\omega_i' u_j' - \omega_j' u_i'} \right) \tag{E.2}$$

$$= A_{ij} + B_{ij} \tag{E.3}$$

E.1.1 Skew-Symmetric Portion of $\overline{\omega_i' u_j'}$

The first step is to examine the Skew-Symmetric portion of the above term. This is done by applying the following identity to Eq. E.3.

$$\epsilon_{mij} \overline{\omega_i' u_j'} = \frac{\partial \overline{(u_m' u_i')}}{\partial x_i} - \frac{\partial k}{\partial x_m} \tag{E.4}$$

$$= \epsilon_{mij} A_{ij} + \epsilon_{mij} B_{ij} \tag{E.5}$$

$$= 0 + \epsilon_{mij} B_{ij} \tag{E.6}$$

Solve the above for B_{ij}.

$$B_{ij} = \frac{\epsilon_{mij}}{2}\left[\frac{\partial\left(\overline{u'_m u'_i}\right)}{\partial x_i} - \frac{\partial k}{\partial x_m}\right] \tag{E.7}$$

E.1.2 Symmetric Portion of $\overline{\omega'_i u'_j}$

The next step is to consider the symmetric portion of $\overline{\omega'_i u'_j}$.

$$A_{ij} = \frac{1}{2}\overline{\left(\omega'_i u'_j + \omega'_j u'_i\right)} \tag{E.8}$$

$$\overline{\omega'_i u'_j} = \overline{\epsilon_{iml}\frac{\partial u'_l}{\partial x_m}u'_j} \tag{E.9}$$

$$= \overline{u'_j\left[\frac{\epsilon_{iml}}{2}\left(\frac{\partial u'_l}{\partial x_m} + \frac{\partial u'_m}{\partial x_l}\right) + \frac{\epsilon_{iml}}{2}\left(\frac{\partial u'_l}{\partial x_m} - \frac{\partial u'_m}{\partial x_l}\right)\right]} \tag{E.10}$$

$$= \overline{u'_j\left[\epsilon_{iml}s'_{lm} + \epsilon_{iml}r'_{lm}\right]} \tag{E.11}$$

$$= \overline{u'_j\epsilon_{iml}r'_{lm}} \tag{E.12}$$

$\overline{u'_j r'_{lm}}$ is a third order tensor. Therefore, in order to maintain the correct tensorial notation this is modeled using the gradient diffusion assumption.

$$\overline{u'_j r'_{lm}} = \frac{\nu_t}{\sigma_r}\frac{\partial \Omega_{lm}}{\partial x_j} \tag{E.13}$$

Combine Eqs. E.7, and E.13 to obtain

$$\overline{u'_j\omega'_i} = \frac{\nu_t}{2\sigma_r}\left[\frac{\partial \Omega_i}{\partial x_j} + \frac{\partial \Omega_j}{\partial x_i}\right] + \frac{\epsilon_{mij}}{2}\left[\frac{\partial\left(\overline{u'_m u'_l}\right)}{\partial x_l} - \frac{\partial k}{\partial x_m}\right] \tag{E.14}$$

E.2 Modeling of $\frac{\partial \overline{u_j' \omega_i' \omega_i'}}{\partial x_j}$

$\overline{u_j' \omega_i' \omega_i'}$ is modeled using a gradient diffusion model.

$$\overline{u_j' \omega_i' \omega_i'} = \frac{-\nu_t}{\sigma_\zeta} \frac{\partial \zeta}{\partial x_j} \tag{E.15}$$

$$\Longrightarrow \frac{\partial \left(\overline{u_j' \omega_i' \omega_i'} \right)}{\partial x_j} = -\frac{\partial}{\partial x_j} \left[\frac{\nu_t}{\sigma_\zeta} \frac{\partial \zeta}{\partial x_j} \right] \tag{E.16}$$

E.3 Modeling of $\overline{\omega_i' \omega_j' s_{ij}'} - \overline{\nu \frac{\partial \omega_i'}{\partial x_j} \frac{\partial \omega_i'}{\partial x_j}}$

$\overline{\omega_i' \omega_j' s_{ij}'} - \overline{\nu \frac{\partial \omega_i'}{\partial x_j} \frac{\partial \omega_i'}{\partial x_j}}$ is modeled using the suggestions given in References [47, 38]

$$\begin{aligned} \overline{\omega_i' \omega_j' s_{ij}'} - \overline{\nu \frac{\partial \omega_i'}{\partial x_j} \frac{\partial \omega_i'}{\partial x_j}} &= \frac{\tilde{\beta}_5 \zeta}{\tau} = \frac{\tilde{\beta}_5 \zeta}{\frac{k}{\epsilon}} \\ &= \frac{\beta_5 \zeta^2}{\left(\frac{k}{\sqrt{2}\nu} \right)} \\ &= \frac{\beta_5 \zeta^{\frac{3}{2}}}{\sqrt{R_t}} \end{aligned} \tag{E.17}$$

where τ is the turbulent time scale and R_t is the turbulent Reynolds number $\frac{k^2}{\nu^2 \zeta}$. The above term was developed for high turbulent Reynolds number and homogeneous turbulence. Therefore, an additional term was added (for $\overline{\omega_i' \omega_j' s_{ij}'}$) to account for low Reynolds number and non-homogeneous effects.

$$\overline{\omega_i' \omega_j' s_{ij}'} - \overline{\nu \frac{\partial \omega_i'}{\partial x_j} \frac{\partial \omega_i'}{\partial x_j}} = \frac{\beta_7 \zeta}{\Omega^2} \Omega_i \Omega_j S_{ij} - \frac{\beta_5 \zeta^{\frac{3}{2}}}{\sqrt{R_t}} \tag{E.18}$$

Based on the research to date, the term that gave the most satisfactory results for the airfoils under consideration was a result of vortex stretching. Because of this, the

above term, which was modeled assuming zero pressure gradient, in now modeled as

$$\overline{\omega_i'\omega_j's_{ij}'} - \nu\overline{\frac{\partial\omega_i'}{\partial x_j}\frac{\partial\omega_i'}{\partial x_j}} = \frac{\beta_7\zeta}{\Omega^2}\Omega_i\Omega_j S_{ij} - \frac{\beta_5\zeta^{\frac{3}{2}}}{\sqrt{R_t}} + \frac{\sigma_p\left(\frac{\partial P}{\partial x_i}\right)^2\left(\frac{\Omega}{P}\right)R_t^{\frac{3}{2}}}{1+\left[\sigma_\rho\frac{a^2M_T^{\frac{5}{2}}}{\nu S^2}\left(\frac{\partial U_i}{\partial x_i}\right)\right]^2} \tag{E.19}$$

E.4 Modeling of $\overline{\omega_i'\omega_j'}$

$\overline{\omega_i\omega_j}$ is modeled by noting the appropriate tensorial notation. Also, when contracted the right hand side must be equal to ζ (from definition of ζ)

$$\overline{\omega_i\omega_j} = \alpha_3\zeta b_{ij} + \frac{\delta_{ij}\zeta}{3} \tag{E.20}$$

$$b_{ij} = \left[\frac{-\overline{u_i'u_j'}}{k} + \frac{2}{3}\delta_{ij}\right] \tag{E.21}$$

where b_{ij} is the anisotropy tensor.

E.5 Modeling of $\overline{\omega_i's_{ij}'}$

$\overline{\omega_i's_{ij}'}$ is modeled by noting the appropriate tensorial notation.

$$\overline{\omega_i's_{ij}'} = \overline{s_{ij}'\epsilon_{ilm}\frac{\partial u_m'}{\partial x_l}} = \overline{s_{ij}'\left[\frac{\epsilon_{ilm}}{2}\left(\frac{\partial u_m'}{\partial x_l}+\frac{\partial u_l'}{\partial x_m}\right)+\frac{\epsilon_{ilm}}{2}\left(\frac{\partial u_m'}{\partial x_l}-\frac{\partial u_l'}{\partial x_m}\right)\right]} \tag{E.22}$$

$$= \overline{s_{ij}'\left(\epsilon_{ilm}s_{ml}'+\epsilon_{ilm}r_{ml}'\right)} \tag{E.23}$$

$$= \overline{s_{ij}'\epsilon_{ilm}r_{ml}'} \tag{E.24}$$

The above tensor, $\overline{s_{ij}'r_{ml}'}$, is symmetric in 'ij' and skew-symmetric in 'ml', therefore, is modeled as

$$\overline{s_{ij}'r_{ml}'} = -\frac{\tau_{ij}}{\rho k}\left[\frac{\beta_4\zeta\Omega_{ml}}{\Omega}+\frac{\beta_8}{\Omega^2}\left(\frac{\partial k}{\partial x_m}\frac{\partial\zeta}{\partial x_l}-\frac{\partial k}{\partial x_l}\frac{\partial\zeta}{\partial x_m}\right)+\beta_6\frac{\nu_t}{\nu}\Omega\Omega_{ml}\right] \tag{E.25}$$

where,

$$\Omega = \sqrt{\Omega_i \Omega_i} \tag{E.26}$$

$$\Longrightarrow \overline{\omega_i' s_{ij}'} = \frac{\tau_{ij}}{\rho k}\left[-\frac{\beta_4 \zeta \Omega_i}{\Omega} + \frac{\epsilon_{ilm}\beta_8}{\Omega^2}\left(\frac{\partial k}{\partial x_l}\frac{\partial \zeta}{\partial x_m} - \frac{\partial k}{\partial x_m}\frac{\partial \zeta}{\partial x_l}\right) - \beta_6 \frac{\nu_t}{\nu}\Omega\Omega_i\right] \tag{E.27}$$

Combine all of the above terms to obtain the incompressible Enstrophy equation.

$$\begin{aligned}\frac{D\zeta}{Dt} = &-\frac{\partial \Omega_i}{\partial x_j}\left(\frac{\nu_t}{\sigma_r}\left[\frac{\partial \Omega_i}{\partial x_j} + \frac{\partial \Omega_j}{\partial x_i}\right] + \epsilon_{mij}\left[\frac{\partial\left(\overline{u_m' u_l'}\right)}{\partial x_l} - \frac{\partial k}{\partial x_m}\right]\right) \\ &+\frac{\partial}{\partial x_j}\left[\left(\nu + \frac{\nu_t}{\sigma_\zeta}\right)\frac{\partial \zeta}{\partial x_j}\right] - \frac{\beta_5}{R_k}\zeta^{\frac{3}{2}} + \left(\alpha_3 \zeta b_{ij} + \frac{2}{3}\delta_{ij}\zeta\right) S_{ij} \\ &-\frac{\zeta \tau_{ij}\Omega_i\Omega_j\beta_4}{\rho k \Omega} + \epsilon_{ilm}\left(\frac{\tau_{ij}}{\rho k}\right)\left(\frac{\partial k}{\partial x_l}\frac{\partial \zeta}{\partial x_m} - \frac{\partial k}{\partial x_m}\frac{\partial \zeta}{\partial x_l}\right)\frac{\Omega_j}{\Omega^2}\beta_8 \\ &-\frac{\beta_6 \tau_{ij}\nu_t}{\rho k \nu}\Omega\Omega_i\Omega_j + \frac{\beta_7 \zeta}{\Omega^2}\Omega_i\Omega_j S_{ij}\end{aligned} \tag{E.28}$$

where

$$R_k = \frac{k}{\nu\sqrt{\zeta}} \tag{E.29}$$

This equation along with the Turbulent Kinetic Energy equation (see Appendix B)

$$\rho\frac{\partial k}{\partial t} + \rho U_m \frac{\partial k}{\partial x_m} = \tau_{im}\frac{\partial U_i}{\partial x_m} - \mu\zeta + \frac{\partial}{\partial x_m}\left[\left(\frac{\mu}{3} + \frac{\mu_t}{\sigma_k}\right)\frac{\partial k}{\partial x_m}\right] \tag{E.30}$$

comprises the current two equation model with the eddy viscosity calculated as

$$\nu_t = \frac{C_\mu k^2}{\nu\zeta} \tag{E.31}$$

F Free Shear Layers

In order to solve the similarity form of the governing equations the momentum, turbulent kinetic energy, and enstrophy equations must be solved simultaneously. The momentum and turbulent kinetic energy equations are derived in Ref. [2] and are reproduced here for convenience.

$$\mathcal{V}\frac{d\mathcal{U}}{d\eta} - \frac{1}{\eta^j}\frac{d}{d\eta}\left[\eta^j N\frac{d\mathcal{U}}{d\eta}\right] = S_u\mathcal{U} \tag{F.1}$$

$$\mathcal{V}\frac{dK}{d\eta} - \frac{1}{\eta^j}\frac{d}{d\eta}\left[\eta^j\frac{N}{\sigma_k}\frac{dK}{d\eta}\right] = S_k K + N\left(\frac{d\mathcal{U}}{d\eta}\right)^2 - E \tag{F.2}$$

where N is the non-dimensional eddy viscosity given by

$$N = C_\mu\frac{K^2(\eta)}{E(\eta)} \tag{F.3}$$

and $K(\eta)$ and $E(\eta)$ are the non-dimensional turbulent kinetic energy and enstrophy, respectively. S_u, S_k, and $\mathcal{V}$ are provided in Table 4.1 Ref. [2]. The solution procedure used is that of Ref. [2] with the exception of replacing the ϵ equation with the ζ equation. Therefore, since the momentum and turbulent kinetic energy equations remain unchanged, the remainder of this appendix deals with the derivation of the similarity form of the ζ equation for the wakes, jets, and mixing-layers.

We begin with the enstrophy equation for a planar two-dimensional incompressible flow and by using the standard boundary layer approximation or thin layer approach.

$$u\frac{\partial\zeta}{\partial x} + v\frac{\partial\zeta}{\partial y} = \frac{\partial}{\partial y}\left[\left(\nu + \frac{\nu_t}{\sigma_\zeta}\right)\frac{\partial\zeta}{\partial y}\right] + \nu_t\left(\frac{\sigma_r - 1}{\sigma_r}\right)\left(\frac{\partial^2 u}{\partial y^2}\right)^2 + \frac{\partial^2 u}{\partial y^2}\frac{\partial u}{\partial y}\frac{\partial\nu_t}{\partial y}$$

$$-\beta_5\frac{\zeta^{\frac{3}{2}}}{R_k}+\frac{\alpha_3\zeta\nu_t}{k}\left(\frac{\partial u}{\partial y}\right)^2+\frac{2}{3}\beta_4\zeta\left|\frac{\partial u}{\partial y}\right|-\frac{4}{3}\frac{\beta_8}{\Omega_3}\left[\frac{\partial k}{\partial x}\frac{\partial \zeta}{\partial y}-\frac{\partial k}{\partial y}\frac{\partial \zeta}{\partial x}\right]$$
$$+\frac{4}{3}\beta_6\frac{\nu_t}{\nu}\left|\frac{\partial u}{\partial y}\right|^3 \tag{F.4}$$

F.1 Plane Wake

$$u(x,y)=U_\infty-\sqrt{\tfrac{D}{\rho x}}\mathcal{U}(\eta)$$
$$k(x,y)=\tfrac{D}{\rho x}K(\eta) \qquad \zeta(x,y)=\tfrac{DU_\infty E(\eta)}{\nu\rho x^2}$$
$$\nu_t=\tfrac{C_\mu K^2(\eta)}{E(\eta)}\left(\tfrac{D}{\rho U_\infty}\right) \qquad N=C_\mu\tfrac{K^2(\eta)}{E(\eta)}$$
$$\eta=y\sqrt{\tfrac{\rho U_\infty^2}{Dx}}$$

The first step is to non-dimensionalize the equations (using the above) and re-write the partial differential equation as a total differential equation.

$$\mathcal{V}\frac{dE}{d\eta}-\frac{d}{d\eta}\left[\frac{N}{\sigma_\zeta}\frac{dE}{d\eta}\right]=2E-\frac{\beta_5}{\sqrt{2}}\frac{E^2}{K}+\alpha_3C_\mu K\left(\frac{d\mathcal{U}}{d\eta}\right)^2+\frac{2}{3}\beta_4E\left|\frac{d\mathcal{U}}{d\eta}\right|$$
$$+\frac{4}{3}\beta_6N\left|\frac{d\mathcal{U}}{d\eta}\right|^3 \tag{F.5}$$

The next step is to solve the ODE using the method described in Reference [2]. This includes applying the Rubel-Melnik transformation [48] to reduce the stiffness of the equation set. This stiffness can be explained by noting that at the edge of the turbulent region the equations become stiff because both k and ζ approach zero. Since we are not interested in solving the equations at the turbulent/non-turbulent interface, we will shift this boundary to infinity by applying the Rubel-Melnik transformation.

$$\frac{d}{d\xi}=\nu_t\frac{\partial}{\partial y} \tag{F.6}$$

or, in terms of the non-dimensional eddy viscosity

$$\frac{d}{d\xi} = N\frac{d}{d\eta} \tag{F.7}$$

From the above transformation, it is seen that as the eddy-viscosity approaches zero, the ξ coordinate will approach infinity, therefore, we simply integrate the equations from the centerline out to some prespecified ξ_{max} which occurs prior to the turbulent/non-turbulent interface.

After applying the Rubel-Melnik transformation the equation for the plane wake takes the form

$$\mathcal{V}\frac{dE}{d\xi} - \frac{d}{d\xi}\left[\frac{1}{\sigma_\zeta}\frac{dE}{d\xi}\right] = 2EN - \frac{\beta_5}{\sqrt{2}}\frac{E^2N}{K} + \frac{\alpha_3 C_\mu K}{N}\left(\frac{d\mathcal{U}}{d\xi}\right)^2 + \frac{2}{3}\beta_4 E\left|\frac{d\mathcal{U}}{d\xi}\right| + \frac{4}{3}\frac{\beta_6}{N}\left|\frac{d\mathcal{U}}{d\xi}\right|^3 \tag{F.8}$$

A similar procedure is used for the Mixing-Layer and the jets.

F.2 Mixing Layer

$$u(x,y) = U_1\mathcal{U}(\eta) \quad v(x,y) = U_1\left[\mathcal{V} + \eta\mathcal{U}\right]$$
$$k(x,y) = U_1^2 K(\eta) \quad \zeta(x,y) = \frac{U_1^3}{\nu x}E(\eta)$$
$$\nu_t = \frac{C_\mu U_1 x K^2(\eta)}{E(\eta)} \qquad N = C_\mu\frac{K^2(\eta)}{E(\eta)}$$
$$\eta = \frac{y}{x}$$

$$\mathcal{V}\frac{dE}{d\eta} - \frac{d}{d\eta}\left[\frac{N}{\sigma_\zeta}\frac{dE}{d\eta}\right] = \mathcal{U}E - \frac{\beta_5}{\sqrt{2}}\frac{E^2}{K} + \alpha_3 C_\mu K\left(\frac{d\mathcal{U}}{d\eta}\right)^2 + \frac{2}{3}\beta_4 E\left|\frac{d\mathcal{U}}{d\eta}\right| - \frac{4}{3}\frac{\beta_8}{\frac{d\mathcal{U}}{d\eta}}\frac{dK}{d\eta}E + \frac{4}{3}\beta_6 N\left|\frac{d\mathcal{U}}{d\eta}\right|^3 \tag{F.9}$$

After the Rubel-Melnik transformation the above equation becomes

$$\mathcal{V}\frac{dE}{d\xi} - \frac{d}{d\xi}\left[\frac{1}{\sigma_\zeta}\frac{dE}{d\xi}\right] = \mathcal{U}EN - \frac{\beta_5}{\sqrt{2}}\frac{E^2N}{K} + \alpha_3\frac{C_\mu K}{N}\left(\frac{d\mathcal{U}}{d\xi}\right)^2$$
$$+\frac{2}{3}\beta_4 E\left|\frac{d\mathcal{U}}{d\xi}\right| - \frac{4}{3}\frac{\beta_8}{\frac{d\mathcal{U}}{d\xi}}\frac{dK}{d\eta}NE + \frac{4}{3}\frac{\beta_6}{N}\left|\frac{d\mathcal{U}}{d\xi}\right|^3 \qquad \text{(F.10)}$$

F.3 Jets (Plane, Round, and Radial)

The two-dimensional axisymmetric form of the enstrophy equation is

$$u\frac{\partial\zeta}{\partial x} + v\frac{\partial\zeta}{\partial y} = \frac{1}{y^m}\frac{\partial}{\partial y}\left[y^m\left(\nu + \frac{\nu_t}{\sigma_\zeta}\right)\frac{\partial\zeta}{\partial y}\right] + \alpha_3\zeta\frac{2\nu_t}{k}\left[\frac{1}{2}\left(\frac{\partial u}{\partial y}\right)^2 + \left(\frac{v}{y^j}\right)^2\right]$$
$$-\frac{\beta_5}{R_k}\zeta^{\frac{3}{2}} - \zeta\left|\frac{\partial u}{\partial y}\right|\beta_4\left[\frac{2\nu_t}{k}\frac{v}{y^j} - \frac{2}{3}\right] - 2\beta_6\frac{\nu_t}{\nu}\left|\frac{\partial u}{\partial y}\right|^3\left(\frac{2\nu_t}{k}\frac{v}{y^j} - \frac{2}{3}\right)$$
$$+\beta_7\zeta\frac{v}{y^j} + \frac{\nu_t}{\sigma_\tau}\left[\frac{2}{y^j}\frac{\partial u}{\partial y}\frac{\partial^2 u}{\partial y^2} - \left(\frac{\partial^2 u}{\partial y^2}\right)^2 - \left(\frac{1}{y^j}\frac{\partial u}{\partial y}\right)^2\right]$$
$$+\frac{\partial\Omega_2}{\partial y}\frac{1}{y^m}\frac{\partial}{\partial y}\left[\nu_t y^m\frac{\partial u}{\partial y}\right] + 2\frac{\beta_8}{\Omega_2}\left(\frac{4\nu_t}{k}\frac{v}{y^j} - \frac{4}{3}\right)\left(\frac{\partial k}{\partial x}\frac{\partial\zeta}{\partial y} - \frac{\partial k}{\partial y}\frac{\partial\zeta}{\partial x}\right) \qquad \text{(F.11)}$$

where the non-dimensionalization parameters are

$$u(x,y) = U_o\mathcal{U}(\eta) \quad v(x,y) = U_o V(\eta)$$
$$\mathcal{U}(\eta) = \frac{(\eta^m F)'}{\eta^m} \quad V(\eta) = \eta\mathcal{U} - F2^{j-1}$$
$$k(x,y) = U_o^2 K(\eta) \quad \zeta(x,y) = \frac{U_o^3 E(\eta)}{\nu x}$$
$$\nu_t = \frac{C_\mu K^2(\eta) U_o x}{E(\eta)} \quad N = C_\mu\frac{K^2(\eta)}{E(\eta)}$$
$$\eta = \frac{y}{x} \quad U_o = \frac{C_1}{x^{\frac{j+1}{2}}}$$

$$j = 0, \quad m = 0 \quad \text{Planar Jets} \qquad \text{(F.12)}$$

$$j = 1, \quad m = 0 \quad \text{Radial Jets} \tag{F.13}$$

$$j = 1, \quad m = 1 \quad \text{Round Jets} \tag{F.14}$$

Substitute in the above and re-write in Dr. Wilcox's notation ($\mathcal{V} = -2^{(j-1)}F$) to obtain

$$\begin{aligned}
\mathcal{V}\frac{dE}{d\eta} - \frac{1}{\eta^m}\frac{d}{d\eta}\left[\eta^m \frac{N}{\sigma_\zeta}\frac{dE}{d\eta}\right] &= \mathcal{U}E\left[1 + 3(2^{j-1})\right] + \frac{\alpha_3 EN}{K}\left[\left(\frac{d\mathcal{U}}{d\eta}\right)^2 + 2j\left(\frac{\eta\mathcal{U}+\mathcal{V}}{\eta^j}\right)^2\right] \\
&- \frac{\beta_5}{\sqrt{2}}\frac{E^2}{K} - \beta_4 E\left|\frac{d\mathcal{U}}{d\eta}\right|\left[\frac{2Nj}{\eta^j K}(\eta\mathcal{U}+\mathcal{V}) - \frac{2}{3}\right] \\
&- 2\beta_6 N\left|\frac{d\mathcal{U}}{d\eta}\right|^3\left[\frac{4Nj}{\eta^j K}(\eta\mathcal{U}+\mathcal{V}) - \frac{4}{3}\right] + \frac{\beta_7 Ej}{\eta^j}(\eta\mathcal{U}+\mathcal{V}) \\
&+ 2\frac{\beta_8}{\frac{d\mathcal{U}}{d\eta}}\left(\frac{4Nj}{\eta^j K}(\eta\mathcal{U}+\mathcal{V}) - \frac{4}{3}\right)\left[2^j K\frac{dE}{d\eta} - 3E\frac{dK}{d\eta}2^{j-1} - E\frac{dK}{d\eta}\right]
\end{aligned} \tag{F.15}$$

After the Rubel-Melnik transformation the above equation becomes

$$\begin{aligned}
\mathcal{V}\frac{dE}{d\xi} - \frac{1}{\eta^m}\frac{d}{d\xi}\left[\eta^m \frac{1}{\sigma_\zeta}\frac{dE}{d\xi}\right] &= \mathcal{U}EN\left[1 + 3(2^{j-1})\right] + \frac{\alpha_3 E}{K}\left[\left(\frac{d\mathcal{U}}{d\xi}\right)^2 + 2N^2 j\left(\frac{\eta\mathcal{U}+\mathcal{V}}{\eta^j}\right)^2\right] \\
&- \frac{\beta_5}{\sqrt{2}}\frac{NE^2}{K} - \beta_4 E\left|\frac{d\mathcal{U}}{d\xi}\right|\left[\frac{2Nj}{\eta^j K}(\eta\mathcal{U}+\mathcal{V}) - \frac{2}{3}\right] \\
&- 2\beta_6\left|\frac{d\mathcal{U}}{d\xi}\right|^3\left[\frac{4Nj}{\eta^j K}(\eta\mathcal{U}+\mathcal{V}) - \frac{4}{3N}\right] + \frac{\beta_7 ENj}{\eta^j}(\eta\mathcal{U}+\mathcal{V}) \\
&+ \frac{2\beta_8 N}{\frac{d\mathcal{U}}{d\xi}}\left(\frac{4Nj}{\eta^j K}(\eta\mathcal{U}+\mathcal{V}) - \frac{4}{3}\right)\left[2^j K\frac{dE}{d\xi} - 3E\frac{dK}{d\xi}2^{j-1} - E\frac{dK}{d\xi}\right]
\end{aligned} \tag{F.16}$$

G Log Layer Analysis

The total shear stress is represented as the sum of the laminar and turbulent stresses.

$$\tau = \tau_l + \tau_t \tag{G.1}$$

From experimental measurements it has been determined that the laminar shear stress accounts for approximately 5% of the total stresses in the log law region. Therefore, in this region we will assume that the laminar shearing stresses are negligible when compared to the turbulent shearing stresses. It is also noted that the total stress is nearly constant in the log law region. As a consequence of the above assumptions we will approximate the total shearing stress in the log law region as

$$\tau = \tau_t \tag{G.2}$$

$$= \tau_w \tag{G.3}$$

where τ_w represents the shear stress evaluated at the wall. Also from experiment, it has been determined that the turbulent kinetic energy, k, is approximately constant in the log law region. Therefore, we can represent the ratio of the turbulent shearing stress to the turbulent kinetic energy as [49]

$$\frac{\tau_t}{k} = \sqrt{C_\mu} \quad where,\ C_\mu = 0.09\ \ (structural\ factor) \tag{G.4}$$

In the log law region the velocity profile is given from the law of the wall,

$$U^+ \approx \frac{1}{\kappa} ln y^+ + B \tag{G.5}$$

where κ is the Karman constant ($\approx .40$) and B is a dimensionless constant (≈ 5.0). The velocity and normal distance in Eq. (G.5) were non-dimensionalized using the friction velocity, u_τ, where

$$u_\tau \equiv \sqrt{\frac{\tau_w}{\rho}} \tag{G.6}$$

Therefore,

$$U^+ \equiv \frac{U}{u_\tau} \tag{G.7}$$

$$y^+ \equiv \frac{u_\tau y}{\nu} \tag{G.8}$$

The Reynolds stress tensor in the log law region is approximated as

$$\tau_t \approx -\overline{\rho u' v'} \tag{G.9}$$

$$= \mu_t \frac{dU}{dy} \tag{G.10}$$

where the eddy viscosity, ν_t is given by

$$\nu_t = \frac{\mu_t}{\rho} = \frac{C_\mu k^2}{\nu\zeta} \tag{G.11}$$

Combine the above relations to obtain

$$\frac{-\overline{u' v'}}{k} = \sqrt{C_\mu} \tag{G.12}$$

$$= \frac{\nu_t}{k}\frac{dU}{dy} \tag{G.13}$$

$$= \frac{\tau_w}{\rho k} \tag{G.14}$$

$$= \frac{u_\tau^2}{k} \tag{G.15}$$

Therefore,

$$k = \frac{u_\tau^2}{\sqrt{C_\mu}} \tag{G.16}$$

Similarly, by solving for ζ in the log law region we obtain

$$\zeta = \frac{u_\tau^3}{\nu \kappa y} \tag{G.17}$$

and the eddy viscosity becomes

$$\nu_t = u_\tau \kappa y \tag{G.18}$$

Next we will examine the vorticity for a two-dimensional cartesian coordinate system.

$$\Omega_i = \epsilon_{ijk} \frac{\partial u_m}{\partial x_j} \tag{G.19}$$

For two-dimensional flows the above reduces to

$$\Omega_1 = \Omega_2 = 0 \tag{G.20}$$

$$\Omega_3 = \left(\frac{\partial V}{\partial x} - \frac{\partial U}{\partial y} \right) \tag{G.21}$$

By also noting that

$$\frac{\partial U}{\partial y} \gg \frac{\partial V}{\partial x} \tag{G.22}$$

$$\Longrightarrow \Omega_3 \approx -\frac{\partial U}{\partial y} \tag{G.23}$$

$$= \frac{-u_\tau}{\kappa y} \tag{G.24}$$

Similarly, the mean strain rate is approximated as

$$S_{ij} = \frac{1}{2} \left(\frac{\partial u_i}{\partial x_j} + \frac{\partial u_j}{\partial x_i} \right) \tag{G.25}$$

$$\approx \frac{1}{2}\frac{\partial U}{\partial y} \tag{G.26}$$

$$= \frac{u_\tau}{2\kappa y} \tag{G.27}$$

and the component of the rotation tensor becomes

$$\Omega_{12} = -\frac{1}{2}\epsilon_{ijk}\Omega_m \tag{G.28}$$

$$= \frac{u_\tau}{2\kappa y} \tag{G.29}$$

Substitute the above relations into the Enstrophy equation in order to obtain a relation between the constants.

$$-\overline{u_j'\omega_i'}\frac{\partial \Omega_i}{\partial x_j} = \frac{-u_\tau^3}{2\kappa\sigma_r}\frac{1}{y^3} \tag{G.30}$$

$$-\frac{\partial}{\partial x_j}\left(u_j'\omega_i'\omega_i'\right) = \frac{u_\tau^4}{\nu\sigma_\zeta}\frac{1}{y^2} \tag{G.31}$$

$$\overline{\omega_i'\omega_j's_{ij}'} - \nu\overline{\frac{\partial\omega_i'}{\partial x_j}\frac{\partial\omega_i'}{\partial x_j}} = -\frac{\beta_5 u_\tau^4\sqrt{C_\mu}}{4\nu\kappa^2 y^2} \tag{G.32}$$

$$\overline{\omega_i'\omega_j'}S_{ij} = \frac{\alpha_3 u_\tau^4\sqrt{C_\mu}}{4\nu\kappa^2 y^2} \tag{G.33}$$

$$\overline{\omega_i's_{ij}'}\Omega_j = \beta_4\frac{u_\tau^4}{3\nu\kappa^2 y^2} + \beta_6\frac{2}{3}\frac{u_\tau^4}{\nu y^2\kappa^2} \tag{G.34}$$

$$\nu\frac{\partial^2\zeta}{\partial x_j\partial x_j} = \frac{u_\tau^3}{\kappa}\frac{1}{y^3} \tag{G.35}$$

Combine the above to obtain

$$\frac{1}{y^2}\left(\frac{u_\tau^4}{2\nu\sigma_\zeta} - \frac{\beta_5 u_\tau^4\sqrt{C_\mu}}{4\nu\kappa^2} + \frac{\alpha_3 u_\tau^4\sqrt{C_\mu}}{4\nu\kappa^2} + \frac{u_\tau^4\beta_4}{3\nu\kappa^2} + \frac{2\beta_6 u_\tau^4}{3\nu\kappa^2}\right)$$

$$+hot = 0 \tag{G.36}$$

From a power series analysis we note that each of the above coefficients must be zero. The $\frac{1}{y^3}$ term is considered a higher order term and is therefore neglected. Therefore, the log-law analysis has provided us the following relation for the model constants.

$$\sigma_\zeta = \frac{6\kappa^2}{\left[3\beta_5\sqrt{C_\mu} - 3\alpha_3\sqrt{C_\mu} - 4\beta_4 - 8\beta_6\right]} \tag{G.37}$$

H Boundary Layer Analysis

Begin with the Reynolds averaged equations of motion for an incompressible, two-dimensional, planar flow

$$\frac{\partial U_i}{\partial x_i} = 0 \tag{H.1}$$

$$\rho\frac{\partial U_i}{\partial t} + \rho U_j\frac{\partial U_i}{\partial x_j} = -\frac{\partial P}{\partial x_i} + \frac{\partial t_{ij}}{\partial x_j}, \tag{H.2}$$

then by making the boundary layer assumptions the above equations reduce to the standard form of the boundary layer equations

$$\frac{\partial U_i}{\partial x_i} = 0 \tag{H.3}$$

$$\rho\frac{\partial U}{\partial t} + \rho U\frac{\partial U}{\partial x} + \rho V\frac{\partial U}{\partial y} = -\frac{\partial P}{\partial x} + \frac{\partial}{\partial y}\left[(\mu + \mu_t)\frac{\partial U}{\partial y}\right] \tag{H.4}$$

This equation set is parabolic in the x direction and, therefore, is solved using a marching procedure as described in Reference [15]. This reduction in the complexity of the equation set reduces the typical run times from several hours to approximately one minute. This reduction in computational effort allows a wide variety of modeling and closure coefficients to be tested.

The k-ζ model was added to the Harris and Blanchard[15] boundary layer code in place of an existing k-ω turbulence model. The only difference in the solution procedure used in the current research as compared to the original code[15] is seen

from the non-dimensionalization of ζ, which uses

$$\zeta = \frac{U_R N_R^* \zeta^*}{L_R} \tag{H.5}$$

$$N_R^* = \frac{U_R L_R \rho_R}{\mu_R} \tag{H.6}$$

where R, *, N_R^* represent a reference quantity, a non-dimensional quantity, and a reference Reynolds number, respectively. The reference Reynolds number is used to scale the Enstrophy in order to maintain numerical accuracy during the solution procedure.

I Near Wall Behavior of k and ζ

Consider the turbulence quantities as you approach a solid surface by expanding the fluctuating velocity components in a power series

$$\begin{aligned} u'(y) &= a_0 + a_1 y + a_2 y^2 + a_3 y^3 + ... \\ v'(y) &= b_0 + b_1 y + b_2 y^2 + b_3 y^3 + ... \\ w'(y) &= c_0 + c_1 y + c_2 y^2 + c_3 y^3 + ... \end{aligned} \tag{I.1}$$

Now impose the conservation of mass for an incompressible fluid

$$\frac{\partial U_i}{\partial x_i} = \frac{\partial u_i'}{\partial x_i} = 0 \tag{I.2}$$

and the 'no slip' boundary condition

$$u'(0) = v'(0) = w'(0) = 0 \tag{I.3}$$

to obtain

$$\begin{aligned} u'(y) &= a_1 y + a_2 y^2 + a_3 y^3 + ... \\ v'(y) &= b_2 y^2 + b_3 y^3 + ... \\ w'(y) &= c_1 y + c_2 y^2 + c_3 y^3 + ... \end{aligned} \tag{I.4}$$

Therefore, from the definition of turbulent kinetic energy we obtain

$$k \equiv \frac{1}{2}\overline{u_i' u_i'} = \frac{1}{2}\left(a_1^2 y^2 + b_2^2 y^4 + c_1^2 y^2\right) \tag{I.5}$$

$$= k_o y^2 \quad as\ y \to 0 \tag{I.6}$$

where k_o is some constant.

A similar analysis is performed for the enstrophy at a solid surface.

$$\zeta = \overline{\omega_i' \omega_i'} \tag{I.7}$$

$$= \overline{\epsilon_{ijk} \frac{\partial u_k'}{\partial x_j} \epsilon_{ilm} \frac{\partial u_m'}{\partial x_l}} \tag{I.8}$$

$$= \overline{\left[\left(\frac{\partial u'}{\partial y} \right)^2 + \left(\frac{\partial w'}{\partial y} \right)^2 \right]} \tag{I.9}$$

$$= \left(a_1^2 + c_1^2 \right) + \ldots$$

$$= \zeta_o \quad as \; y \to 0 \tag{I.10}$$

where ζ_o is some constant.

J Homogeneous shear flows

A homogeneous shear flow

$$S_{ij} = \begin{bmatrix} 0 & S & 0 \\ S & 0 & 0 \\ 0 & 0 & 0 \end{bmatrix}$$

is given by enforcing a linear velocity profile with no dependence on the x or z coordinate directions. In other words, the following must be imposed

$$\frac{\partial U}{\partial y} = Constant \tag{J.1}$$

$$\frac{\partial U}{\partial x} = \frac{\partial U}{\partial z} = 0 \tag{J.2}$$

$$\frac{\partial^2 U}{\partial y^2} = 0 \tag{J.3}$$

where U is the mean velocity.

The above constraints reduce the k and ζ equations to

$$\frac{\partial k}{\partial t} = \nu_t \left(\frac{\partial u}{\partial y}\right)^2 - \nu\zeta \tag{J.4}$$

$$\frac{\partial \zeta}{\partial t} = \frac{\alpha_3 C_\mu k}{\nu}\left(\frac{\partial u}{\partial y}\right)^2 - \frac{\beta_5 \zeta^2\sqrt{2}}{\left(\sqrt{\zeta} + \frac{k}{\nu}\right)} + \frac{2}{3}\zeta\beta_4\left|\frac{\partial u}{\partial y}\right| + \frac{4}{3}\frac{\beta_6 C_\mu k^2}{\nu^2\zeta}\left|\frac{\partial u}{\partial y}\right|^3 \tag{J.5}$$

Now apply the following non-dimensionalization (* superscript represent a non-dimensional quantity)

$$k = k_o k^* \tag{J.6}$$

$$\zeta = \frac{\zeta^* S k_o}{2\nu} \tag{J.7}$$

$$t = \frac{t^*}{S} \tag{J.8}$$

$$S = \frac{\partial u}{\partial y} \tag{J.9}$$

to obtain

$$\frac{\partial k^*}{\partial t^*} = \frac{C_\mu (k^*)^2}{\zeta^*} - \zeta^* \tag{J.10}$$

$$\frac{\partial \zeta^*}{\partial t^*} = \alpha_3 C_\mu K^* - \frac{\beta_5 (\zeta^*)^2}{\sqrt{2}\left(k^* + \sqrt{\frac{\zeta^* S\nu}{2k_o}}\right)} + \frac{2}{3}\beta_4 \zeta^* + \frac{4}{3}\frac{\beta_6 C_\mu (k^*)^2}{\zeta^*} \tag{J.11}$$

The above ODE's are solved using a fourth order runge-kutta integration scheme to determine the decay rate of turbulence for a homogeneous shear flow. An initial condition , corresponding to setting production equal to dissipation, gives a homogeneous shear parameter of $\frac{SK_o}{\epsilon_o}$ at $t = 0$, to begin the integration.

It should be noted that many modelers use this type of flow to calibrate closure coefficients, however, since we were primarily interested in wall bounded shear flows and free shear layers we chose not to use the decay of homogeneous turbulence as a method of determining constants. Instead, we used homogeneous shear flow as a test case for the current two-equation model.

The data from our test case includes an examination of the shear parameter $\left(\frac{SK}{\epsilon}\right)$, anisotropy tensor (b_{ij}), and the predicted decay rates of k and ζ as per suggestion of Reference [37].

K Free Stream Boundary Condition

In this case, the equation governing k and ζ can be written as

$$\frac{dk}{dt} = -\nu\zeta \tag{K.1}$$

$$\frac{d\zeta}{dt} = -\beta_5 \frac{\zeta^{\frac{3}{2}}}{\left(R_t^{\frac{1}{2}} + \delta\right)} \tag{K.2}$$

where

$$R_t = \frac{k^2}{\nu^2\zeta} = \frac{1}{C_\mu}\frac{\nu_t}{\nu} \tag{K.3}$$

Dividing Eq. (K.1) by Eq. (K.2) gives

$$\frac{dk}{d\zeta} = \frac{k}{\beta_5\zeta} + \frac{\delta\nu}{\beta_5\zeta^{\frac{1}{2}}} \tag{K.4}$$

Equation (K.4) is a first order linear equation. Its solution can be written as

$$k = 2\delta\nu\frac{\zeta^{\frac{1}{2}}}{(\beta_5 - 2)} + C\zeta^{\frac{1}{\beta_5}} \tag{K.5}$$

where C is a constant to be determined from initial conditions. It can be seen from Eq. (K.5) that

$$\frac{k}{\nu\zeta^{\frac{1}{2}}} = \frac{2\delta}{(\beta_5 - 2)} + \frac{C}{\nu}\zeta^{\left(\frac{1}{\beta_5} - \frac{1}{2}\right)} \tag{K.6}$$

For $\beta_5 = 2.37$, the above equations show that as $\zeta \to 0$, R_t and ν_t increase without bound. Therefore

$$C = 0 \tag{K.7}$$

and initial values of ζ must be chosen such that

$$\frac{\nu_t}{\nu} = C_\mu R_t \leq C_\mu \left(\frac{2\delta}{(\beta_5 - 2)} \right)^2 \tag{K.8}$$

Thus, for decaying homogeneous turbulence k and ζ approach zero in such a way that $\frac{\nu_t}{\nu}$ remains constant. This, in turn, implies that during the decay process

$$\zeta \propto k^2 \tag{K.9}$$

Substituting Eq. (K.9) into (K.1) yields

$$k \propto t^{-1} \quad , \quad \zeta \propto t^{-2} \tag{K.10}$$

L Final k-ζ Equation Set

The final form for the modeled k-ζ equations can be written as

$$\rho\frac{Dk}{Dt} = \tau_{im}\frac{\partial U_i}{\partial x_m} - \mu\zeta + \frac{\partial}{\partial x_m}\left[\left(\frac{\mu}{3}+\frac{\mu_t}{\sigma_k}\right)\frac{\partial k}{\partial x_m}\right] - C_1\rho\frac{k}{\tau_\rho} \tag{L.1}$$

$$\begin{aligned}\rho\frac{D\zeta}{Dt} = {} & \frac{\mu_t}{\sigma_r}\frac{\partial\Omega_i}{\partial x_j}\left(\frac{\partial\Omega_i}{\partial x_j}+\frac{\partial\Omega_j}{\partial x_i}\right) - \frac{C_{\zeta_1}\rho\sqrt{2\zeta}\Omega}{\tau_\rho} + \frac{\partial}{\partial x_j}\left[\left(\mu+\frac{\mu_t}{\sigma_\zeta}\right)\frac{\partial\zeta}{\partial x_j}\right] \\ & - \frac{\rho\beta_5}{R_k+\delta}\zeta^{\frac{3}{2}} + \left(\alpha_3\rho\zeta b_{ij} + \frac{2}{3}\delta_{ij}\rho\zeta\right)S_{ij} - \frac{\beta_4\zeta\tau_{ij}\Omega_i\Omega_j}{k\Omega} \\ & + \max\left[2\beta_8\epsilon_{ilm}\left(\frac{\tau_{ij}}{k}\right)\left(\frac{\partial k}{\partial x_l}\frac{\partial\zeta}{\partial x_m}\right)\frac{\Omega_j}{S^2}, 0.0\right] \\ & - 2\frac{\beta_6\tau_{ij}\nu_t}{k\nu}\Omega\Omega_i\Omega_j + \frac{\beta_7\rho\zeta}{\Omega^2}\Omega_i\Omega_j S_{ij} \\ & + \max\left[\frac{\partial(\rho U_i P)}{\partial x_i}, 0.0\right]\frac{k\Omega}{\nu P\sigma_p}\frac{1}{(1+\delta\rho)}\end{aligned} \tag{L.2}$$

where

$$\tau_{ij} = 2\mu_t\left[S_{ij} - \frac{\delta_{ij}}{3}S_{kk}\right] - \frac{2}{3}\delta_{ij}\rho k \quad , \quad \nu_t = C_\mu\frac{k^2}{\nu\zeta}$$

$$S^2 = S_{ij}S_{ij} \quad , \quad \Omega^2 = \Omega_i\Omega_i \quad , \quad R_k = \frac{k}{\nu\sqrt{\zeta}} \quad , \quad R_t = R_k^2$$

$$\delta\rho = \frac{\sigma_\rho}{\rho}\sqrt{\frac{kR_t}{\zeta}\left(\frac{\partial\rho}{\partial x_i}\right)^2} \quad , \quad C_1 = 0.60 \quad , \quad C_{\zeta_1} = 2.10$$

$$\frac{1}{\tau_\rho} = \frac{1}{\rho}\sqrt{\left(\epsilon_{ijk}U_j\frac{\partial\rho}{\partial x_k}\right)^2\frac{k}{U_l^2}}$$

9 Tables

Table 9.1: Free Shear Flow Spreading Rates

Flow	Enstrophy	Epsilon	Measured
Far Wake	0.3130	0.256	0.365
Mixing Layer	0.1054	0.098	0.115
Plane Jet	0.1143	0.109	0.100 - 0.110
Round Jet	0.0906	0.120	0.086 - 0.095
Radial Jet	0.0965	0.094	0.096 - 0.110

Table 9.2: Turbulence Model Closure Coefficients - Original

Constants	$k-\zeta$
α_3	0.35
β_4	0.42
β_5	2.37
β_6	0.10
β_7	1.50
β_8	1.15
σ_p	0.6
σ_ρ	5.6
$\frac{1}{\sigma_k}$	1.80
$\frac{1}{\sigma_\zeta}$	1.46
$C_{\mu 1}$	32.0
$C_{\mu 2}$	32.0
δ	0.10

Table 9.3: Turbulence Model Closure Coefficients - Final

Constants	$k-\zeta$
α_3	0.35
β_4	0.42
β_5	2.37
β_6	0.10
β_7	1.50
β_8	1.15
σ_r	0.07
σ_p	0.065
σ_ρ	91.9
$\frac{1}{\sigma_k}$	1.80
$\frac{1}{\sigma_\zeta}$	1.46
δ	0.10

Table 9.4: Cases Considered

Flat Plate	Mach #	Re		Grid
	0.20	$9.0x10^6$		NAx201 (BL code)
Airfoil	Mach #	Re	AOA	Grid
NACA 0012	0.50	$2.91x10^6$	2.06°	287x81
NACA 0012	0.799	$9.0x10^6$	0.00°	287x81
RAE 2822	0.73	$6.5x10^6$	2.80°	321x91
RAE 2822	0.73	$6.5x10^6$	2.80°	231x51
RAE 2822	0.73	$6.5x10^6$	2.80°	143x41
NACA 4412	0.20	$1.5x10^6$	13.87°	237x91
NACA 0012	0.55	$9.0x10^6$	8.34°	287x71
NACA 0012	0.799	$9.0x10^6$	2.26°	287x71
RAE 2822 (case 9)	0.73	$6.5x10^6$	2.80°	321x91
RAE 2822 (case10)	0.75	$6.2x10^6$	2.72°	231x61
Cylinder-Flare	Mach #	Re		Grid
	2.89	$15.0x10^6$		87x99x99

10 Figures

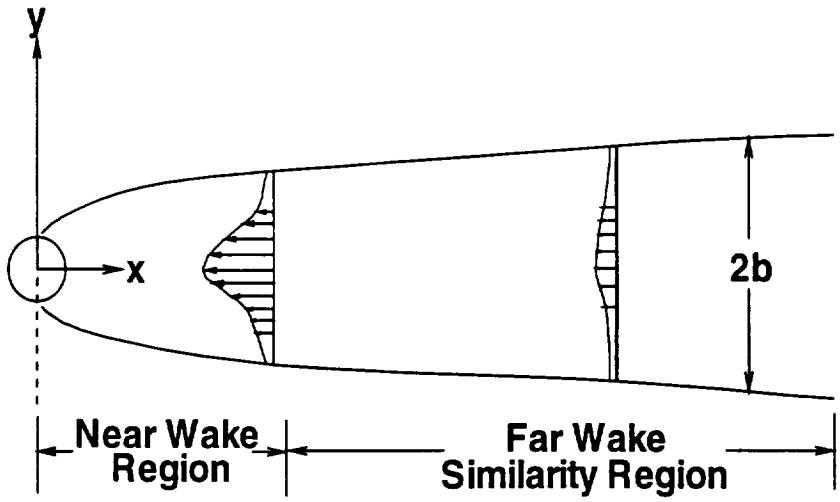

Figure 10.1: Wake flow schematic

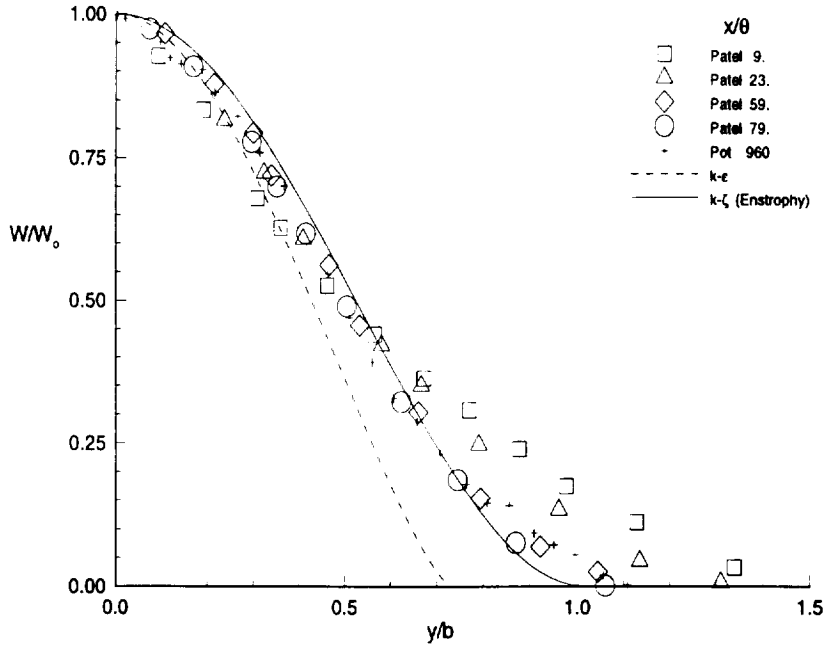

Figure 10.2: Self-similar velocity (Planar Wake)

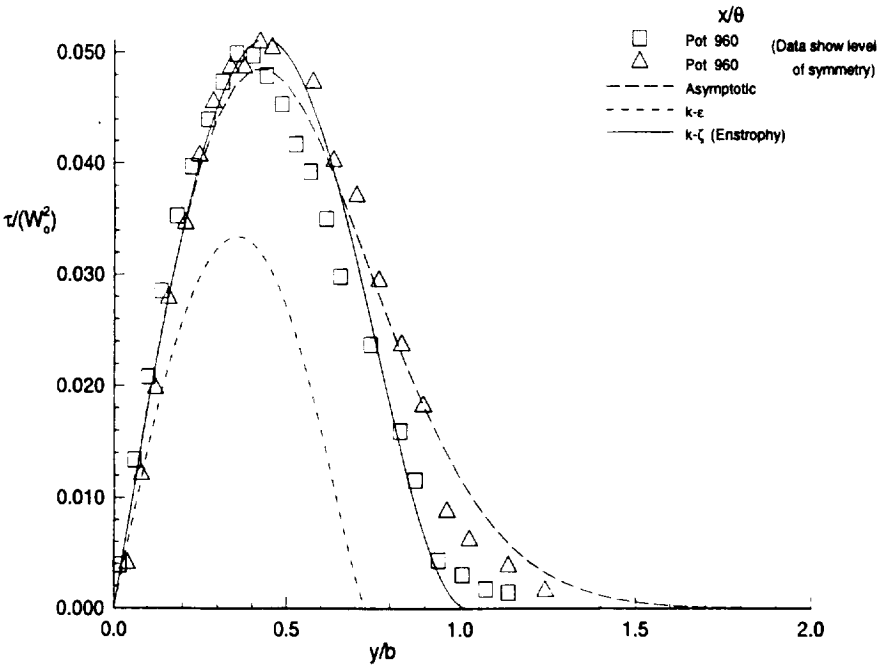

Figure 10.3: Self-similar shear stress (Planar Wake)

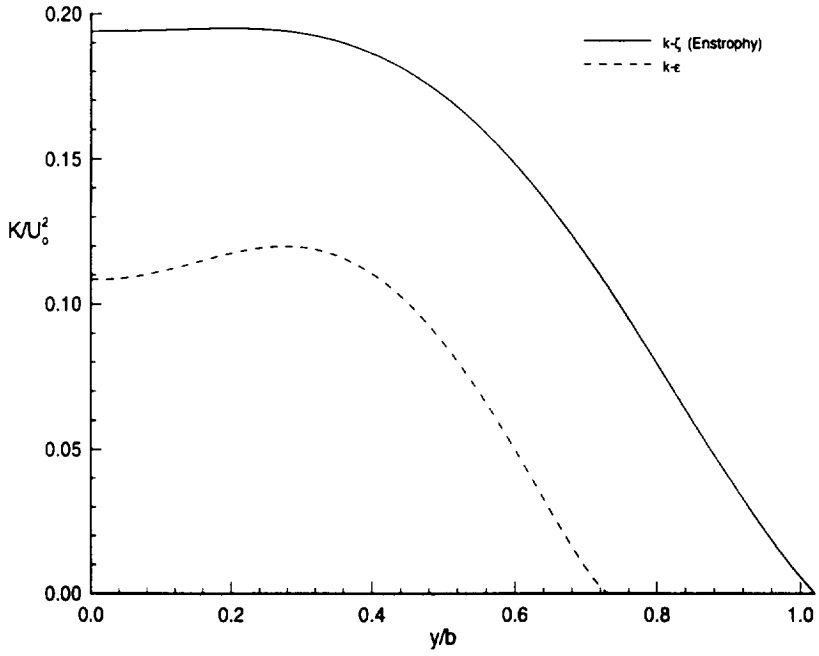

Figure 10.4: Self-similar turbulent kinetic energy (Planar Wake)

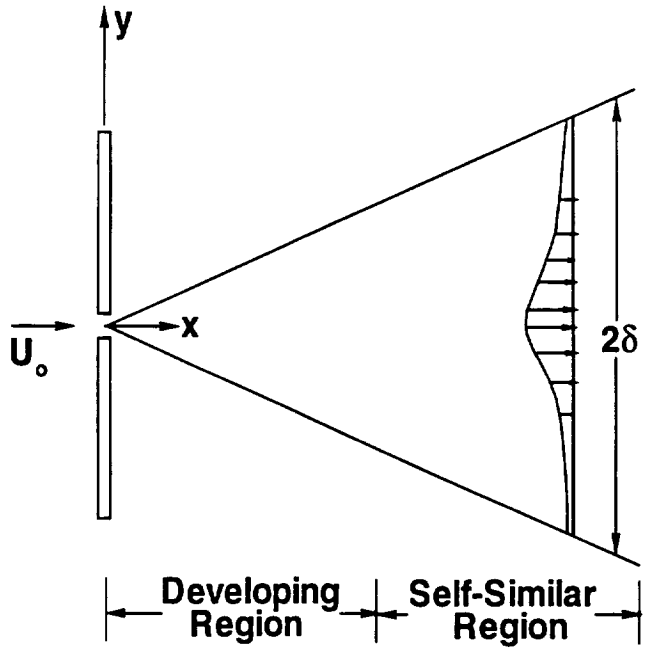

Figure 10.5: Schematic diagram of planar jet

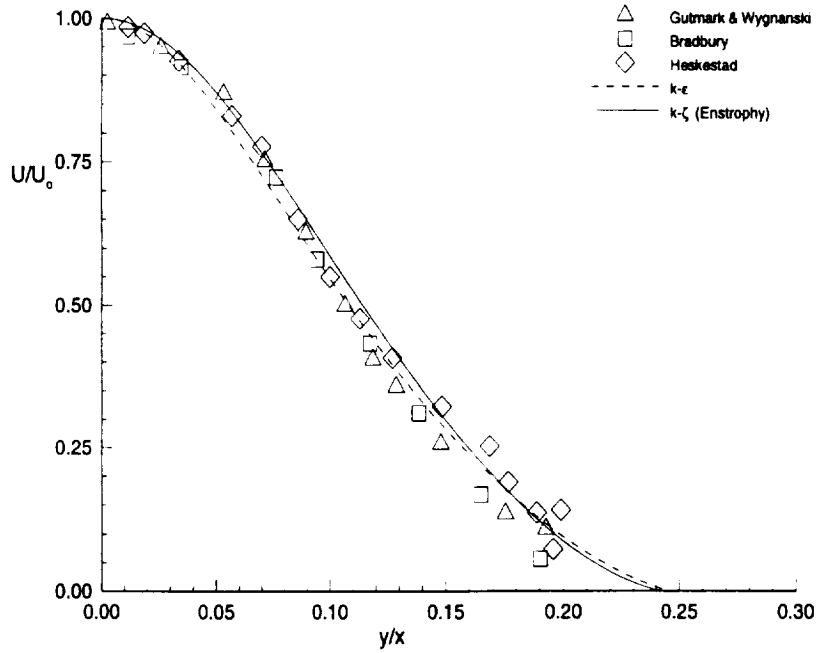

Figure 10.6: Self-similar velocity (Planar Jet)

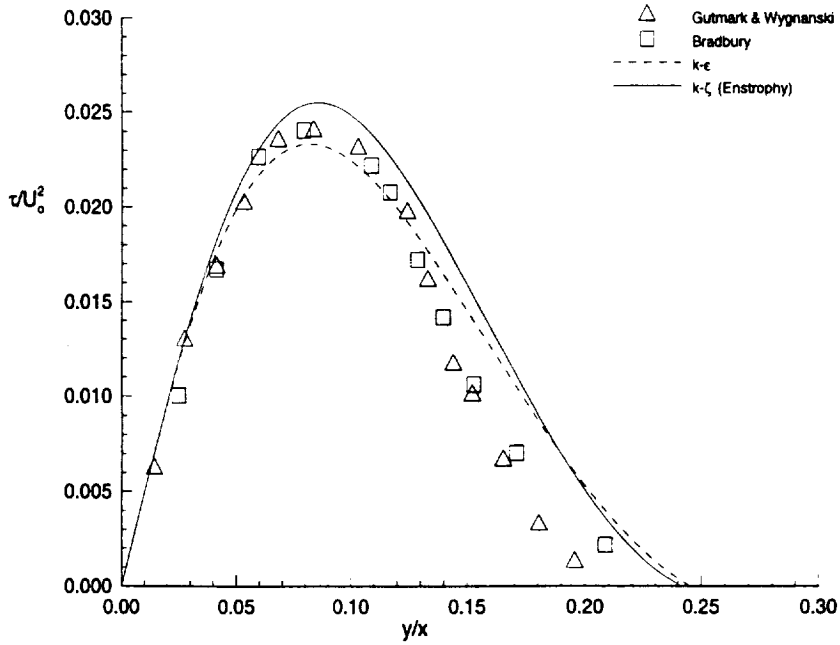

Figure 10.7: Self-similar shear stress (Planar Jet)

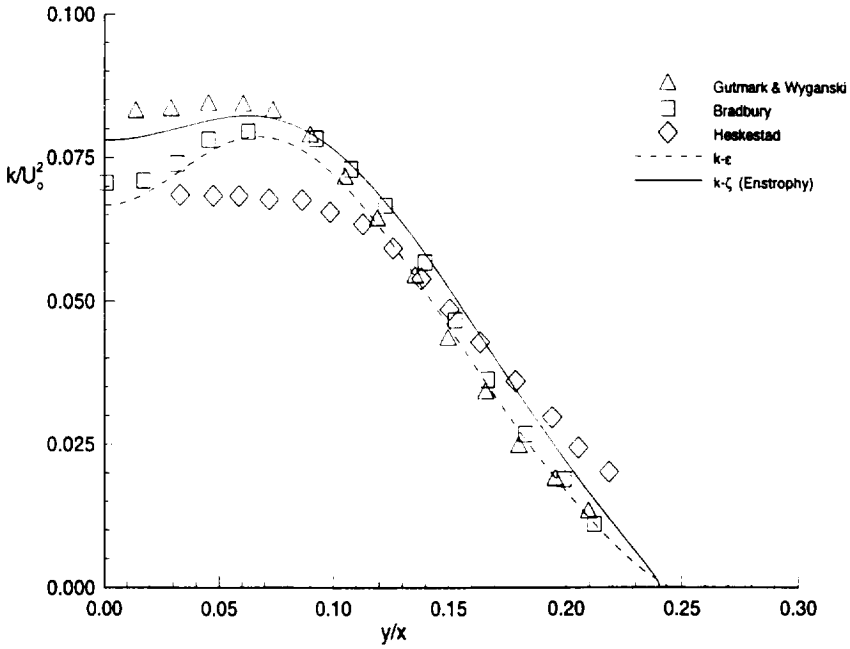

Figure 10.8: Self-similar turbulent kinetic energy (Planar Jet)

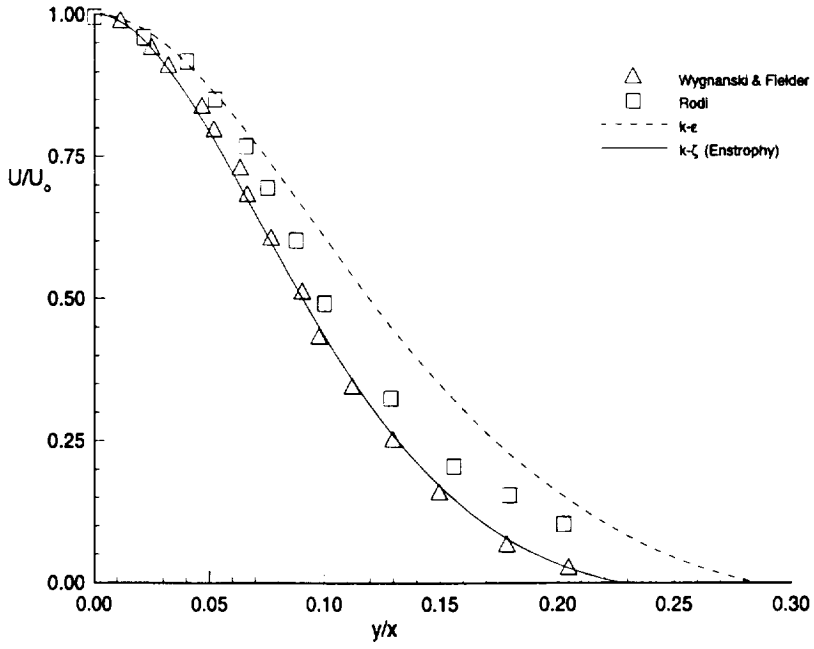

Figure 10.9: Self-similar velocity (Round Jet)

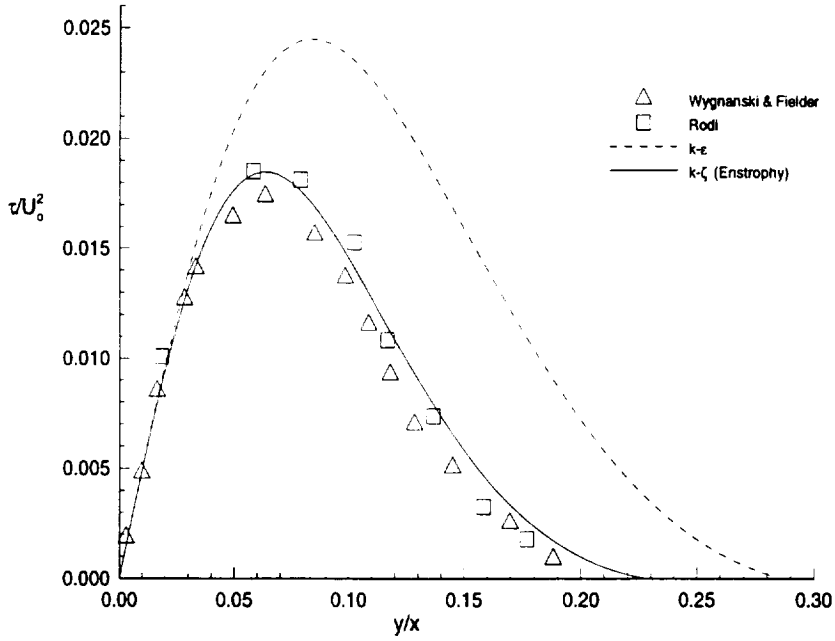

Figure 10.10: Self-similar shear stress (Round Jet)

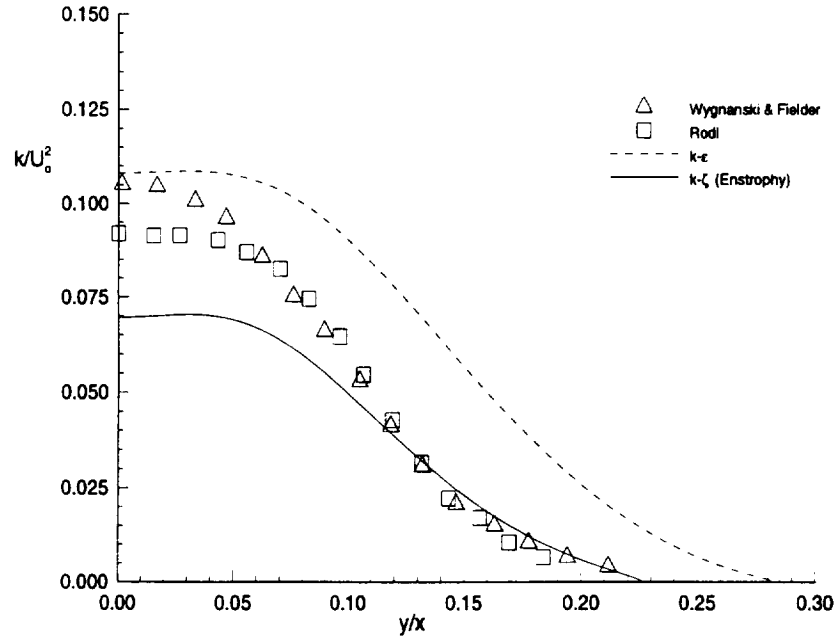

Figure 10.11: Self-similar turbulent kinetic energy (Round Jet)

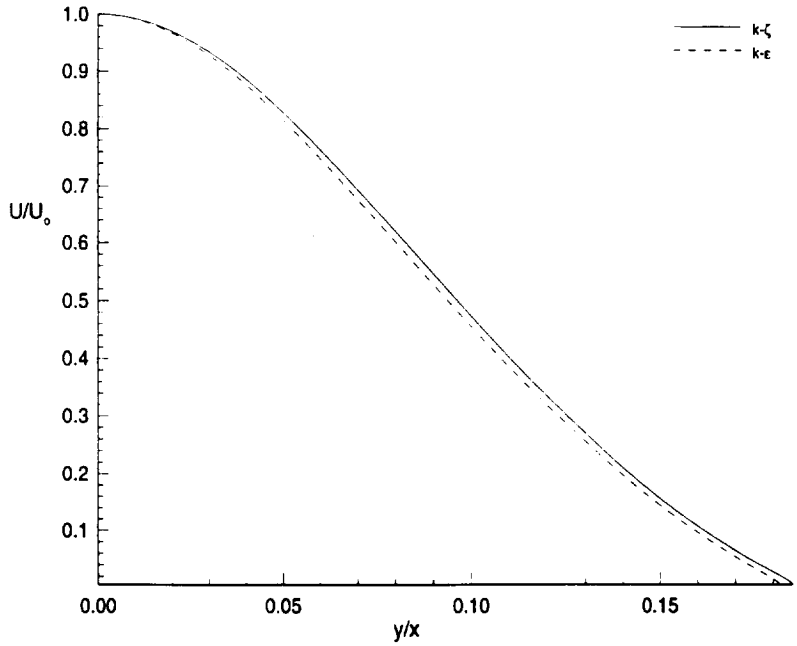

Figure 10.12: Self-similar velocity (Radial Jet)

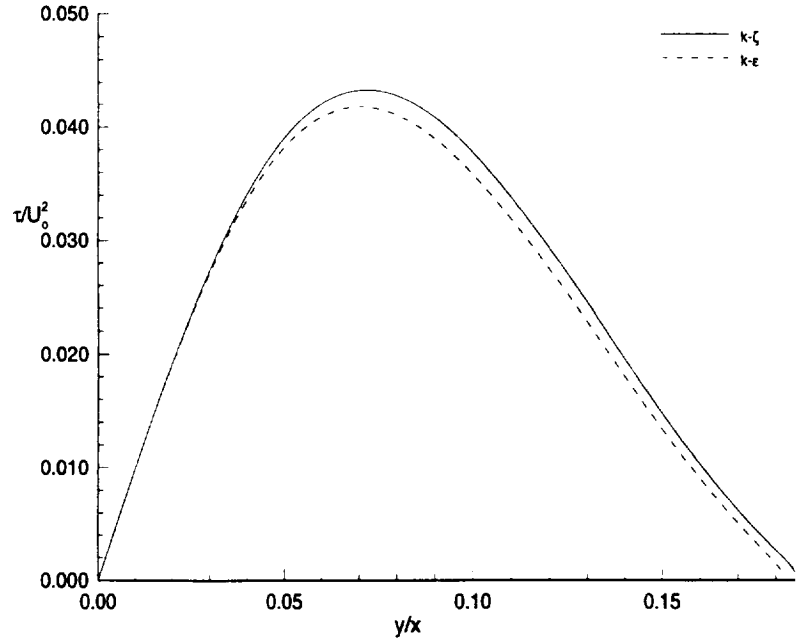

Figure 10.13: Self-similar shear stress (Radial Jet)

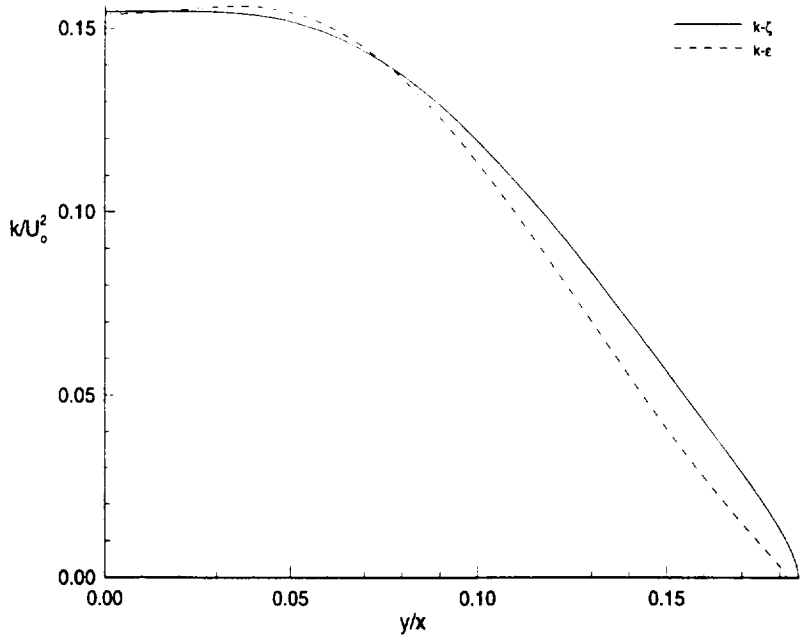

Figure 10.14: Self-similar turbulent kinetic energy (Radial Jet)

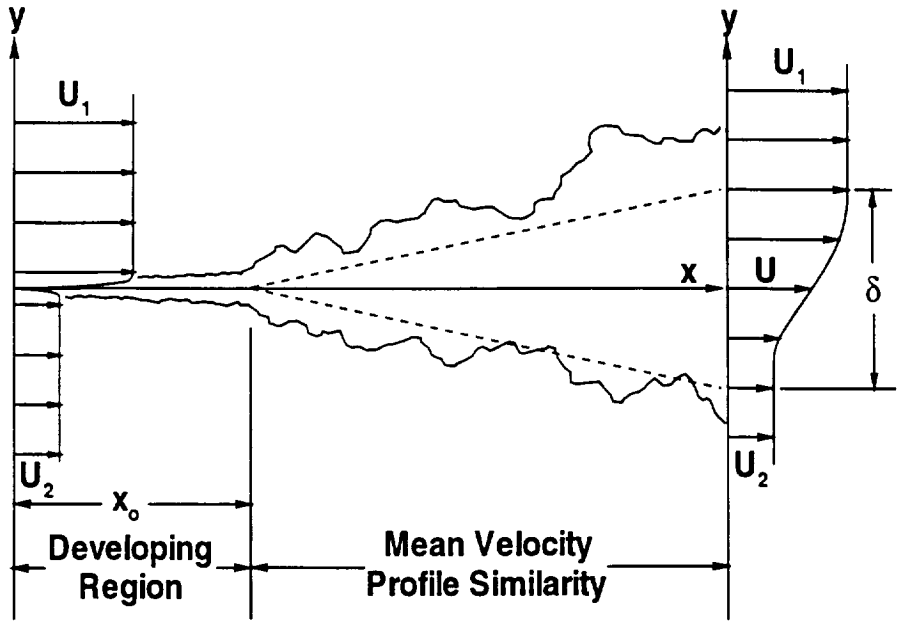

Figure 10.15: Schematic diagram of mixing layer

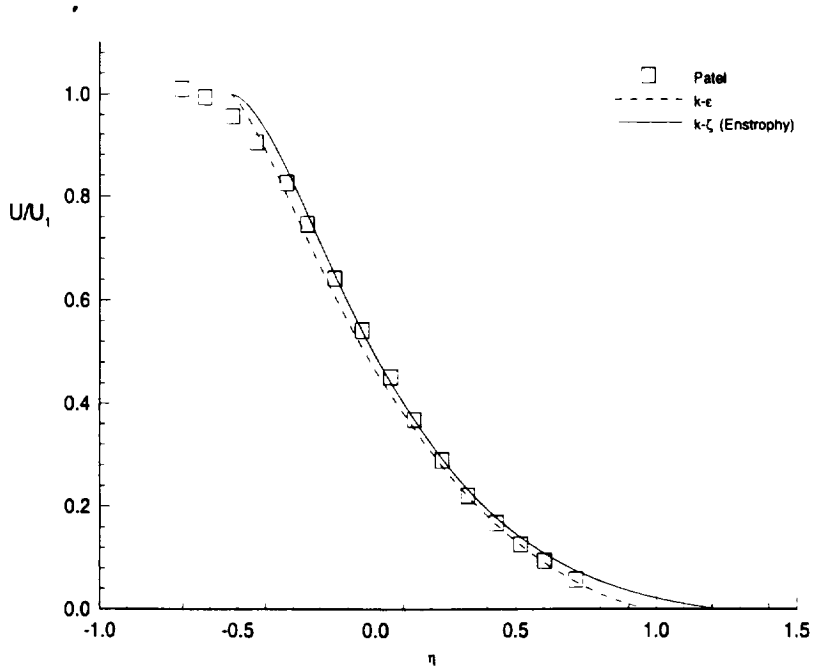

Figure 10.16: Self-similar velocity (Mixing Layer)

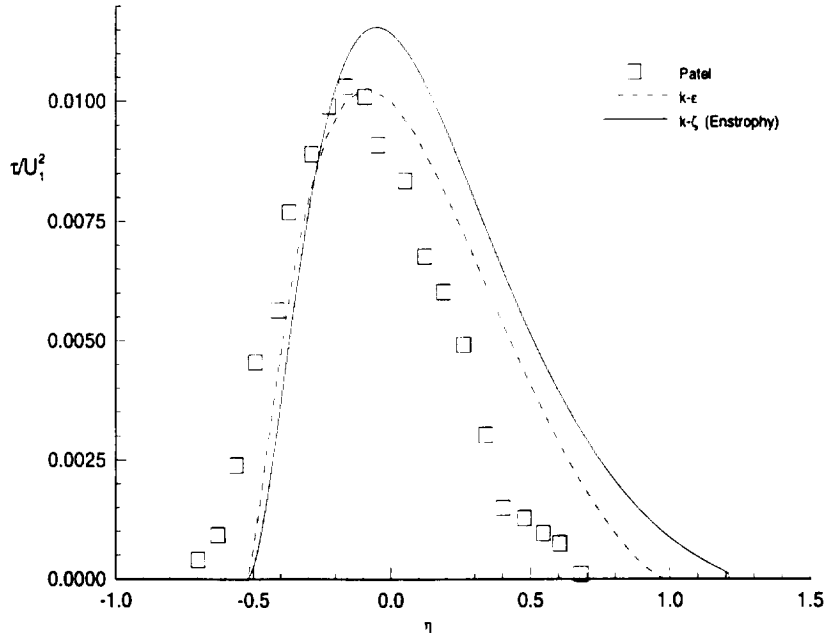

Figure 10.17: Self-similar Shear Stress (Mixing Layer)

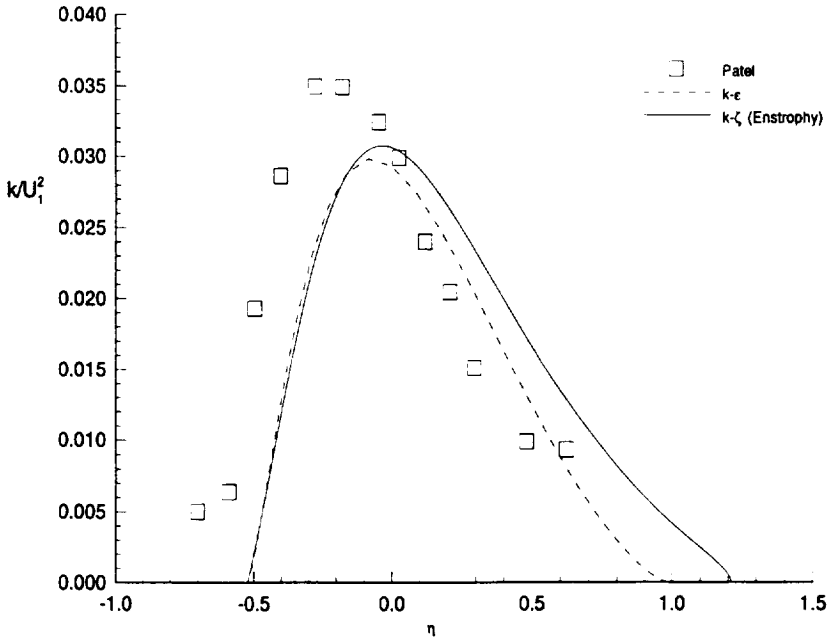

Figure 10.18: Self-similar turbulent kinetic energy (Mixing Layer)

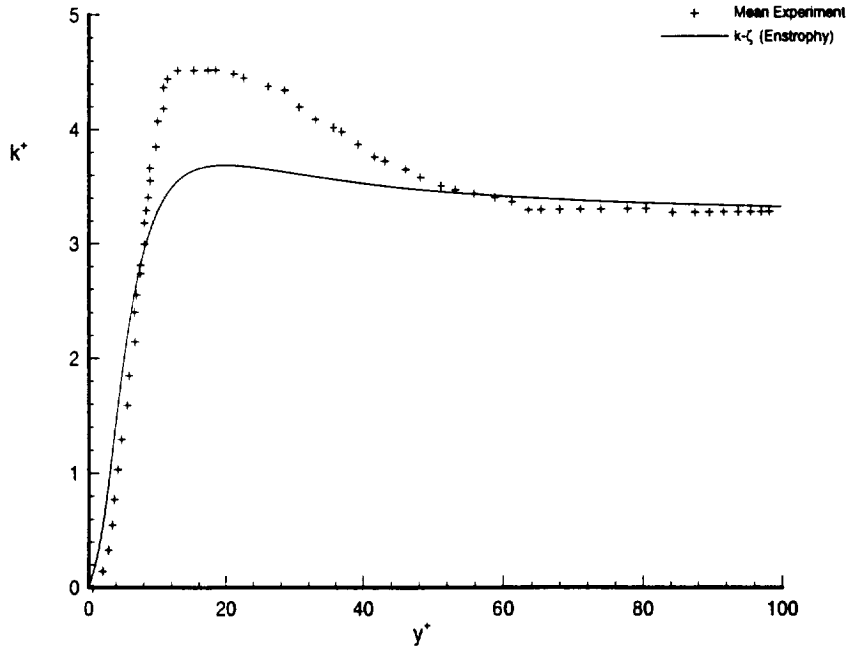

Figure 10.19: Near wall turbulent kinetic energy for flat plate

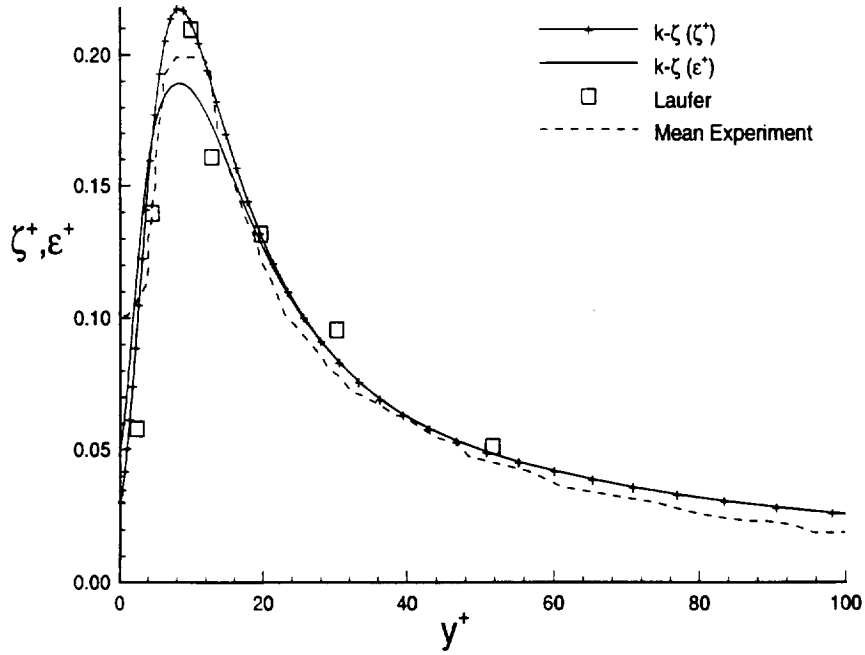

Figure 10.20: Near wall Enstrophy for flat plate

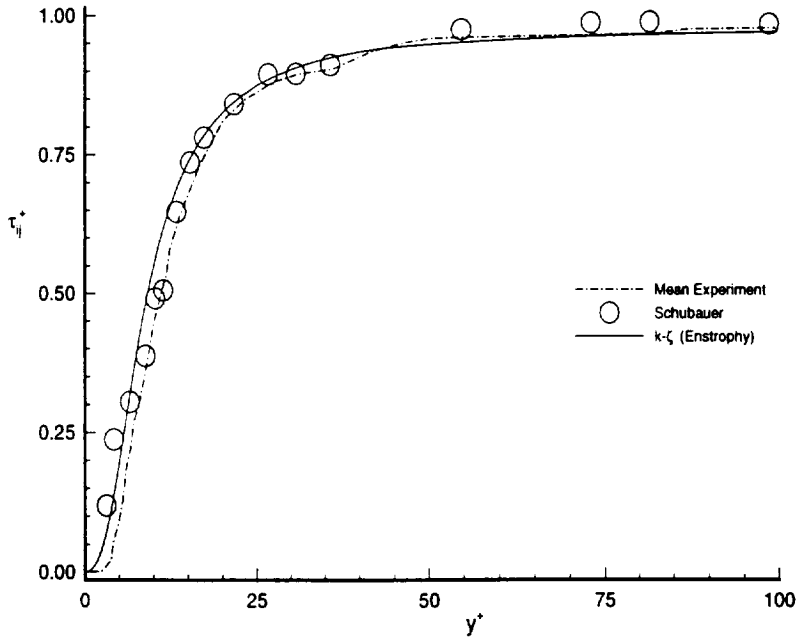

Figure 10.21: Near wall shearing stress for flat plate

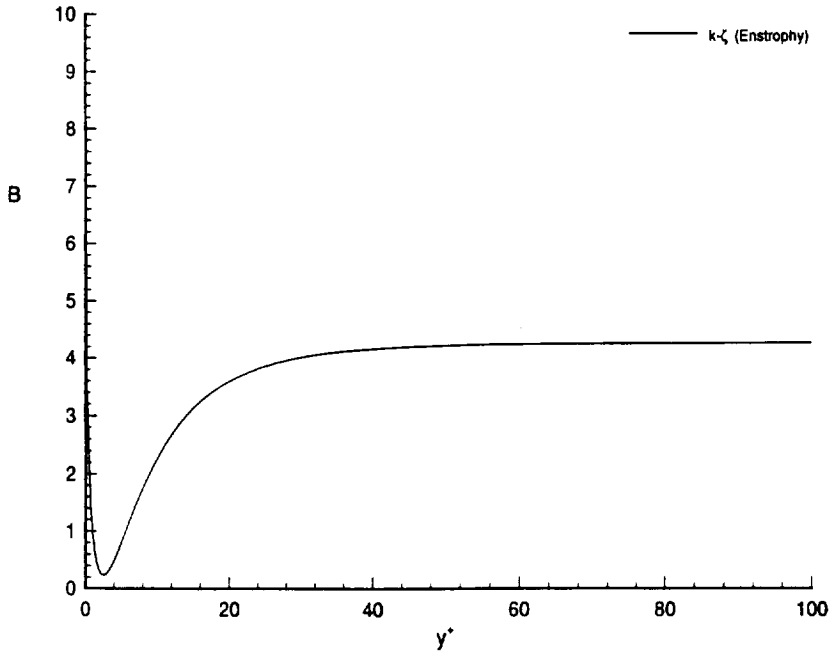

Figure 10.22: Flat plate log-law constant

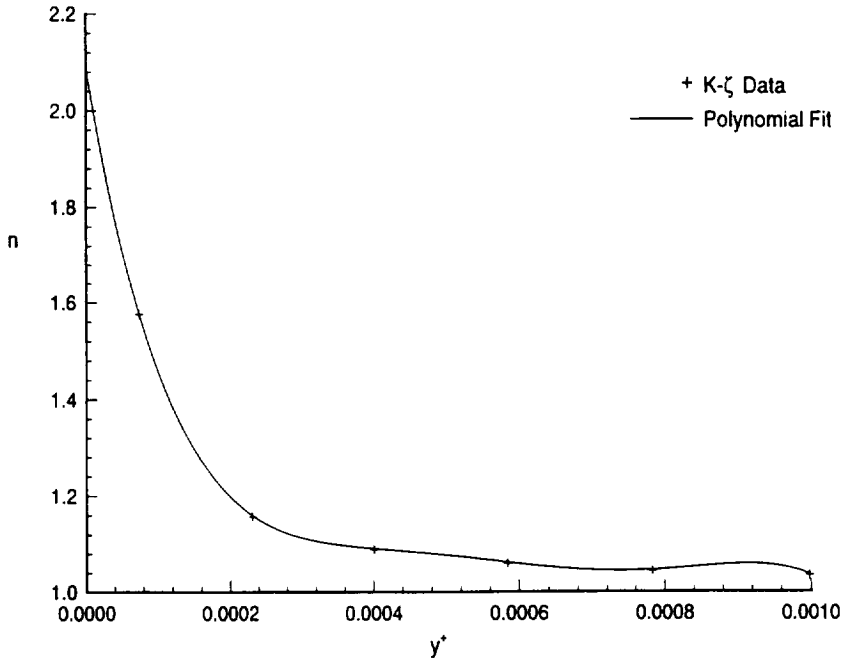

Figure 10.23: Near wall variation of turbulent kinetic energy $k = k_o y^n$

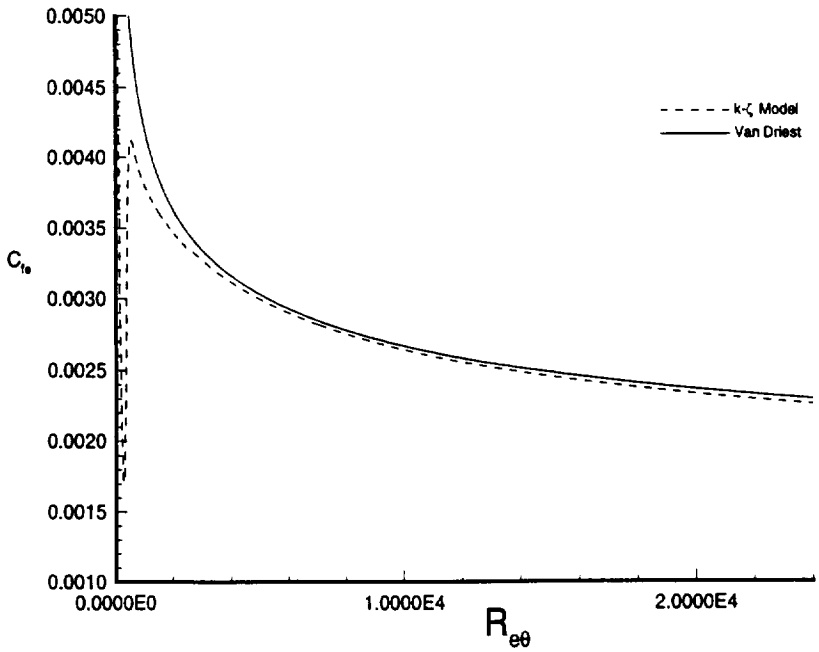

Figure 10.24: Flat plate skin friction coefficient

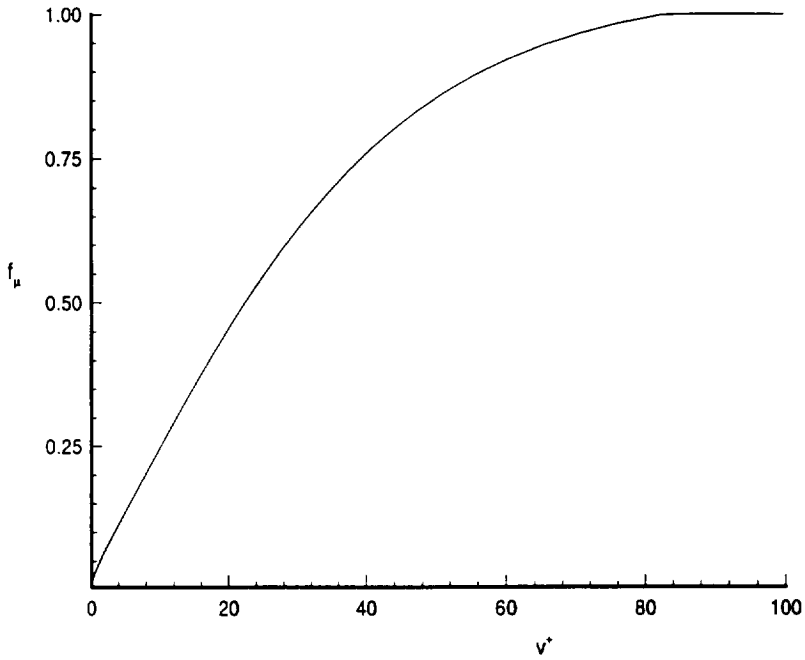

Figure 10.25: Flat plate wall damping function

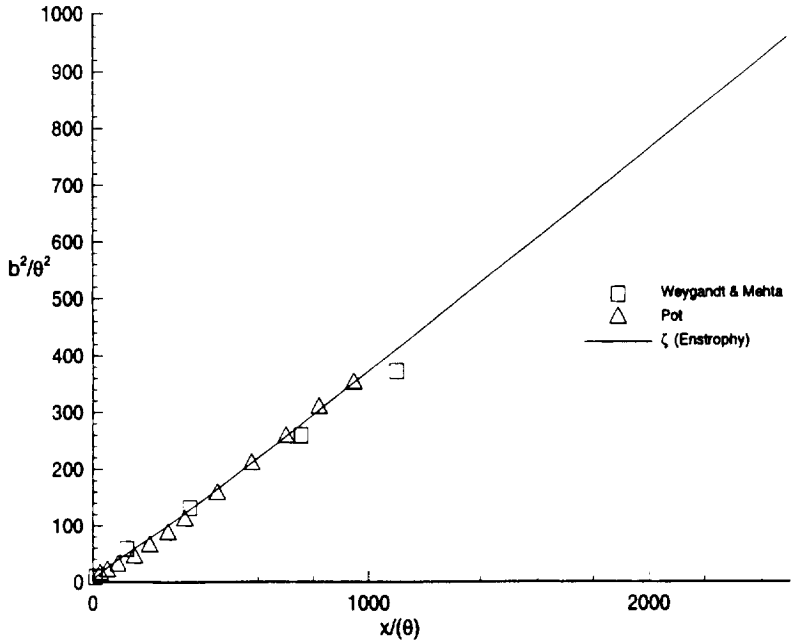

Figure 10.26: Near wake growth rate

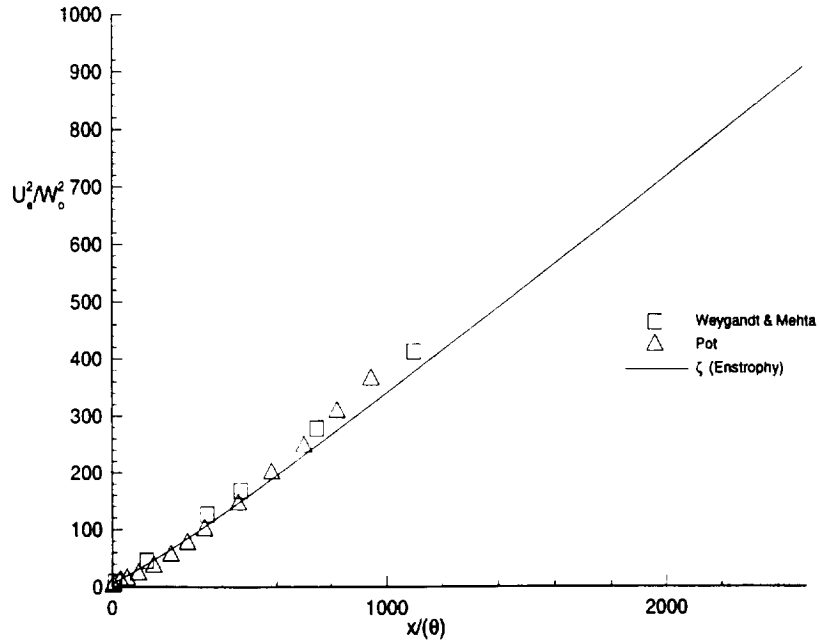

Figure 10.27: Centerline Defect velocity profiles

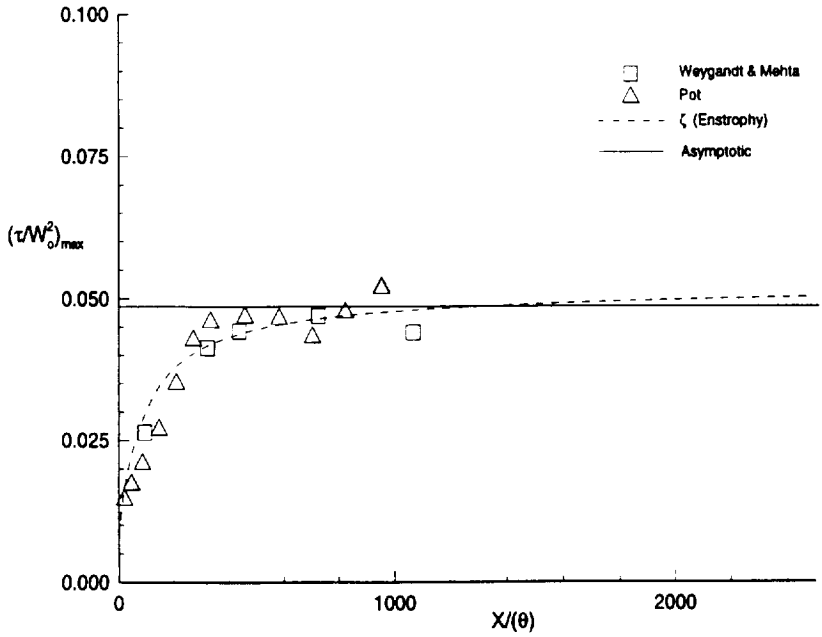

Figure 10.28: Peak shearing stress for near wake region

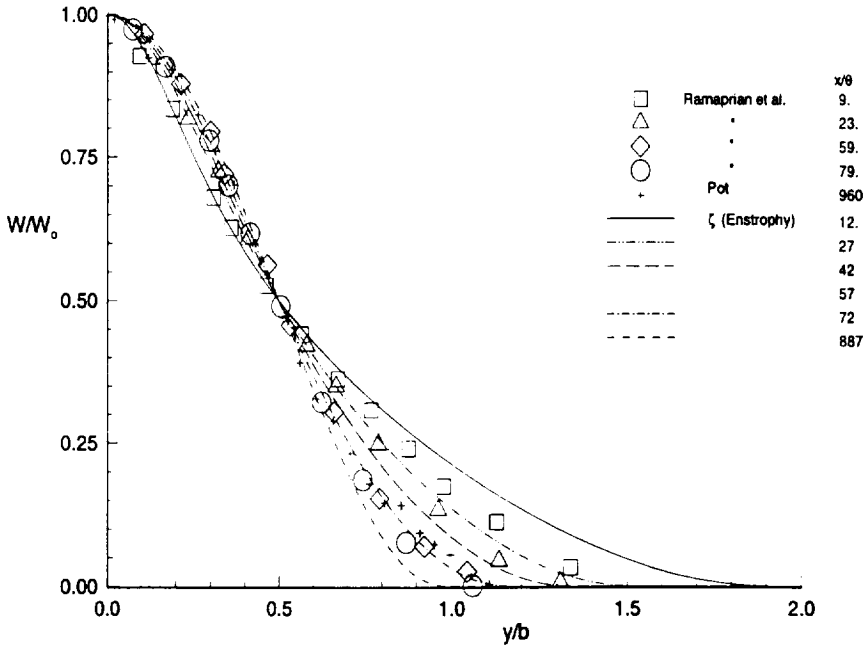

Figure 10.29: Defect velocity profiles

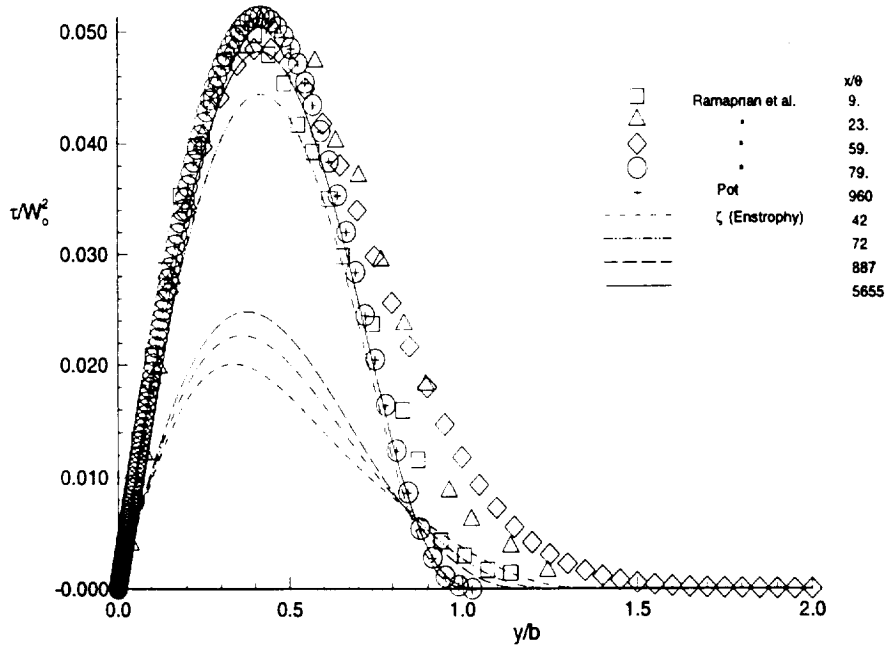

Figure 10.30: Wake shear stress profiles

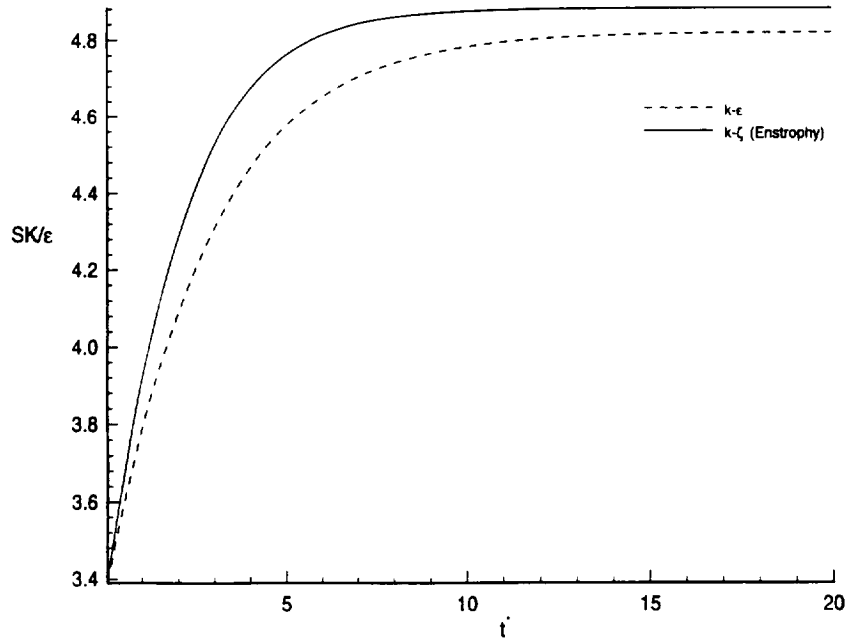

Figure 10.31: Time decay of Homogeneous shear parameter

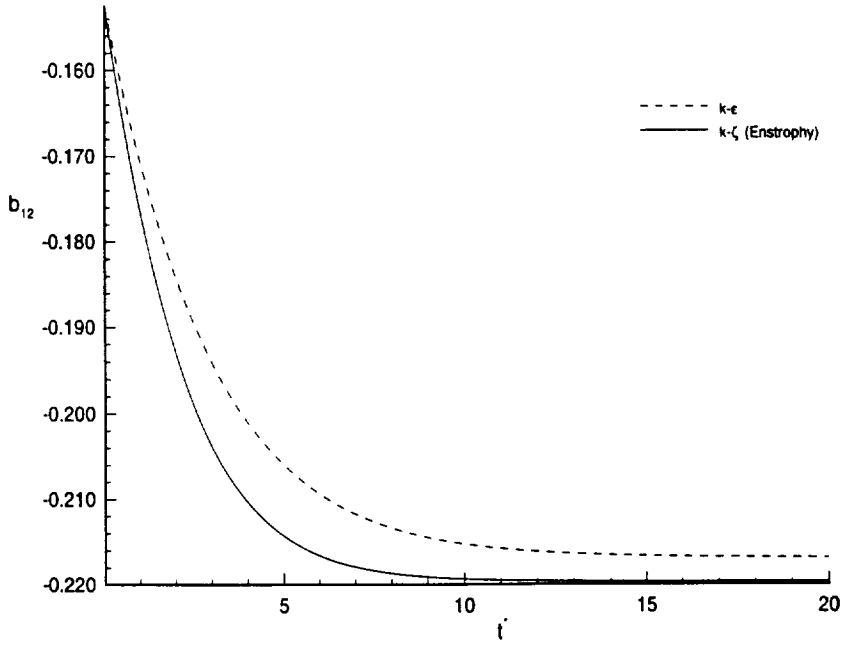

Figure 10.32: Anisotropy tensor for homogeneous shear flow

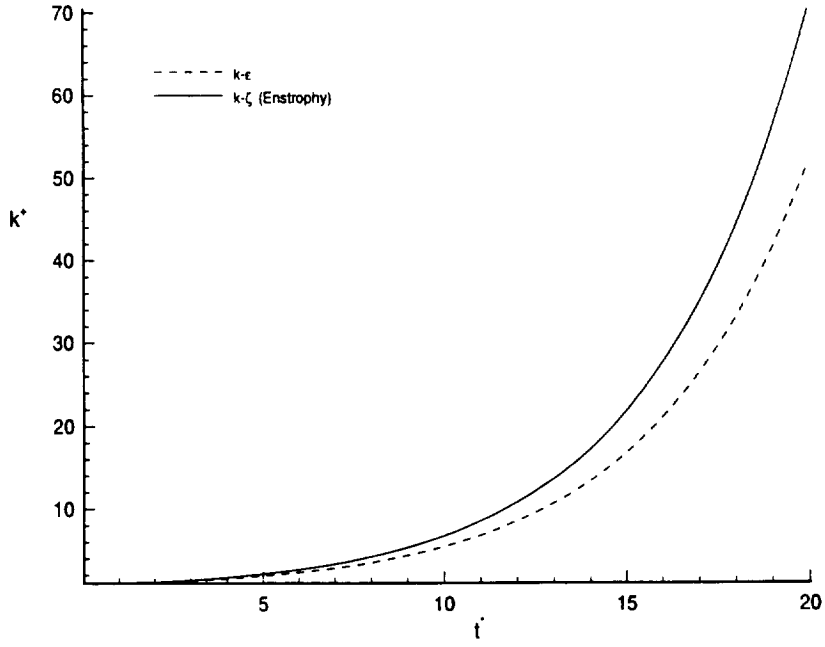

Figure 10.33: Time decay of k^+

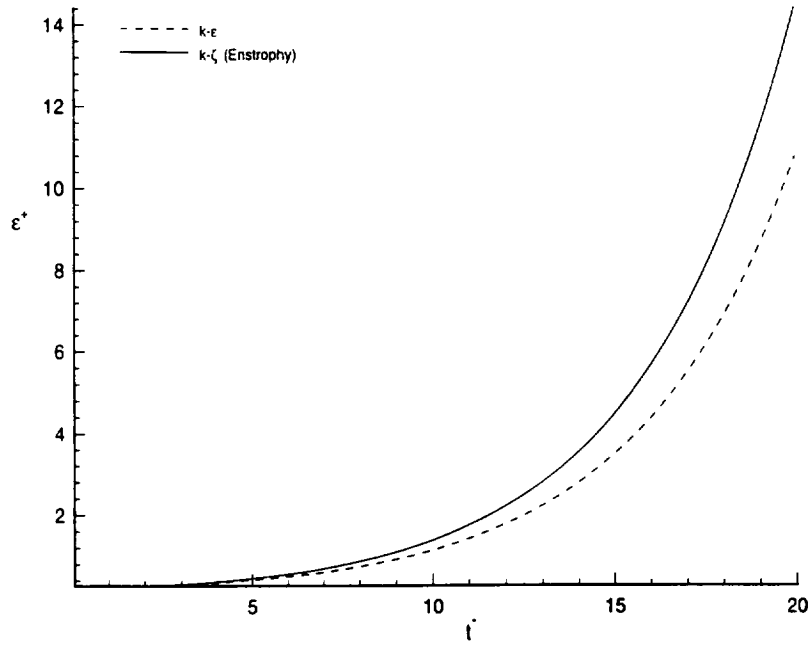

Figure 10.34: Time decay of ϵ^+

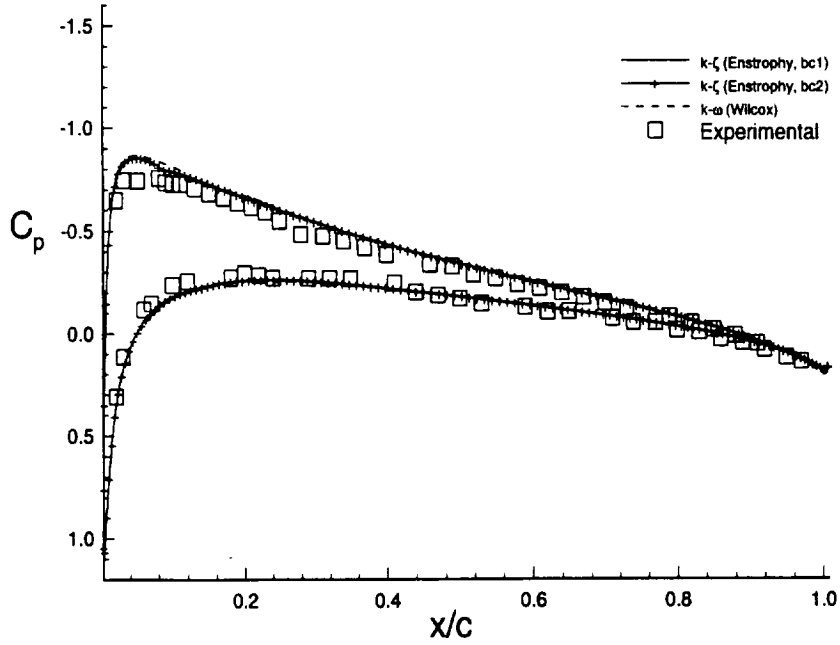

Figure 10.35: Boundary condition comparison of pressure coefficient for NACA 0012 ($M_\infty = .502, R_\infty = 2.91e6, \alpha = 2.06$)

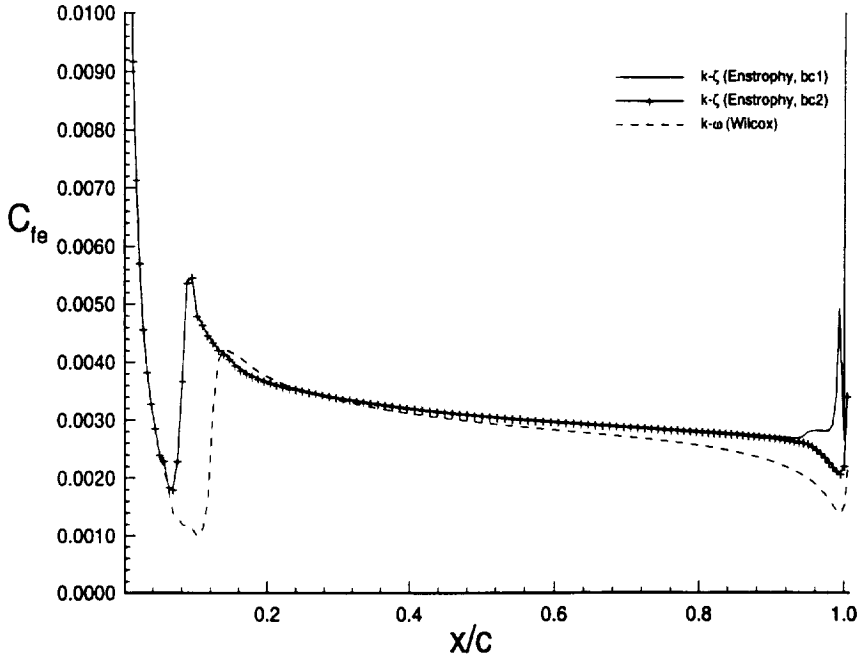

Figure 10.36: Boundary condition comparison of skin friction coefficient for NACA 0012 ($M_\infty = .502, R_\infty = 2.91e6, \alpha = 2.06$)

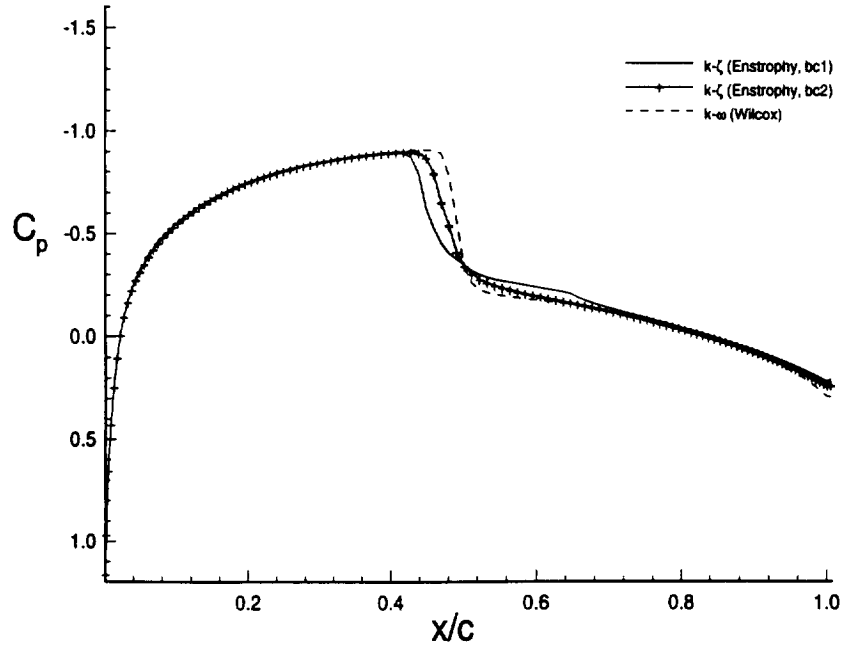

Figure 10.37: Boundary condition comparison of pressure coefficient for NACA 0012 ($M_\infty = 0.8, R_\infty = 9.0e6, \alpha = 0.0$)

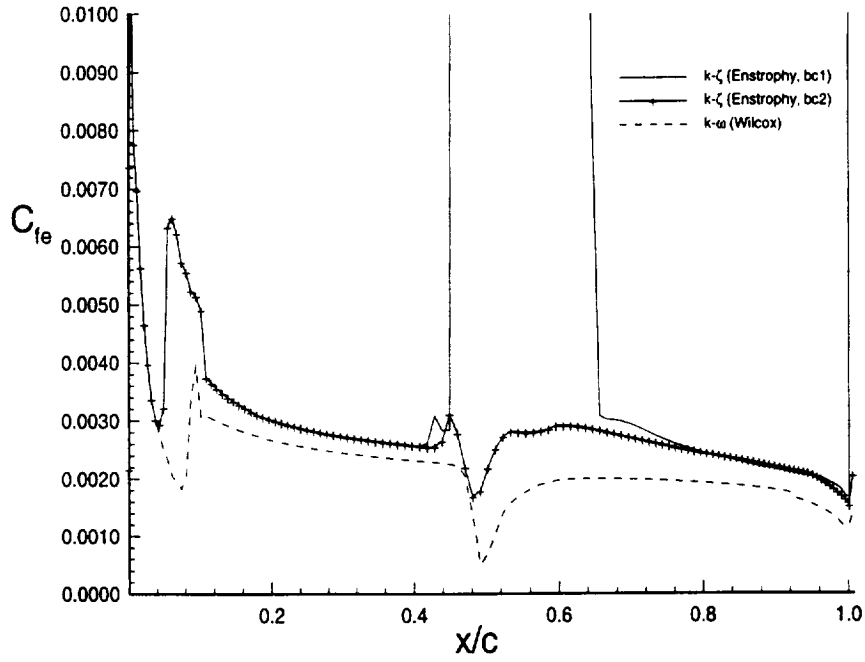

Figure 10.38: Boundary condition comparison of skin friction coefficient for NACA 0012 ($M_\infty = 0.8, R_\infty = 9.0e6, \alpha = 0.0$)

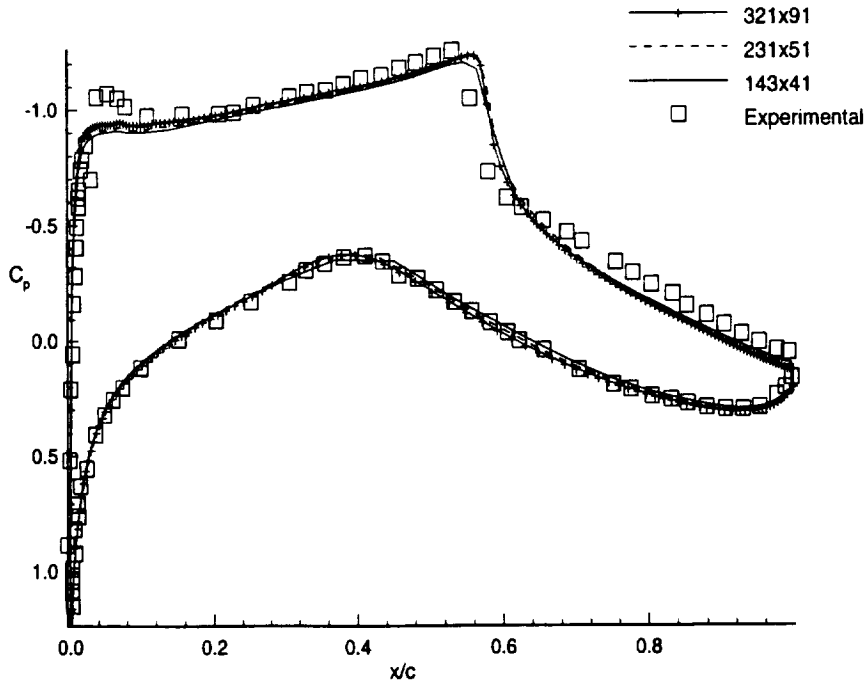

Figure 10.39: Pressure coefficient for RAE2822 grid study

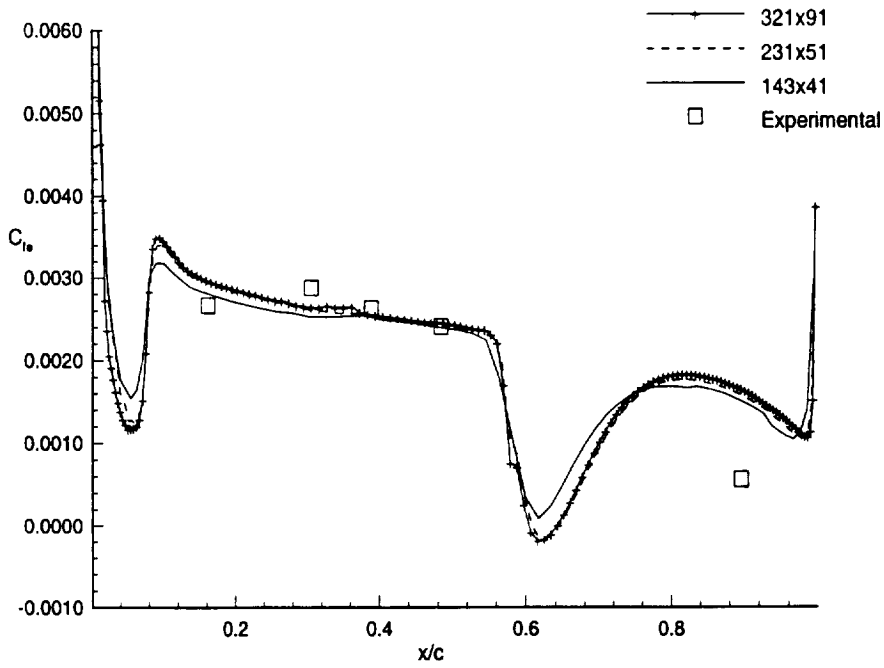

Figure 10.40: Skin friction coefficient for RAE2822 grid study

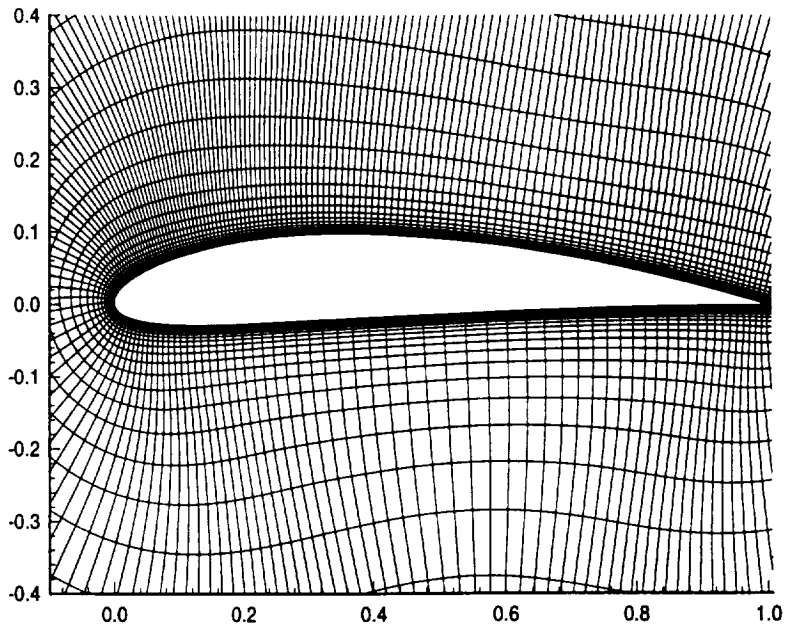

Figure 10.41: Airfoil geometry for NACA 4412

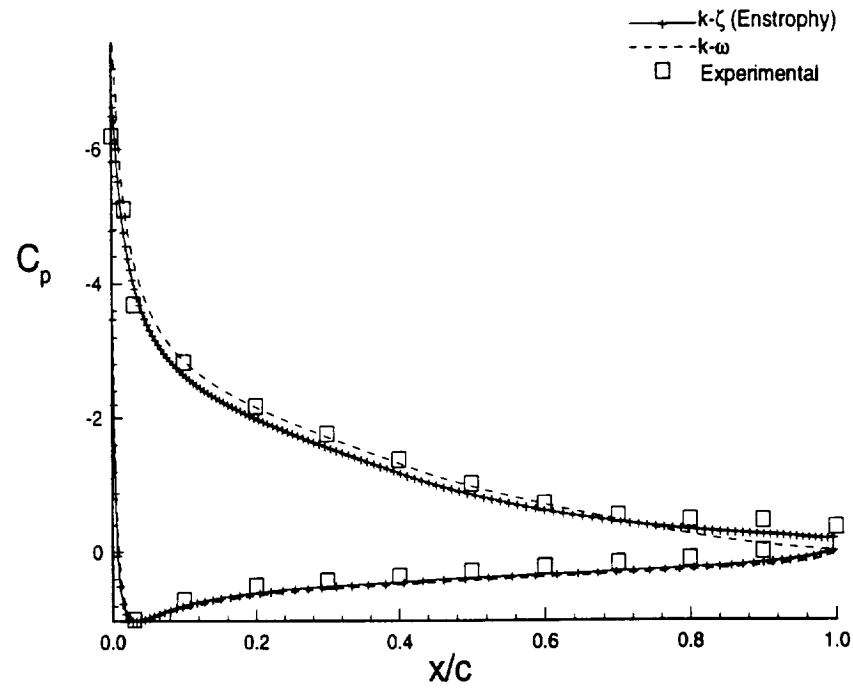

Figure 10.42: NACA 4412 Pressure coefficient

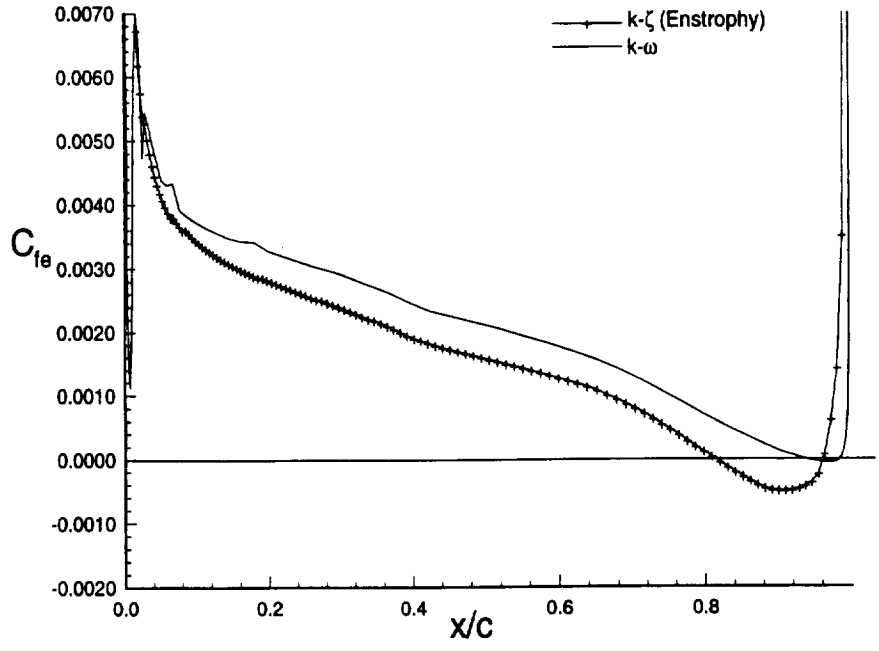

Figure 10.43: NACA 4412 Skin friction coefficient

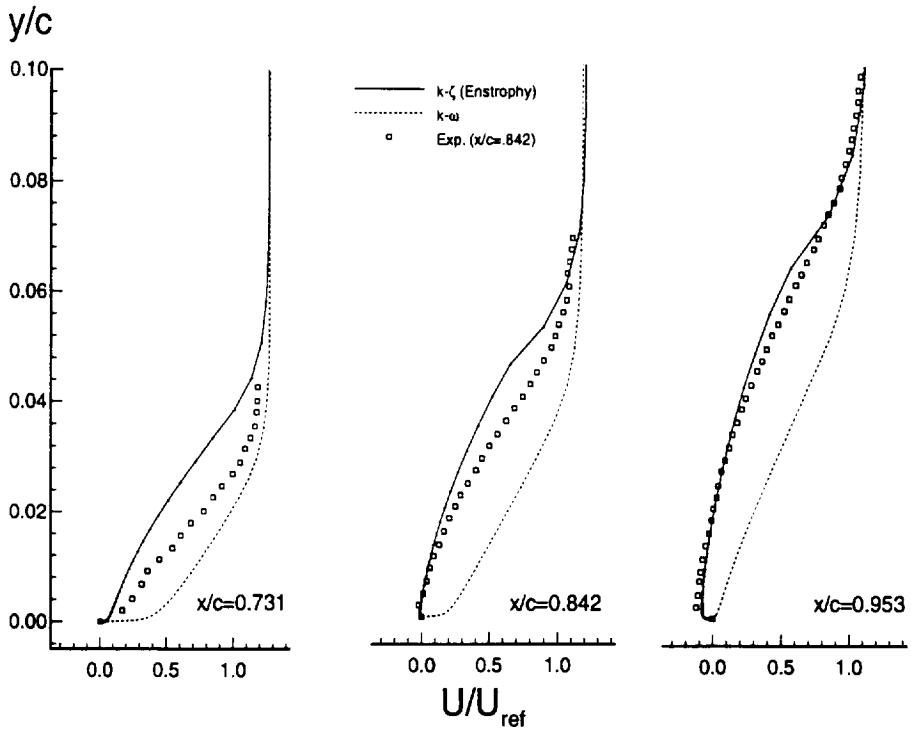

Figure 10.44: NACA 4412 Velocity profiles

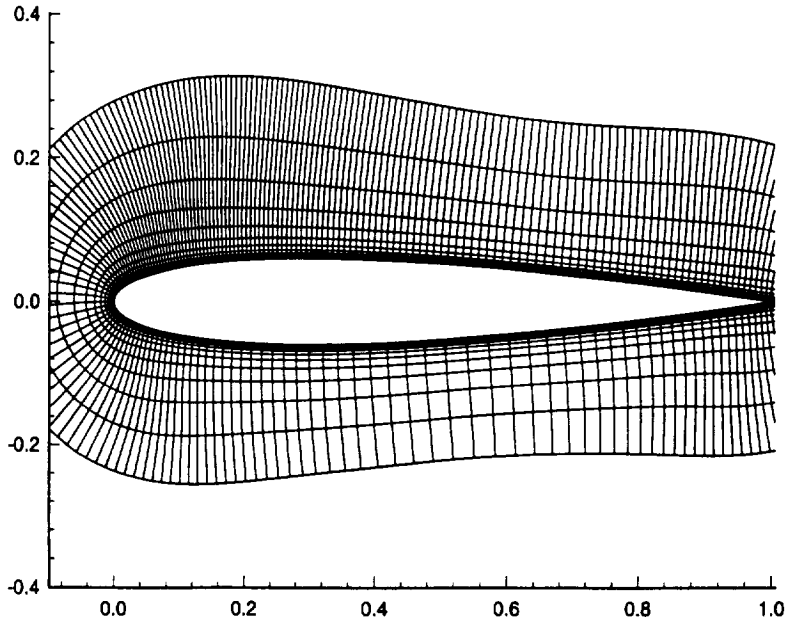

Figure 10.45: Airfoil geometry for NACA 0012

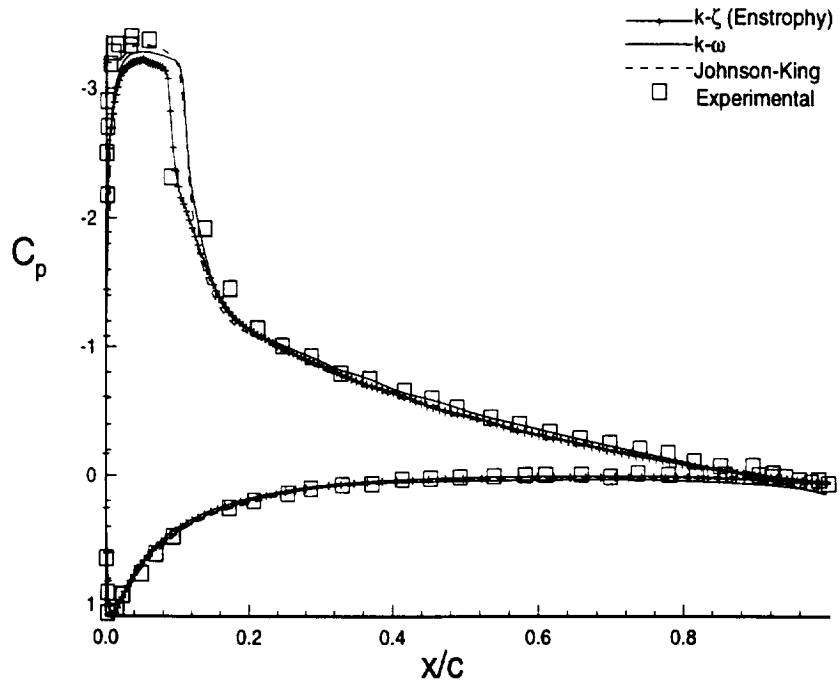

Figure 10.46: NACA 0012 (Case 1) Pressure coefficient

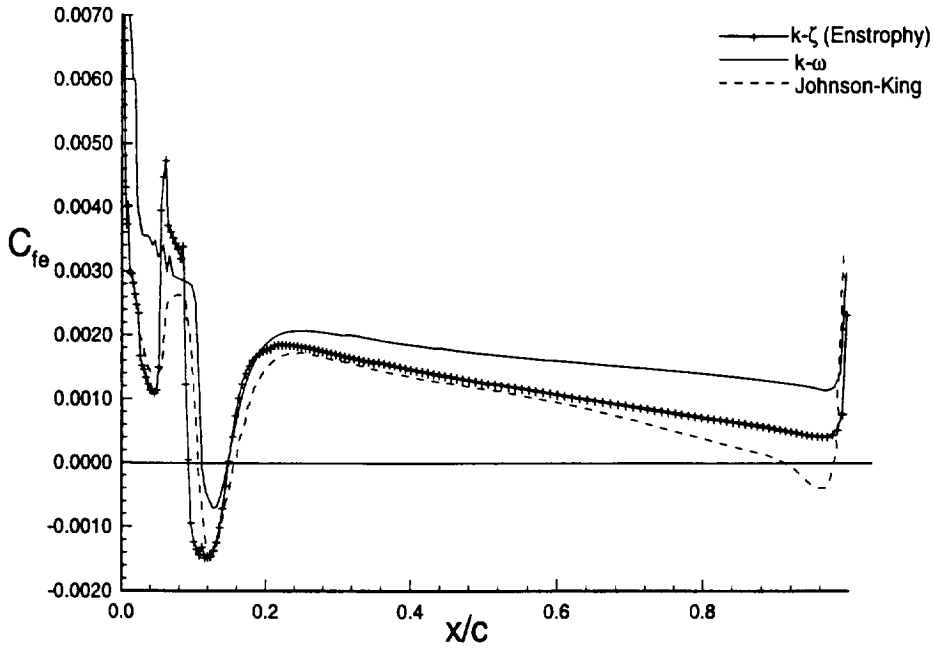

Figure 10.47: NACA 0012 (Case 1) Skin friction coefficient

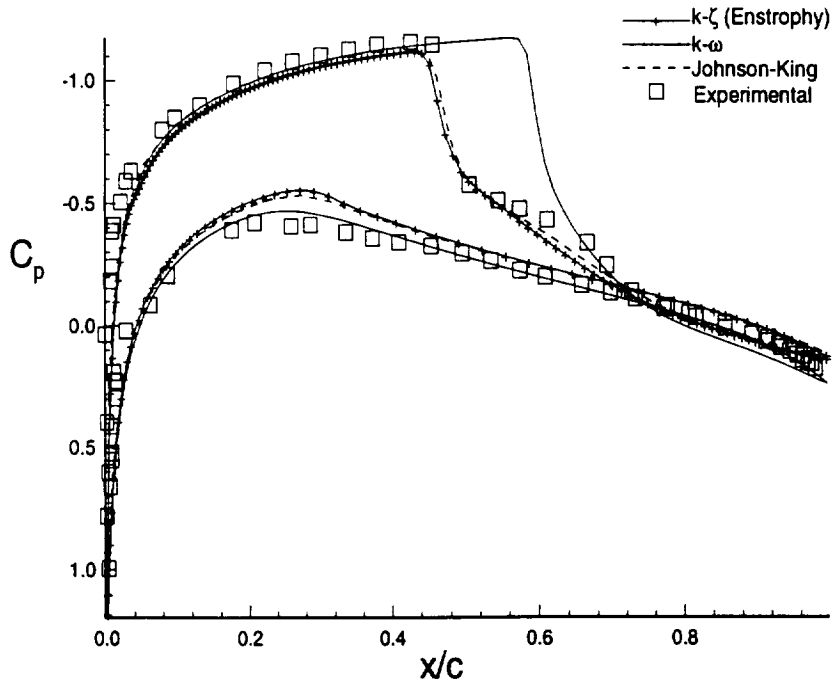

Figure 10.48: NACA 0012 (Case 2) Pressure coefficient

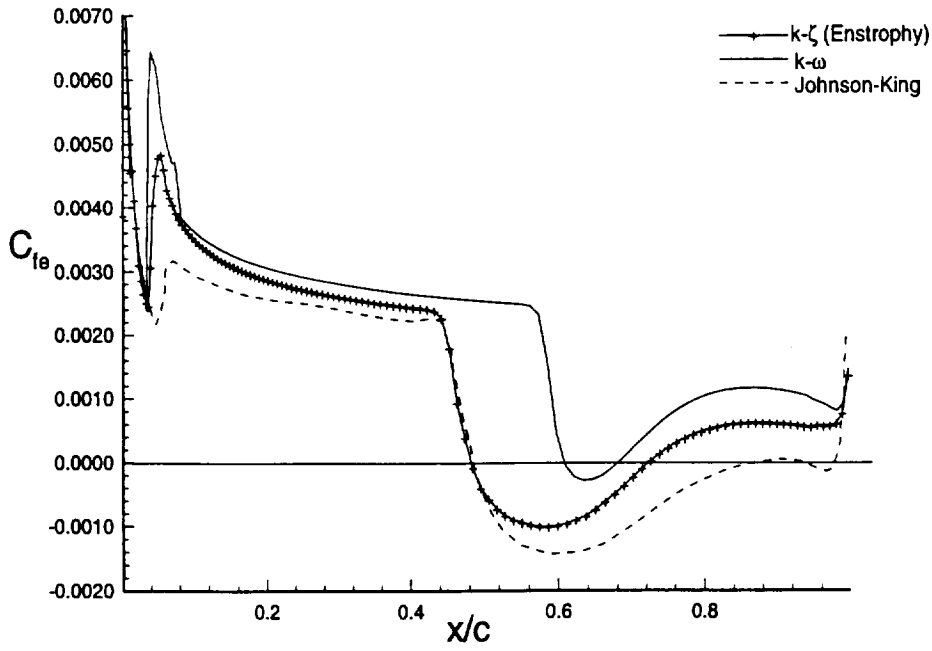

Figure 10.49: NACA 0012 (Case 2) Skin friction coefficient

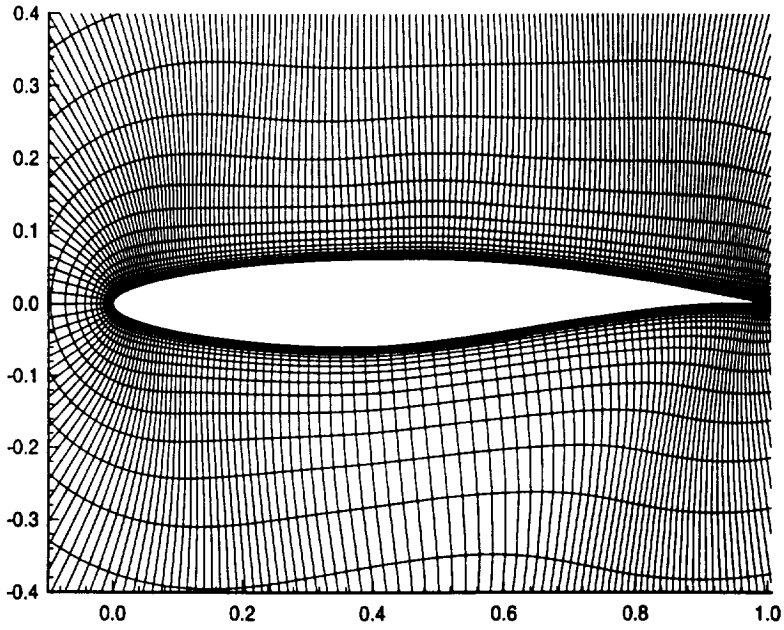

Figure 10.50: Airfoil geometry for RAE 2822

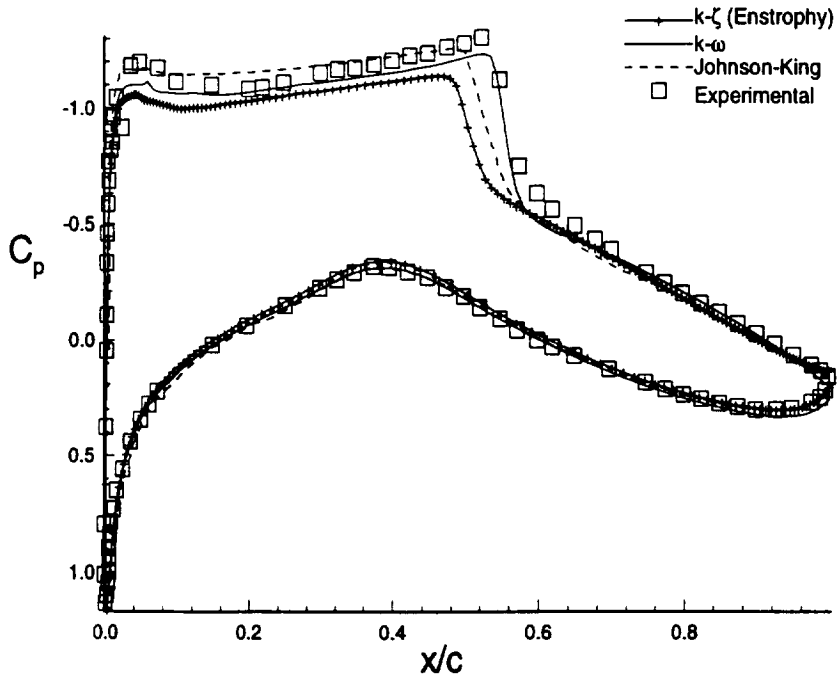

Figure 10.51: RAE 2822 (Case 9) Pressure coefficient

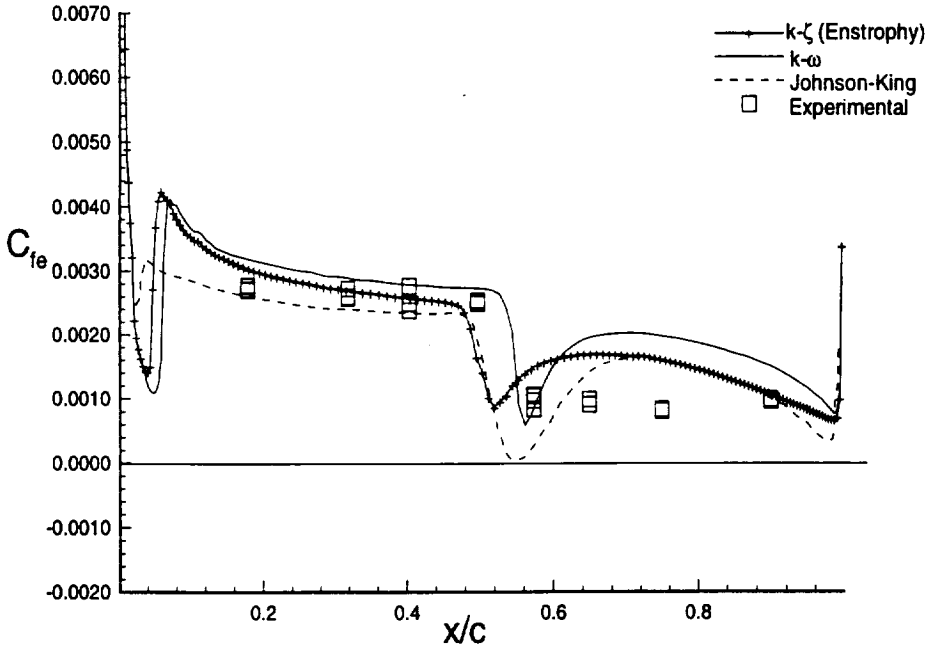

Figure 10.52: RAE2822 (Case 9) Skin friction coefficient

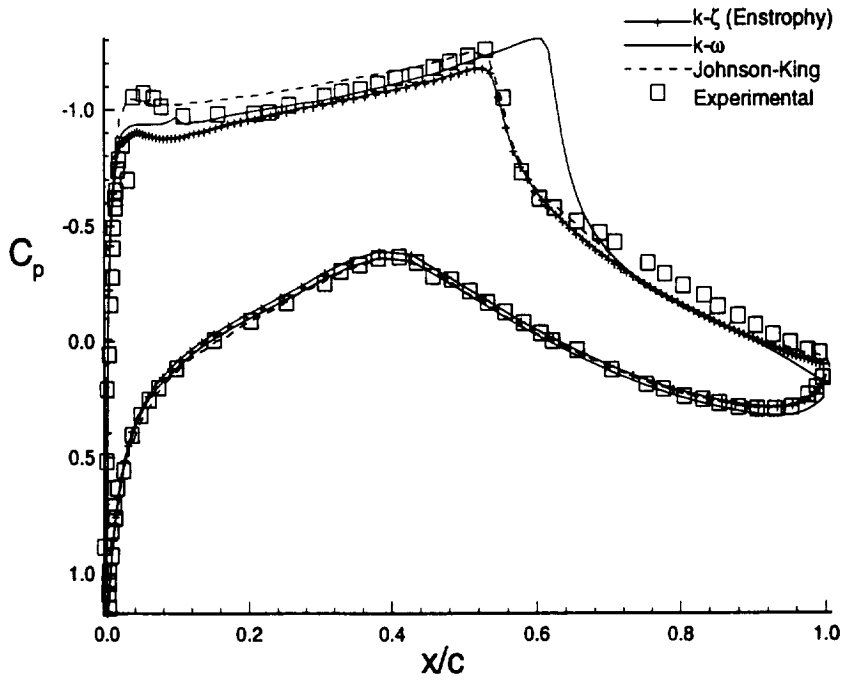

Figure 10.53: RAE 2822 (Case 10) Pressure coefficient

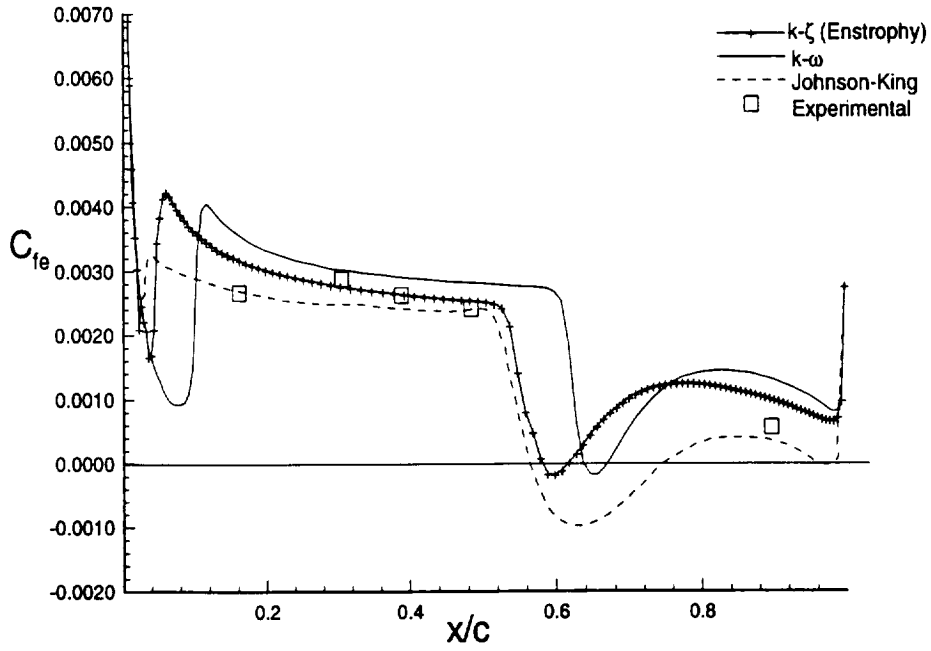

Figure 10.54: RAE2822 (Case 10) Skin friction coefficient

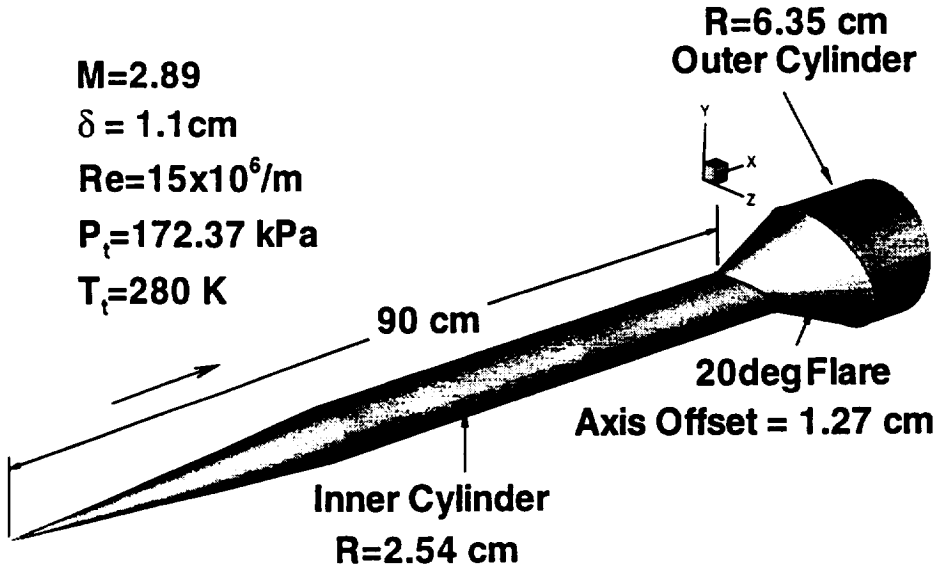

Figure 10.55: Geometry of cylinder/offset-flare juncture

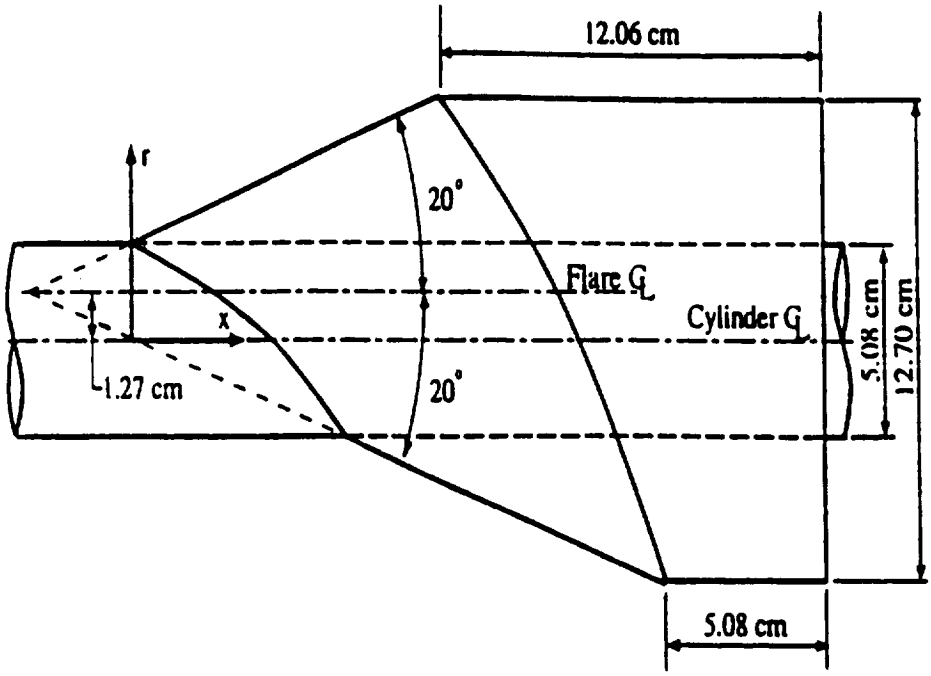

Figure 10.56: Schematic of offset three-dimensional flare

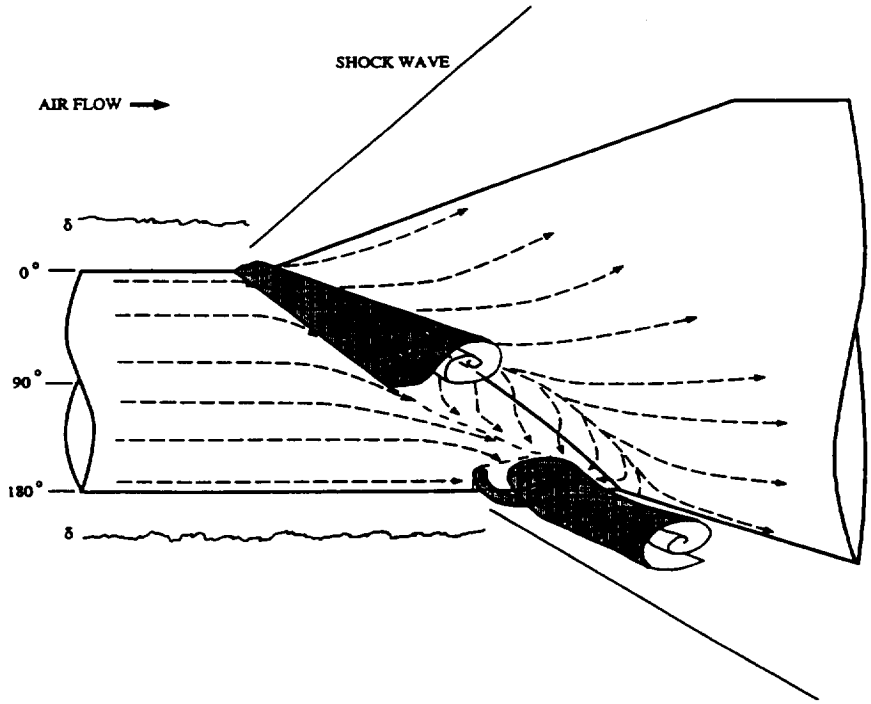

Figure 10.57: Postulated flow structure

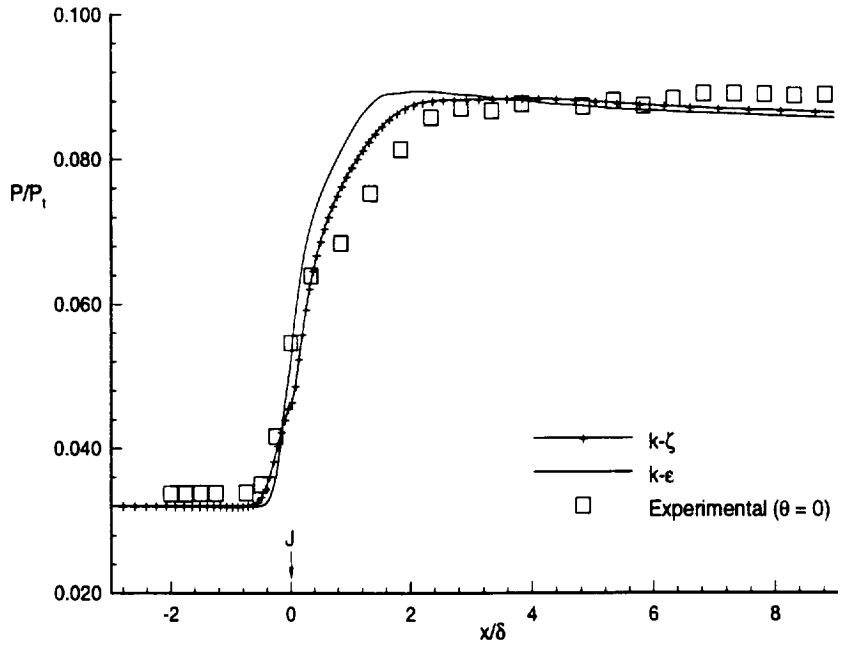

Figure 10.58: Streamwise pressure comparison for $\theta = 0$ plane

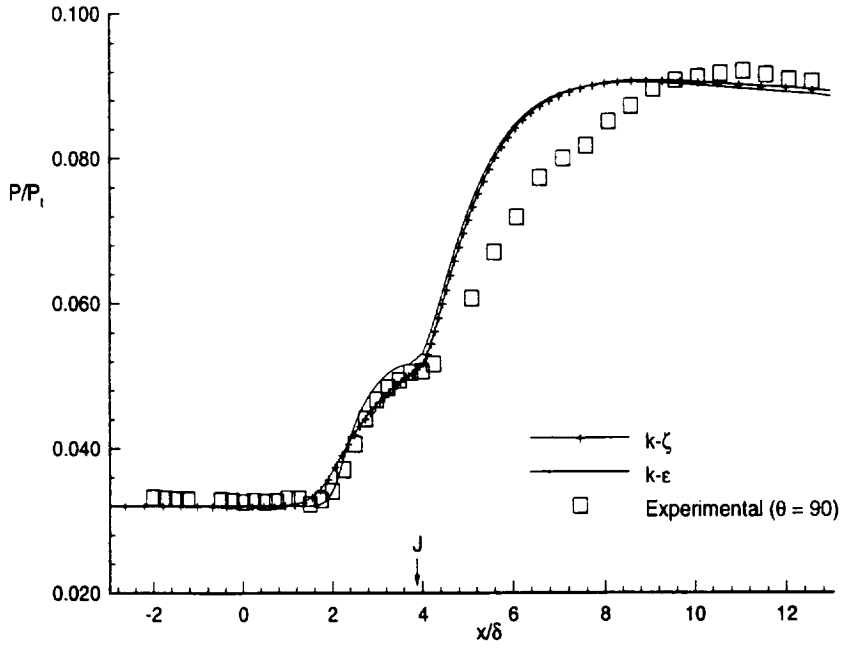

Figure 10.59: Streamwise pressure comparison for $\theta = 90$ plane

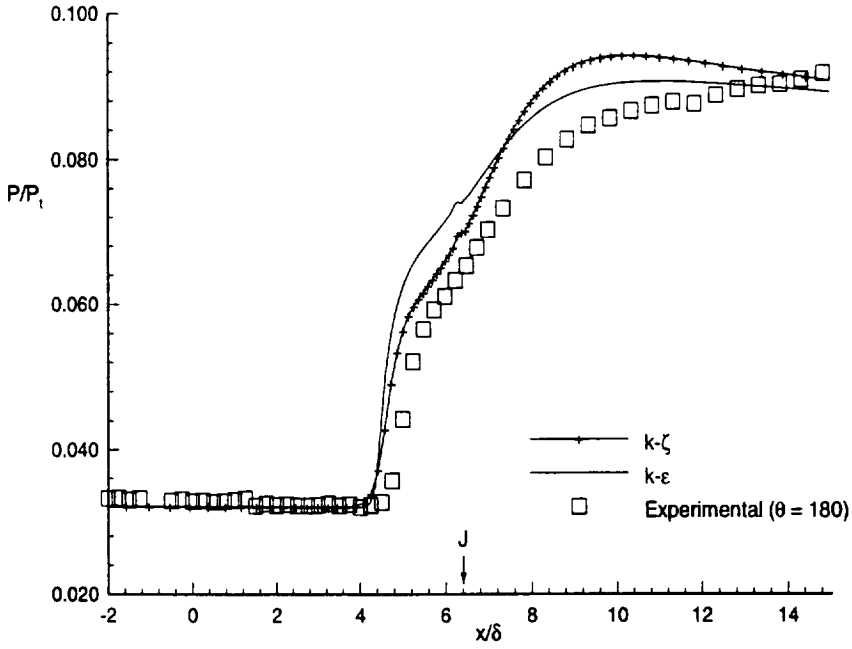

Figure 10.60: Streamwise pressure comparison for $\theta = 180$ plane

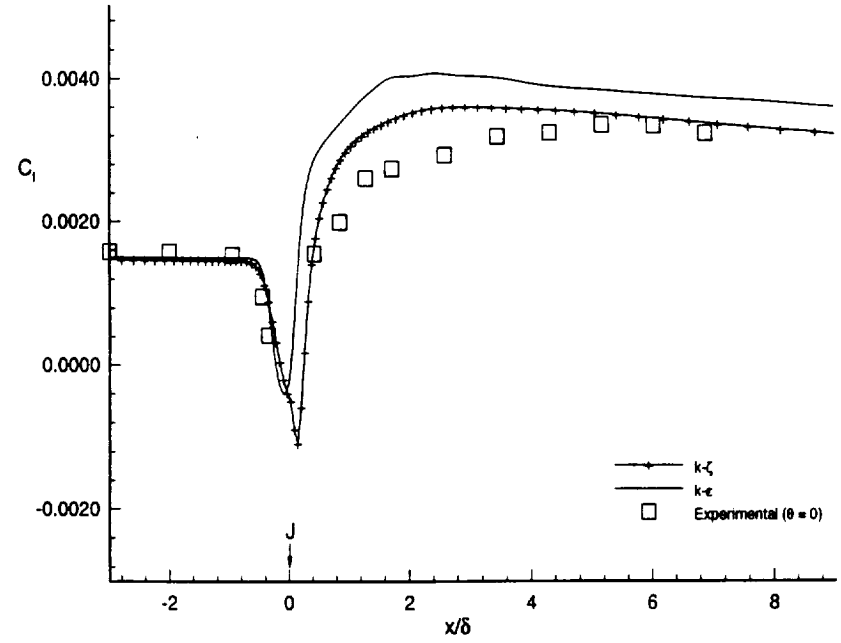

Figure 10.61: Skin friction coefficient for $\theta = 0$ plane

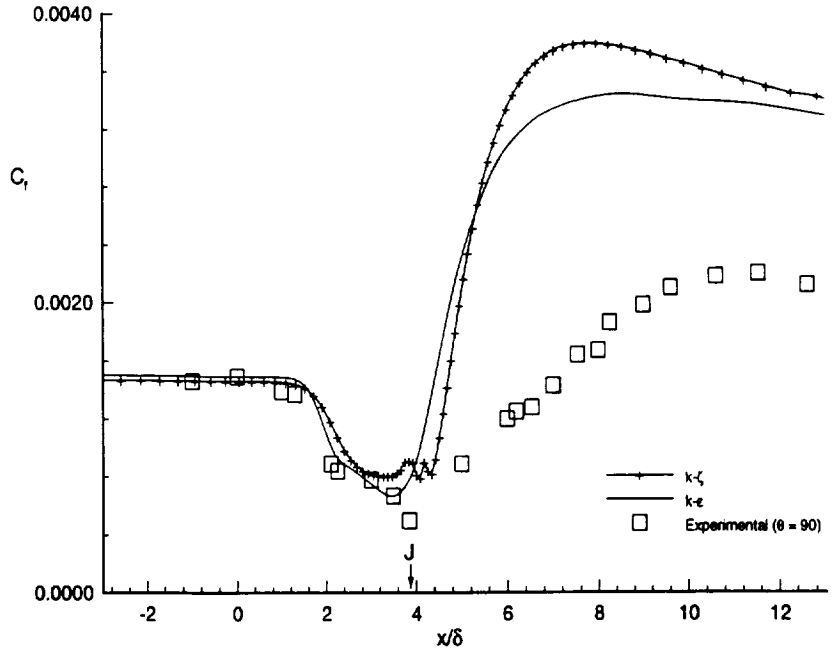

Figure 10.62: Skin friction coefficient for $\theta = 90$ plane

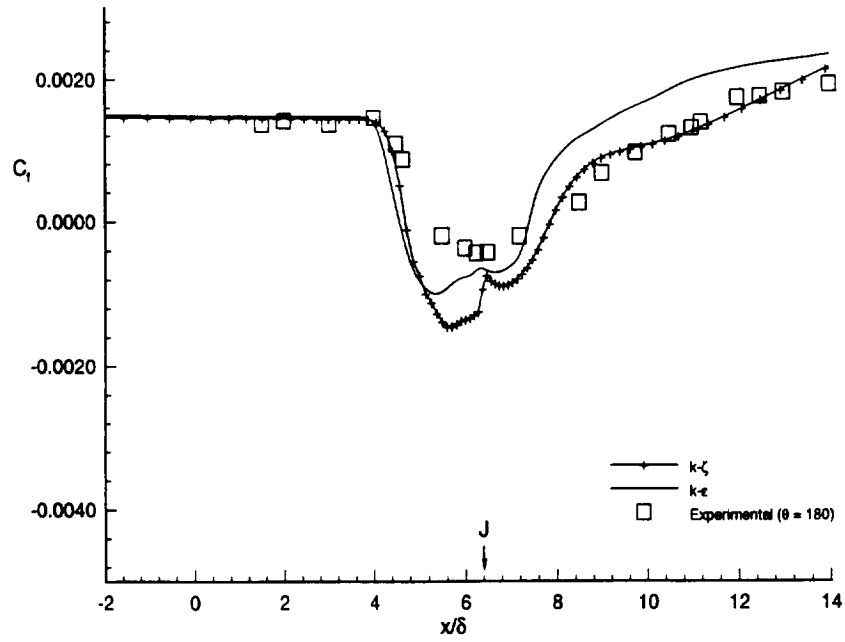

Figure 10.63: Skin friction coefficient for $\theta = 180$ plane